A Study of Chemoenzymatic and Multi-enzymatic Microreactor Cascades for the Synthesis of Pharmaceutical Compounds in Continuous Flow

Mariana Santos

A Thesis Submitted for the Degree of
Doctor of Philosophy

Department of Biochemical Engineering
University College London

Declaration

I, Mariana Santos confirm that the work presented in this thesis is my own. Where information has been derived from other sources, I confirm that this has been indicated in the thesis.

Acknowledgement

I would like to thank my supervisor Prof. Nicolas Szita for the opportunity to be part of his research group and for guiding me through my Ph.D studies. I would also like to thank Prof. John Ward and Prof. Rolland Wohlgemuth for the invaluable discussions during this research project.

I am grateful to Dr Marco Marques and Dr Brian O'Sullivan for their guidance and much appreciated help in the lab. A special thanks is also due to Dr Pia Gruber for showing me the ropes in the microfluidic lab and for giving me the tools to continue her research.

I would also like to thank all my office and lab colleagues for making this journey much more enjoyable and keeping me sane throughout all the hard times. In particular, I want to acknowledge Sofia Nunes for her constant emotional support, for always checking on me before she left for the day, and for making sure I had food if I was staying late. Her kindness and generosity knew no bounds, and I am deeply thankful for her friendship.

Finally, but most importantly, I would like to thank my friends and family. Their unwavering belief in me and their encouragement helped me to overcome many challenges and persevere through the toughest times. Thank you for always being there for me and for being such an important part of my life. I certainly would not be where I am without them. Words cannot express how grateful I am to my parents, José and Marina, for their unconditional love and support during my entire life. Last, thank you, Goncalo, for being my rock throughout this journey. Thank you for your patience, understanding, and support throughout the writing of this thesis. I couldn't have done it without you.

Abstract

Biocatalytic cascades have emerged as efficient tools in the synthesis of valuable pharmaceutical compounds. Multi-enzymatic and chemoenzymatic cascades offer several advantages. Some examples are the ability to produce complex chiral molecules from simple building blocks, the reduced need for isolation of intermediates, and the potential to shift reaction equilibrium towards product synthesis. Their performance, however, requires the optimisation of several parameters to overcome incompatible reaction conditions and inhibitory interactions between the cascade components. Continuous flow microreactors, with their small reagent requirements, efficient mass and heat transfer and improved spatial control of reaction steps, are a promising technology for developing biocatalytic cascades.

In this work, continuous flow techniques were explored in the development of two novel biocatalytic cascades. The first reaction investigated the coupling of a Diels-Alder reaction, catalysed by aluminium chloride, with a transketolase-catalysed reaction for the synthesis of 1-(3,4-dimethyl-3-cyclohexen-1-yl)-1,3-dihydroxypropan-2-one. The different catalysts were combined thanks to the spatial separation of reaction steps afforded by microreactors. Optimisation of reaction conditions led to the complete conversion of substrates and a total process yield of 5 mM of product. Further process intensification strategies were developed to increase the cascade productivity. These included a numbering-up approach of identical microreactors and product purification methods *via* enzyme immobilisation and integration of an in-line tangential flow filtration.

The second enzymatic cascade was designed to synthesise the only glycolytic metabolite commercially unavailable, 1,3-biphosphoglycerate. Several enzyme combinations and starting substrates were investigated under different operation modes. A three-enzyme cascade was established to realise the synthesis with *in situ* co-factor regeneration. The metabolite prepared in the cascade can serve as an effective substrate to phosphoglycerate kinase to produce adenosine triphosphate. Operational guidelines are proposed to assist in the efficient enzymatic preparation of 1,3-biphosphoglycerate for posterior isolation and use in scientific research.

Impact Statement

This work has developed two biocatalytic cascades in continuous flow for the synthesis of valuable pharmaceutical compounds. A chemoenzymatic cascade compromising a Diels-Alder reaction and a transketolase reaction for the synthesis of chiral pharmaceutical intermediate was demonstrated, for the first time, in a continuous flow system with complete conversion of substrates. The chiral intermediate synthesised is a precursor of several antibiotics, such as thiamphenicol and chloramphenicol. Its efficient synthesis is, therefore, of interest to the pharmaceutical industry. Complete conversion of substrates was only possible thanks to the compartmentalisation of reactions enabled by continuous flow microreactors, showcasing the advantages of microreactors over conventional batch reactors for establishing biocatalytic cascades with incompatible reaction conditions. Moreover, the results obtained further underpin the applicability of chemoenzymatic cascades to organic synthesis in the pharmaceutical industry. The transketolase-catalysed reaction replaces several chemical reactions and purification steps, making the synthesis of this compound more environmentally and economically sustainable. The process considerations explored in this thesis for coupling a chemical catalyst and biocatalyst in flow can be applied to any chemoenzymatic cascade reaction.

In this research, a *de novo* multi-enzymatic cascade for the synthesis of a non-commercially available glycolytic metabolite was also designed. The synthesis of this metabolite is of high value for scientific research since it may enable a new fundamental understanding of metabolism and lead to the developing of new therapies. Additionally, continuous flow process intensification strategies through upstream and downstream processing were explored in this research work. A micro-scale tangential flow filtration device with a reversible clamp sealing, allowing for the utilisation of different filtration membranes as needed, was used to remove reaction products from the biocatalyst completely. The device can be further used in research with other enzymatic microreactors operated with free enzymes. An enzyme immobilisation method is also presented that can be further used to support the development of other biocatalytic reactions in flow. The strategies developed will enable future research into scalable continuous flow biocatalytic processes.

List of Presentations and Publications

Conferences

European Symposium on Biochemical Engineering Sciences (ESBES), Virtual Conference, 2021 – Oral presentation.

24th International Conference on Miniaturized Systems for Chemistry and Life Science (MicroTAS), Virtual conference, 2020 – Poster presentation.

4th International Symposium on Biocatalysis and Biotransformations (BioTrans), Groningen, The Netherlands, 2019 - Poster presentation.

5th International Conference Implementation of Microreactor Technology in Biotechnology (IMTB), Cavtat, Croatia, 2019 – Oral presentation.

Publications

Santos M., Gruber P., O'Sullivan B., Wohlgemuth R., Marques M., Szita N. "Chemoenzymatic Reactions in Flow: First Coupling of a Catalytic Diels-Alder Reaction with a Transketolase-catalysed reaction" (in preparation).

Abbreviations

2,3-BPG	2,3-biphosphoglycerate
3-FBA	3-formylbenzoic acid
3-PGA	3-phosphoglycerate
ABT	(2*S*,3*R*)-2-amino-1,3,4-butanetriol
ADP	Adenosine diphosphate
AK	Acetate kinase
APIs	Active pharmaceutical ingredients
APTES	3-aminopropyltriethoxysilane
ATP	Adenosine triphosphate
BPGM	Biphosphoglycerate mutase
BPR	Back pressure regulator
BSA	Bovine serum albumin
BZA	Benzylamine
CAL-B	*Candida antarctica lipase B*
CCA	3,4-dimethyl-3-cyclohexene-1-carboxaldehyde
DA	Diels-Alder
DAADH	d-amino acid dehydrogenase
DA-TK	Diels-Alder-transketolase
DCDHP	1-(3,4-dimethyl-3-cyclohexen-1-yl)-1,3-dihydroxypropan-2-one
DDI	DNA-directed immobilization
DHAP	Dihydroxyacetone phosphate
DKR	Dynamic kinetic resolution
EM	Embden-Meyerhof
ERY	Erythrulose
FDH	Formate dehydrogenase
FEP	Fluorinated ethylene propylene
FID	flame ionization detector
FLLEX	Flow Liquid–Liquid Extraction
GA	Glycolaldehyde
GAP	Glyceraldehyde-3-phosphate
GAPDH	Glyceraldehyde 3-phosphate dehydrogenase

GC	Gas chromatography
GK	Glycerol kinase
HEWT	Halomonas elongata
HHDH	Halohydrin dehalogenase
HLADH	Alcohol dehydrogenase
HNL	Hydroxynitrile lyase
HPA	Hydroxypyruvate
HPLC	High-performance liquid chromatography
LB	Lysogeny broth
LBL	Layer-by-layer
LDH	Lactate dehydrogenase
L-DOPA	3,4-dihydroxy-L-phenylalanine
MBA	(S)-α-methylbenzyl-amine
MPIR	Multipoint injection microreactor
MS	Mass spectrometry
MTBE	Methyl tertiary-butyl ether
NAD+	Nicotinamide adenine dinucleotide
NADP	Nicotinamide adenine dinucleotide phosphate
OD	Optical Density
PAMAM	Polyamidoamine
PBS	Phosphate-buffered saline
PDMS	Polydimethylsiloxane
PEEK	Polyether ether ketone
PEI	Polyethylenimine
PFA	Perfluoroalkoxy
PGAM1	Phosphoglycerate mutase 1
pgK	3-phosphoglyceryl-lysine
PGK	Phosphoglycerate kinase
PMMA	Poly(methyl methacrylate)
PTFE	Polytetrafluoroethylene
RO	Reverse osmosis
TEA	Triethylamine borane
TFA	Trifluoroacetic acid

TFF	Tangential Flow filtration
ThDP	Thiamine diphosphate
TK	Transketolase
TLC	Thin layer chromatography
TPI	Triosephosphate isomerase
TTN	Total turnover number

Table of contents

List of Figures

List of Tables

1 Introduction

1.1 Biocatalysis for efficient and sustainable synthesis of pharmaceutical intermediates

Biocatalysis is one of the most promising technologies for the green and sustainable synthesis of pharmaceutical intermediates. Compared to traditional chemical synthesis, enzyme-catalysed reactions offer many advantages that contribute to greener and more efficient production of pharmaceuticals. One of the main characteristics of biocatalysis is its ability to reduce the environmental footprint of pharmaceutical manufacturing significantly. Thanks to enzymes' high chemo-, regio- and stereo-selectivity, biocatalytic reactions can efficiently convert substrates into desired products with minimal by-product formation and waste generation. Consequently, biocatalytic processes produce fewer pollutants, helping to mitigate environmental pollution and conserve valuable resources. The excellent selectivity of biocatalysts gives them an advantage over chemical catalysts, leading to a superior atom economy, which is a fundamental principle of green chemistry. Enzymatic reactions excel in achieving superior atom economy as they can directly convert starting materials into desired products without the need for excessive reagents or the formation of undesirable side products. This not only reduces waste but also optimises the use of resources, aligning perfectly with sustainability goals.

Furthermore, obtaining single enantiomers of chiral intermediates in pharmaceutical synthesis is often critical. Enzymes' exceptional selectivity makes them invaluable, eliminating the need for complex and often hazardous chemical steps such as chiral resolution. This streamlines the synthesis process while reducing the use of toxic reagents (Woodley, 2008; Hoyos, Pace and Alcántara, 2019; Alcántara *et al.*, 2022).

Biocatalysis also simplifies synthetic routes by eliminating the need for laborious protective group strategies and deprotection steps. This reduces the overall number of synthetic steps and curtails the consumption of resources and hazardous reagents.

Additionally, enzymes operate under mild temperature and pressure conditions, unlike many traditional chemical processes that demand harsh conditions. These mild reaction conditions enhance both the safety of the synthesis process and energy

efficiency. Lower energy consumption translates into reduced greenhouse gas emissions and a smaller carbon footprint for pharmaceutical production. Also, enzymes are non-toxic, biodegradable proteins, ensuring the safety of both the production process and the final pharmaceutical products. They eliminate the need for toxic chemicals, thereby creating pharmaceuticals that are safer for patients and the environment.

Enzymes can be immobilised and reused in multiple reaction cycles, significantly enhancing efficiency and sustainability. Moreover, biotechnology advances enable enzyme engineering to enhance their activity, selectivity, and stability for specific pharmaceutical synthesis processes. Technological advances in enzyme screening, bioinformatics, and protein engineering have greatly expanded the biocatalytic toolbox. These innovations have facilitated the discovery and optimisation of biocatalysts, paving the way for novel and greener processes in pharmaceutical production (Patel, 2006; Ghislieri and Turner, 2014; Fuchs, Farnberger and Kroutil, 2015; Hughes and Lewis, 2018).

A well-known example is the industrial application of an engineered transaminase for the synthesis of sitagliptin, the active ingredient in Januvia, a leading drug used to treat type II diabetes and commercialised by Merck (Savile et al., 2010). The previous chemical synthesis of sitagliptin lacked the stereoselectivity of transaminase, resulting in a product stream contaminated with rhodium where several purification steps were necessary. Compared with the chemical process, the biocatalytic process has increased overall productivity by 53% and reduced the total waste, making the manufacturing process more cost-efficient. Since this first demonstration, transaminases have become an attractive alternative to metal catalysts for the synthesis of chiral amino compounds under mild conditions and efficient reaction steps (Green, Turner and O'Reilly, 2014).

The manufacturing of Saxagliptin, a DPP-IV inhibitor like Januvia, commercialised by Bristol-Myers Squibb to improve blood glucose control for diabetics, has also benefited from enzymatic catalysis. Here, an enzymatic reductive amination was carried out with two engineered enzymes, phenylalanine dehydrogenase and formate dehydrogenase, to synthesise a chiral (S)-amino acid for Saxagliptin. Both enzymes were expressed in a single recombinant *Escherichia coli* and formate dehydrogenase was used to regenerate the co-factor of phenylalanine dehydrogenase the enzyme

responsible for the synthesis of the amino acid (Cao *et al.*, 2007). The use of a recombinant *Escherichia coli* expressing formate dehydrogenase to recycle NAD+ back to NADH necessary as a co-factor for leucine dehydrogenase has been applied in the preparation of (S)-tertiary leucine, a chiral amino acid required for the synthesis of Atazanavir, a drug used to treat HIV (Patel, 2013).

Another example marketed by Merck is the enzymatic synthesis of a key intermediate in the synthesis of montelukast sodium (Singulair), a drug used to control the symptoms of asthma and allergies. Here, a ketoreductase was engineered to be highly selective and active in a mixed aqueous and organic media leading to a process yield above 95% in a biocatalytic process at a >200 kg scale (Liang et al., 2010).

A recent study by Bong and co-wokers has described the development of an enzymatic oxidation of pyrmetazole to esomeprazole using an engineered Baeyer-Villiger monooxygenase (Bong et al., 2018). This method could potentially be a better alternative for the kagan sulfoxidation used by Astra Zeneca to produce esomeprazole, the API of their blockbuster drug Nexium, used to treat certain stomach and oesophagus problems, such as acid reflux and ulcers. Although successful at a laboratory scale (30 g), the process has encountered some mass challenge limitations during scale-up and therefore further optimisations are necessary to achieve a successful production at an industrial scale.

In the last few decades, several biocatalytic processes have been explored, with some being successful in the development of single enantiomers of drug intermediates with applications in the pharmaceutical industry. Regardless, the full potential of biocatalysis for industrial applications still needs to be realised, and it is dependent on the development and availability of biocatalysts robust enough to sustain high selectivity, stability, and activity at an industrial scale in combination with chemical transformations. Progress in bioinformatics and DNA and protein engineering technologies will continue to contribute to the availability and design of novel biocatalysts with properties suited to the desired process conditions. However, in combination with these advances, further optimisations of bioreactor process modes (batch, fed-batch, perfusion and continuous processing) to facilitate the scale-up of biocatalytic processes and their combination with chemical steps in sequential reactions are needed (Sun *et al.*, 2018). Recently, special attention has been given to

continuous flow reactors. These enable spatial compartmentalisation of reaction conditions avoiding the interference of other reaction conditions with the biocatalysts' stability and activity. Therefore, their application to enzymatic and chemoenzymatic processes is worth investigating (Britton, Majumdar and Weiss, 2018).

1.2 Continuous Flow Biocatalysis

Over the last two decades, continuous flow reactors have gained attention as a novel technology with the potential to address batch-process challenges and improve biocatalytic process development and intensification.

Continuous flow synthesis at a micro-scale offers several advantages over conventional batch systems. Unlike macro-scale systems, flow microreactors have short diffusion paths and high surface-to-volume ratios, which leads to enhanced mass and heat transfer and a laminar flow regime that allows for better control over reaction conditions. These flow characteristics result in improved space-time yields and increased productivity and are particularly important for multiphase processes in which the large surface to volume ratios and interphases are essential for efficient mixing of reactants. Furthermore, the small dimensions of flow reactors reduce the process equipment's footprint and lower the energy consumption and reagent input, reducing waste and leading to an overall more cost-effective process.

Continuous flow reactors can also be integrated with *in situ* condition monitoring technologies, such as temperature and pH sensors, as well as in-line feeding, quenching and analysis methods. These integrations allow for highly efficient high-throughput screening and process optimization, which further contributes to the higher productivity and selectivity of processes performed in microfluidic reactors compared to traditional systems.

One of the major benefits of flow reactors for process intensification is their modular configuration that allows for the compartmentalization of reactions. The ability to spatially confine reactions in different compartments inside one reactor or inside different reactors connected in-line facilitates the development of multi-step reactions with incompatible reaction conditions. Additionally, the modular configuration of flow systems also enables scalability simply by numbering-up reactors in parallel. Having multiple flow reactors with the same configuration and size operating

simultaneously in identical conditions means that the reaction conditions remain the same and are not affected by any scaling-out level.

All the characteristics mentioned above make continuous flow reactors ideal tools to for the development of biocatalytic processes.

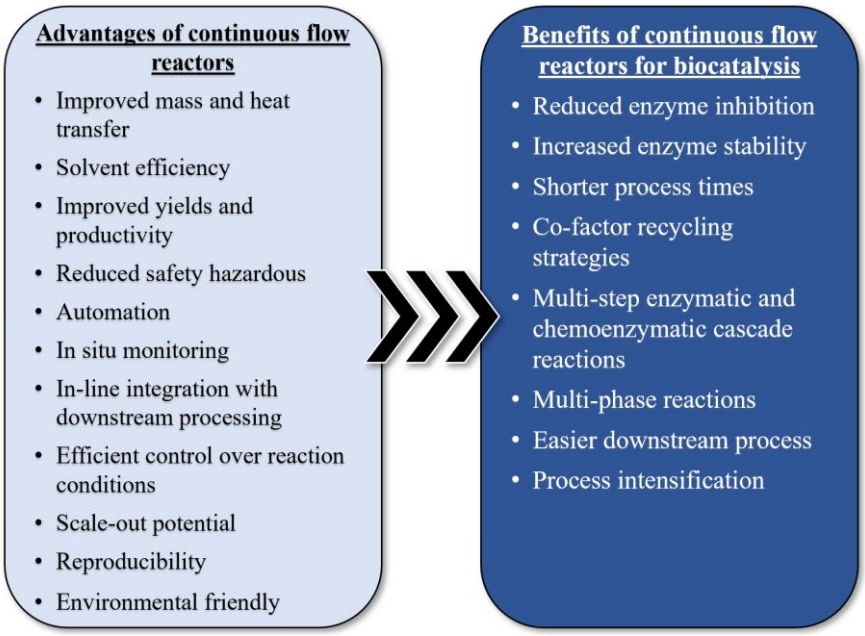

Figure 1.1: Overview of the advantages of continuous flow reactors over batch reactors and the benefits of continuous flow reactors for biocatalysis.

The possibility of screening for several reaction conditions with minimal amounts of biocatalysts is crucial to evaluate large libraries of biocatalysts that may have limited availability until further protein engineering developments are made. Furthermore, the easy testing and optimization of different process conditions in flow reactors allows for selecting the best process options before scaling up.

The small dimensions of the microchannels of continuous flow reactors reduces diffusion limitations between the enzyme and substrates and allows for mixing to occur by molecular diffusion avoiding harsh mixing that can affect the biocatalysts lifetime. In addition, the cost-efficiency and sustainability of the process can be further improved by the continuous feeding and feedback loop strategies of substrates and co-factors to the reaction as well as *in situ* product removal methods. For biocatalytic reactions, these methods can improve the process efficiency by overcoming the

inhibitory effects of substrates and products on the biocatalyst and shifting unfavourable reaction equilibrium.

Continuous flow reactors can be fabricated from inert materials such as glass, metal, polymers, and ceramics. Depending on the inner diameter and volume of the channels, flow reactors can be classified as microfluidic microreactors or mesoreactors. Microfluidic microreactors typically have an internal diameter <500 μm and a volume in the μL range. They usually take the form of microcapillaries and microchips and are characterized by low Reynolds numbers (generally below 250) and laminar flow regime. On the other hand, mesoreactors are generally considered to have internal diameters between 500 μm and several millimetres (Tamborini *et al.*, 2018; Fernandes and de Carvalho, 2021). Depending on the flow rate at larger dimensions (>1mm), it may not be easy to maintain a laminar regime. Mesoreactors can have different designs, and the most common for biocatalysis are coil and packed-bed reactors.

Coil reactors made from polymers such as PFA (perfluoroalkoxy) are easy to fabricate in the laboratory and, thus are one of the most used flow reactors. However, they may not be ideal for high-pressure reactions, and small chemicals can diffuse through the reactor tubing. On the other hand, chip microreactors are challenging to fabricate but can be operated at high pressures and temperatures. Both coils and chip microreactors can easily become blocked; therefore, for immobilised enzymes, packed-bed reactors are more popular since they typically have a bigger inner diameter.

Microreactors enable efficient mixing at laminar flow and can be operated at high pressures and temperatures. However, they can be easily blocked and require challenging and expensive fabrication techniques such as micromachining, laser ablation, photolithography and plasma etching. Therefore, mesoreactors such as coil reactors made from polymers like PFA (perfluoroalkoxy) that are easy to fabricate in the laboratory are one of the most used flow reactors. Packed-bed reactors are more popular for immobilised enzymes since they typically have a bigger inner diameter. Another mesoreactor design is a tube-in-tube or membrane reactor used for enzymatic reactions involving an aqueous and gas phase physically separated by a membrane. Recently, stereolithography technologies also known as rapid prototyping or 3D printing have been used to fabricate customisable continuous flow reactors for biocatalysis.

The choice of material and microreactor design usually depends on the operating conditions and the configuration of the biocatalyst in the microreactor. Like in conventional batch reactors, in continuous flow reactors biocatalysts can be used in cell-free enzymes or whole cells. Cell-free enzymes, either used free in solution or immobilised, are the most common biocatalyst configuration used since whole-cell systems have slower reaction rates and preventing side reactions and cross-inhibitions is more complex. Although using free enzymes dissolved in solution is easier, separating the product and the enzyme from the reaction mixture may require extra costs and complicated downstream processing. Therefore, from a commercial point of view, immobilised enzymes are preferred. Besides facilitating downstream processing and product purification, immobilization strategies can improve reaction rates and enzyme stability.

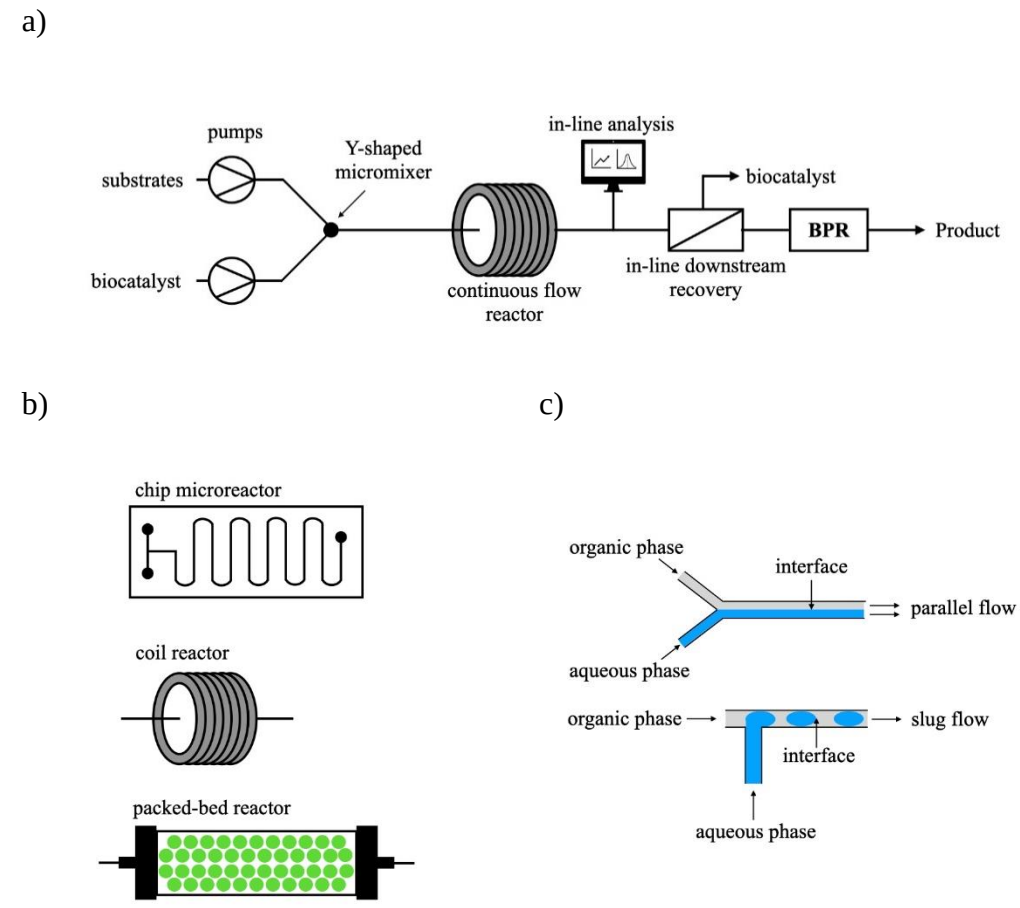

Figure 1.2: Overview of the continuous flow reactors designs and operation mode.

a) Schematic of a typical continuous flow system for biocatalysis composed of pumps, a micromixer and a continuous flow reactor. Additionally extra modules can be integrated into the system, such as an in-line analysis modules and an in-line downstream processing unit, to separate the reaction mixture and a backpressure regulator (BPR) to pressurize the system. b) Examples of the three most used types of continuous flow reactors for biocatalysis (chip microreactor, coil reactor and packed-bed reactor). c) Schematic of the type of flow inside the channel of the flow reactor when running immiscible liquids. The streams can run either in parallel flow or in slug flow.

Enzymes can be immobilised onto solid supports by absorption, entrapment, cross-linking, affinity, and covalent bonding. There are several enzyme immobilization techniques to choose from depending on the enzyme characteristics, the solid support used and the reaction conditions. Selecting the right immobilization support is not trivial since it will affect the enzyme structure and directly impact enzymatic activity and stability. Although there is no preferred method since each reaction system is different, in continuous flow systems, enzymes are usually immobilised in: (i) packed-bed reactors, where enzymes are immobilised on beads or particles that are used to pack the reactor; (ii) wall-coated reactors, where the enzyme is directly attached on the inner wall of the microchannels or on materials coating the inner wall; (iii) monolithic reactors, where the enzyme is immobilised onto the surface of the microchannel of the monolithic structure (Laurenti and dos Santos Vianna Jr., 2016).

The configuration of microchannels makes them ideal supports for enzyme immobilization due to their large surface area that allows for high enzyme loading with minimum diffusion limitation (Valikhani, Bolivar and Nidetzky, 2020; Žnidaršič-Plazl, 2021). Additionally, some immobilization methods allow for the specific spatial distribution of the enzymes inside the microreactor, which is essential for conducting efficient multi-enzymatic cascade reactions. Regardless, not all biocatalysts are suitable for all the immobilization methods, and many enzymes will lose considerable activity when immobilised. Thus, the choice between using free or immobilised enzymes depends on the activity and stability of the biocatalyst and the overall operational and reaction conditions.

A)

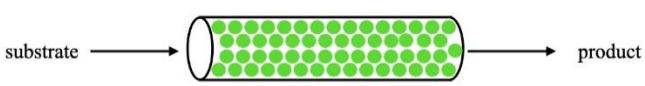

b)

c)

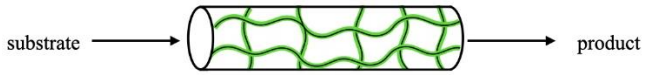

Figure 1.3: Examples of the different types of enzyme-immobilised continuous flow reactors.
a) Packed-bed reactor, where the enzyme is pre-immobilised onto beads/particles used to pack the reactor; b) Monolithic reactor, where the enzyme is immobilised on the pores/channels of the monolithic structure; c) Wall-coated enzyme immobilised reactors where the enzyme is directly bound to the inner wall of the microchannel, or on a supporting coating material on the inner walls.

Independently of biocatalyst configuration and reactor design in continuous flow reactors the reaction rate will depend on the residence time inside the microchannels and enzyme activity. The residence time (τ) is calculated from the volume of the reactor (V) and the flow rate used (Q):

$$\tau = \frac{V}{Q} \qquad 1.1$$

Therefore, in order to compare batch and flow enzymatic reaction rates the residence time needs to be normalized for both operation modes taking into account enzyme activity and reactor volume. Accordingly to Marques et al. (Marques *et al.*, 2012) the normalized residence time (σ) in a batch reactor can be expressed as:

$$\sigma = \frac{E_t . t}{V} \qquad 1.2$$

where E_t represents the total enzyme activity (U), t is the reaction time (min), and V is the volume of reaction (mL). In continuous mode, σ is expressed as:

$$\sigma = \frac{E_t}{Q} \qquad 1.3$$

Where Q corresponds to the flow rate ($mL.min^{-1}$). This normalization of residence time ($U.min.mL^{-1}$) allows us to compare batch and continuous operation modes.

1.2.1 Biocatalytic reactions in continuous flow reactors

The most straightforward approach to flow biocatalysis is to operate in a single liquid phase, where a substrate and a free-enzyme solution are simultaneously pumped into separate inlets of the microreactor, typically with high-pressure syringe pumps, and the reaction occurs along the microchannel. This approach was used for the laccase-catalysed oxidation of 3,4-dihydroxy-l-phenylalanine (l-DOPA) (Tušek *et al*., 2013) and for the glycosidase-catalysed hydrolysis of oligosaccharides (Kanno *et al.*, 2002). In both cases, reaction rates were improved 2 to 5-fold in chip microreactors versus batch reactors, showcasing the efficiency of continuous flow systems for the development of biocatalytic reactions.

An alternative approach is a two-phase aqueous/organic flow system, where two fluids run through the microchannel in parallel or slug-flow. Kanno and co-workers developed a biphasic flow system for the enzymatic synthesis of oligosaccharides to reduce the water concentration in the reaction media and consequently shift the equilibrium of the reverse reaction (Kanno *et al.*, 2002). In biphasic conditions, a hydrophobic product can be continuously extracted by an organic solvent from the aqueous phase. This can shift the reaction equilibrium towards product formation and facilitates product recovery and enzyme recycling. Furthermore, in an aqueous/organic phase system, the solubility of a hydrophobic substrate, which can often be a rate-limiting step, can be enhanced. For example, applying a two-phase flow system in microreactors for the lipase-catalysed synthesis of isoamyl acetate from an extremely hydrophobic substrate, resulted in orders of magnitude faster reaction rates versus conventional batch esterification of isoamyl acetate (Pohar, Plazl and

Nidar Si C-Plazl, 2009; Žnidaršič-Plazl and Plazl, 2009). The two-phase system was operated in parallel and slug-flow with continuous product separation. In slug-flow, the interfacial area between the two phases is increased and controlled by the size of the solvent segments, leading to highly efficient mixing inside the microchannels and improved mass transfer. This flow pattern was also applied in a capillary microreactor for the enzymatic synthesis of the antibiotic cephalexin from extremely hydrophobic substrates. Once again, the two-phase slug-flow facilitated *in situ* product extraction and enzyme recycling leading to reaction rates that were not feasible in batch (Vobecká et al., 2020). The examples mentioned above rely on the flow regime being laminar throughout the whole microchannel. If this is not the case, the surface of the microchannel can be chemically modified to become hydrophobic or hydrophilic and allow phase separation (Maruyama *et al*., 2003).

Another technique to separate the biocatalyst from the reaction mixture was proposed by O'Sullivan et al. In their approach, a substrate with a biocatalyst in a free solution were pumped through a microreactor connected in-line with a tangential flow filtration system. Complete enzyme retention and product extraction were achieved in the filtration system, demonstrating the potential for microfluidic platforms to integrate upstream and downstream unit operations to develop whole biocatalytic processes (O'Sullivan *et al.*, 2012).

Although continuous flow microreactors exhibit higher yields than batch reactors, the productivity of microreactors can be limited by enzyme inhibition and denaturation caused by high substrate concentrations. To address this issue, Lawrence *et al.* developed a multi-input microreactor capable of substrate feeding at multiple points for the transketolase-catalyzed synthesis of L-erythrulose (Lawrence *et al.*, 2013). The multi-input reactor allowed for a 4.5-fold increase in output concentration and a 5-fold increase in throughput compared with a single-input reactor. The results showcase the flexibility of microreactors to be adapted to bioprocess needs.

Table 1.1 presents further details of the examples mentioned of microreactors using free enzymes that outperformed batch reactors.

Table 1.1: Examples of biocatalytic reactions with free enzymes in continuous flow reactors

Biotransformation	Microreactor	Comments	Refs
Laccase-catalysed oxidation of catechol and 3,4-dihydroxy-L-phenylalanine(L-DOPA)	Glass chip microreactor with Y-shaped inlet and outlet	Oxidation rates in the microreactor in aqueous media were 18 – 167-fold higher than in a batch reactor, and two times higher than the rates observed in a cuvette.	(Tušek *et al.*, 2013)
β-galactosidase-catalysed hydrolysis of *p*-nitrophenyl-β-D-galactopyranoside and transgalactosylation of *p*-nitrophenyl-2-acetamide-2-deoxy-β-D-glucopyranoside	PMMA chip microreactor with Y-shaped inlet	Hydrolysis was performed in aqueous media while transgalactosyation was performed in a buffer-acetonitrile solvent system, to minimize reverse reactions. Both reactions were enhanced as compared to the batch system, with the hydrolysis of p-nitrophenyl-β-D-galactopyranoside being 5 times faster in the microreactor than in batch.	(Kanno *et al.*, 2002)
Lipase-catalysed isoamyl acetate synthesis	Glass chip microreactor with Y-shaped inlet and outlet	The esterification of isoamyl alcohol and acetic acid occurred at the interface between n-hexane and an aqueous phase with dissolved lipase B from Candida antarctica. The two-phase flow system allowed for continuous product separation from the aqueous phase to the organic phase. Faster reaction rates were observed in the continuous flow microreactor than in batch reactors	(Žnidaršič-Plazl and Plazl, 2009)

	Glass chip microreactor with Ψ-shaped inlet and single outlet	The ionic-liquid/organic two-phase system operated in slug flow proven to be highly efficient for esterifications. The system allowed for simultaneous extraction and product removal with a 3-fold increase in the reaction rate when compared to conventional batch operation.	(Pohar, Plazl and Nidar Si C-Plazl, 2009)
Penicillin acylase catalysed synthesis of cephalexin	Teflon microcapillary reactor with Y-shaped inlet	The aqueous two-phase slug-flow system allowed for simultaneous reaction product separation and enzyme recycle. The recycling loop also contained a microdialysis unit for removal of the side product, phenylglycine to prevent clogging.	(Vobecká *et al.*, 2020)
Transketolase catalysed reaction of lithium hydroxypyruvate (HPA) and glycolaldehyde (GA) to l-erythrulose (ERY)	PMMA microreactor connected in-line with a filtration unit based on PDMS gasket and regenerated cellulose filter	Full substrate conversion and complete enzyme retention and product separation was achieved; the reaction rate was comparable to batch reactors.	(O'Sullivan *et al.*, 2012)
	Multi-input PMMA microreactor	The multi-input microreactor system, capable of substrate feeding at multiple points, showed an 8-fold improvement of productivity over fed-batch microplate reactions and a 5-fold increase in throughput compared with a single input microreactor.	(Lawrence *et al.*, 2013)

Despite the success of several continuous flow systems with free enzymes dissolved in solution, the full potential of continuous flow biocatalysis requires efficient product removal and enzyme retention for multiple conversion rounds. To achieve this, immobilizing the enzymes on continuous flow systems is a key enabling technology to move from batch to flow synthesis.

The most straightforward continuous flow reactor configuration for immobilised enzymes is a packed-bed reactor in which enzymes are immobilised on physical supports used to pack the reactor. Packed-bed reactors are usually easy to fabricate from long-lasting commercial materials and offer a high enzyme-loading capacity and a high surface area-to-volume ratio, which ensures short diffusion paths between substrates and enzymes. A wide variety of materials can be used as support for enzyme immobilization. Porous silica is one of the most widely used inorganic supports due to its thermal and chemical resistance, biocompatibility, high binding capacity and easy functionalization. Nagy et al. developed an efficient and easy-to-perform method for the covalent immobilization of lipase from *Burkholderia* (Lipase PS) on hollow silica microspheres (M540). Surface activation of M540 support was investigated using a variety of bisepoxide activating agents to maximize the stability and activity of the enzyme after immobilization. It was demonstrated that the developed immobilised method in continuous flow allowed for an almost five-fold higher biocatalytic activity value to the free form of Lipase PS (Nagy *et al.*, 2019). Another example of standard support used is hydrogel-based beads. A study by Liu and co-workers showed that enzyme leaching from porous acrylic resin beads was lower in microreactors compared with batch reactors (Liu *et al.*, 2019a).

In order to overcome some of the drawbacks of packed-bed reactors, such as high-pressure drops and possible leakage at higher flow rates, an approach is to pack the microchannels with monolith materials and have enzymes immobilised onto them. In this reactor configuration, the microchannels are filled by a monolithic material with interconnected porous structures that facilitate higher flow rates and lower pressure drops. The higher backpressure allows fast diffusion of substrates, and therefore high productivity can be achieved. For example, Szymańska *et al.* developed monolithic silica rods in a continuous flow reactor that could operate at flow rates up to about 20 $mL.min^{-1}$ at backpressures until 2.5 bar. After the covalent attachment of invertase, used as a model enzyme, the monolithic reactor allowed for the hydrolysis of sucrose at a maximum velocity over 1000 times faster than in a batch system (Szymańska *et al.*, 2013).

Although monolithic reactors allow for a relatively high protein loading, they may not be ideal for large-scale processing since the fabrication of monolithic materials is usually time-consuming and poorly reproducible. Another more reproducible approach is to directly attach the biocatalyst to the microchannels' inner wall or materials coating the inner wall. This approach overcomes backpressure limitations and provides a large interfacial area per unit volume. However, given that the available surface wall area is limited, the enzyme loading capacity is low. Therefore, researchers have developed methods to increase protein loading on the inner surface of microchannels. One feasible solution is to increase the immobilization layers on the walls, also referred to as the layer-by-layer (LBL) assembly approach. Bi *et al.* opted for a multi-layer deposition process to immobilize *Candida antarctica* lipase B (CAL-b) on the microreactor surface. Their approach consisted of a polydopamine layer as a primer followed by layer-by-layer coatings composed of polyethylenimine (PEI) and lipase. The multiple depositions of PEI and lipase were critical in increasing the enzyme loading on the microreactor. After 8 PEI/lipase layers, enzyme loading on the inner surface of the microchannel reached a maximum (350 μg to 400 μg), compared with approximately 20 μg in a single layer (Bi *et al.*, 2017).

Some representative examples of different immobilization approaches on packed-bed, monolithic and wall-coated reactors are given in Table 1.2.

Table 1.2: Examples of biocatalytic reactions with immobilised enzymes in continuous flow reactors

Biotransformation	Immobilization technique	Comments	Refs
Biocatalyst in packed-bed reactors			
Lipase from *Burkholderia* (Lipase PS) -catalyzed kinetic resolution of racemic 1-phenylethanol	Immobilization by absorption on porous hollow silica microspheres (M540) by bisepoxide activation	High specific activity and enantiomer selectivity was achieved in the developed immobilization method in continuous flow versus the free form of Lipase PS and commercially available covalently immobilised Lipase PS	(Nagy *et al*., 2019)
Candida antarctica Lipase B (CaLB) catalysed synthesis of 1-caffeoylglycerol	immobilization in acrylic resin beads (Novozym 435)	Compared to the batch reactor, the reaction time was reduced by 75%, the reuse times of lipase increased by 2.29-fold, the external mass and transfer coefficients increased 10 times	(Liu *et al*., 2019b)
ω-Transaminase from *Halomonas* (H. 35xample35) catalysed oxidation of 16 (aryl)alkyl amines with methyl/ethyl side chain with pyruvate	immobilization in epoxy-resin beads	The developed system allowed for an easy catalyst recovery and activity was unchanged when assessed over several cycles. The process was implemented with an integrated in- line purification step for the recovery of the pure amines.	(Planchestainer *et al*., 2017)

β-Glucosidase catalysed hydrolysis of 4-Nitrophenyl β-d-glucopyranoside	immobilization in tetraethyl orthosilicate-polyethylene oxide and alginate hydrogels	The immobilization in hydrogels proved to be an effective method to increase the thermal stability and long-term activity of the enzymes; the results suggest alginate hydrogels to be preferred to silica	(Kazan *et al*., 2017)
Biocatalyst immobilised on monoliths			
ω-Transaminase-catalysed kinetic resolution of the chiral amine, 4-bromo-α-methylbenzylamine	covalent immobilization using glutaraldehyde as a coupling agent in 36xample36lular silica monoliths	The porous structure of the monolith ensured effective mass transfer and transaminases retained their stability, activity and enantioselectivity on stream and during storage.	(Biggelaar, Soumillion and Debecker, 2017)
Invertase catalysed hydrolysis of sucrose	covalent immobilization using glutaraldehyde crosslinking	Over 1000 times faster hydrolysis and notably larger enzyme affinity to the substrate versus batch system.	(Szymańska *et al*., 2013)
Benzaldehyde lyase catalysed synthesis of ®-Benzoin and ®-2-hydroxy-1-phenylpropan-1-one from benzaldehyde and acetaldehyde	His6-tagged benzaldehyde lyase immobilised on Ni-NTA functionalized monolithic glass/polymer composite material	®-Benzoin was isolated in 99% yield; immobilization lead to enhanced activity and stability of the biocatalyst	(Dräger *et al*., 2007)

Biocatalyst immobilised on the inner surface of the microchannel			
β-Glucosidase catalysed hydrolysis of cellobiose into glucose	covalent immobilization by the APTES/GA method	The microreactor afforded enhanced pH and thermal stability, increased conversion rates of cellobiose, and reduced product inhibition in comparison with conventional batch systems. The maximum conversion rate of was 76% at 50 °C and pH=4.8 when the microreactor operated continuously for over 10 h at a flow 7 μL/min	(Wei *et al*., 2018)
Candida antarctica Lipase B (CaLB) catalysed transesterification of soybean oil to produce fatty acid methyl ester (FAME, biodiesel)	Layer-by-layer ionic binding Self-oxidation of dopamine was applied to modify the inner surface of the polytetrafluoroethylene (PTFE) microchannel followed by the deposition of alternating layers of polyethylenimine (PEI) and lipase	The multiple deposition of PEI and lipase was the key factor of increasing the enzyme loading on the coil reactor. Enzyme loading saturation was reached after 8 PEI/lipase layers. A 95.2% conversion rate of biodiesel was achieved in 53 min under optimised conditions, instead of a couple of hours in the traditional batch reaction	(Bi *et al*., 2017)
Transketolase-catalysed synthesis of l-erythrulose	His-tag/Ni-NTA binding	The 1-step-immobilisation described is based on the affinity of the His-tag/Ni-NTA interaction and does not require prior amination of the PMMA surface. The simplified immobilisation method required fewer chemicals and less time for preparation of the immobilised microfluidic device compared to the 3-step method while achieving higher specific enzyme activity.	(Kulsharova *et al.*, 2018a)

Trypsin catalysed hydrolysis of *N*α-benzoyl-L-arginine ethyl ester	DNA-directed immobilization (DDI) technique applied to a fused-silica capillary modified with polyamidoamine (PAMAM) dendrimers	The results demonstrated that this trypsin capillary enzyme microreactor had high reusability, good stability and satisfactory renewability properties. It combines the advantages of both PAMAM and DDI technology, enabling fabrication of an enzyme microreactor with high enzyme loading and also allowing renewable enzyme immobilization for regeneration of the microreactor. The method results in a microreactor with unique performance qualities because of its increased enzyme loading and reusability.	(Wu *et al.*, 2018)

Many more examples have documented the enhancements that continuous flow reactors can bring to biocatalytic reactions over conventional batch systems. The advantages of carrying out reactions in continuous flow include improved mixing, mass transfer, better control over reaction conditions, in-line product removal and purification, and integration with process analytical technology. All of these lead to improved reaction rates and enzyme stability and lifetime. Therefore, combining biocatalysis with continuous flow technologies presents an exciting opportunity to access new process windows and accelerate the discovery of novel reactions.

1.3 Biocatalytic Cascade Reactions

A cascade reaction is, by general definition, a combination of at least two transformations that occur consecutively in the same reaction apparatus. In a cascade, the starting compound is transformed into the compound necessary to initiate the subsequent reaction step, whose product again becomes the starting compound for the following reaction, and so on until the desired product is achieved. The advantage of cascade reactions compared to traditional multi-step reactions is the elimination of downstream intermediates recovery and purification steps, as the intermediate produced in one step is used in the following reaction. This results in an improved process efficiency due to the decreased use of reagents, catalysts and solvents (Nicolaou, Edmonds and Bulger, 2006; Kroutil and Rueping, 2014) (Figure 1.4).

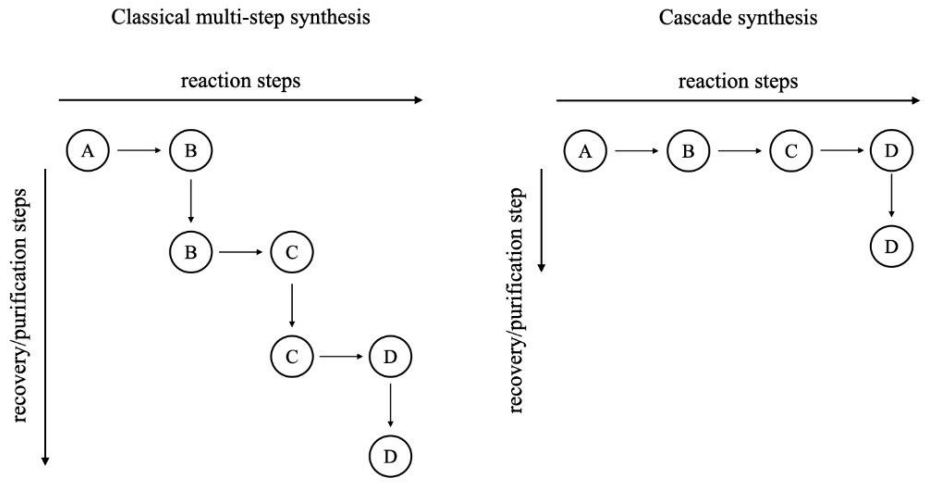

Figure 1.4: Classic multi-step synthesis versus a cascade synthesis.

In a biocatalytic cascade, at least one of the reactions is catalysed by an enzyme. If the cascade only involves biocatalysts, it is referred to as an enzymatic cascade, whereas if there are also chemical catalysts involved, the reactions are usually referred to as chemoenzymatic cascades. Compared with chemical catalysts, enzymes have specific characteristics that make their combination in multistep cascade reactions easier. Generally, enzymes share compatible reaction conditions, primarily if sourced from a common organism. In contrast, conventional chemical catalysts and reactions may require different and, in some cases, non-compatible solvents and conditions (pH and temperatures). Moreover, unlike most chemical catalysts, enzymes can carry out transformations in water which facilitates the matching of reaction media between each cascade step. Another unique advantage of enzymatic cascades is that the occurrence of side reactions is minimised by the high specificity of enzymes, especially towards their natural substrates. Furthermore, enzymatic cascades make it easier to work with unstable intermediates since these can be generated and immediately converted by adding a subsequent biocatalytic step. The addition of another enzymatic step can also be used to shift the equilibrium towards the desired product and complete substrate conversion (France *et al.*, 2017; Cutlan *et al.*, 2020; Paradisi *et al.*, 2022).

Biocatalytic cascades can be conducted with whole cells (*in vivo*) or purified enzymes (*in vitro*). *In vivo*, biocatalytic cascades can be more cost-effective since they offer the possibility of expressing multiple enzymes in a single cell, and co-factor-dependent enzymes can be used without supplementing co-factors (Wohlgemuth and Littlechild, 2022). However, the cell membrane can impose limitations on the diffusion between substrates and enzymes. In addition, in whole cells, the enzymes are exposed to several other reactions happening in the cell simultaneously, which may lead to substrate competition or biocatalyst inhibition resulting in low product yields. Another issue *in vivo* systems is the isolation of products from all the intermediates and enzymes in the cell. On the other hand, in *in vitro* enzymatic cascades, enzymes are extracted and purified from the cell. Therefore, challenges related to potential competing reactions or toxicity of other reaction intermediates in the cell are no longer an issue. However, the purification of enzymes adds extra costs to the overall process (Wilding *et al.*, 2018; Claassens *et al.*, 2019).

At an industrial scale, the high cost of biocatalysts may be a limiting step for the application of biocatalytic reactions. Biocatalysts' cost usually depends on their availability, selectivity, activity, stability, and lifetime. Protein engineering methods can improve enzyme activity and stability, and enzyme lifetime can be extended using membrane filtration systems (Sen *et al.*, 2012) or enzyme immobilisation strategies for enzyme recycling (Zhao *et al.*, 2018). Immobilisation strategies allow enzyme reusability while improving enzyme stability at the same time.

In an *in vitro* cascade reaction, the enzymes are no longer in a metabolic context within the cell. Therefore, in the case of co-factor-dependant enzymes, stoichiometric amounts of co-factors may need to be supplied to the system to sustain enzymatic activity, increasing the overall cost of the process and, in some cases leading to the inhibition of other enzymes in the cascade. The need for co-factor regeneration systems led to some of the first biocatalytic cascades using chemical, electrochemical and enzymatic strategies for *in situ* co-factor regeneration (Sperl and Sieber, 2018; Grunwald, 2019; Siedentop *et al*., 2021).

Nicotinamide adenine dinucleotide (NADH) and thiamine pyrophosphate (ThDP) are examples of co-factors often recycled in biocatalytic processes. NADH is involved in numerous redox reactions and is crucial in various enzymatic processes. Recycling methods include chemical, enzymatic, and electrochemical approaches. Chemical methods employ agents like formate or glucose to chemically regenerate NADH by reducing its oxidized form, NAD^+. Enzymatic methods involve alcohol dehydrogenases or glucose dehydrogenases that utilize substrates such as ethanol or glucose to reduce NAD^+ back to NADH enzymatically. Electrochemical methods employ electrodes to facilitate NADH regeneration, offering precise control without introducing additional chemicals (Schrittwieser *et al.*, 2018).

ThDP is a co-factor involved in decarboxylation reactions and is crucial for specific enzymatic functions. In most ThDP dependent enzymes, the holoenzyme facilitates the cleavage of carbon-carbon bonds in a donor substrate, forming a highly reactive intermediate. This intermediate subsequently undergoes condensation with an acceptor molecule, generating a new product, while ThDP is regenerated and made available for further catalysis (Nilsson *et al.*, 1997; Bunik, 2013). Recycling methods encompass chemical, enzymatic, and electrochemical strategies. Chemical methods

utilize reducing agents like sodium borohydride ($NaBH_4$) or triethylamine borane (TEAB) for ThDP regeneration. Enzymatic methods involve enzymes such as pyruvate decarboxylase or engineered enzymes naturally employing ThDP as a co-factor. Electrochemical approaches offer controlled ThDP reduction and integration into biocatalytic processes. Recycling co-factors in biocatalysis offers cost-effectiveness by reducing the need for expensive co-factors, minimizes environmental impact by reducing additional chemical usage and waste generation, ensures reaction efficiency by maintaining high co-factor concentrations, and aligns with sustainable chemistry principles (Bettendorff and Wins, 2013).

A well-known example of an enzymatic cascade with a enzymatic co-factor regeneration method is the two-step, three-enzyme cascade process for the synthesis of a key intermediate in the manufacture of atorvastatin, the active ingredient of Lipitor a cholesterol drug (Ma *et al.*, 2010). In the first step of the cascade, a ketoreductase (KRED) catalyses the reduction of ethyl-4-chloroacetoacetate in combination with a NADP-dependent glucose dehydrogenase (GDH) for co-factor regeneration. In the second step, a halohydrin dehalogenase (HHDH) was used to catalyse the conversion of the product of the first reaction step into the key hydroxynitrile intermediate. All the enzymes used were engineered to improve their catalytic activity, and in the case of HHDH a 2500-fold improvement in comparison with the wild-type enzyme was achieved. This enzymatic cascade was more economically and environmentally friendly than traditional chemical processes.

In the past decade, enzymatic cascades have evolved from simple enzyme combinations for co-factor regeneration to respected alternatives to conventional chemical synthesis, in particular for the complex synthesis of chiral intermediates and active pharmaceutical ingredients (APIs) (Abdelraheem *et al.*, 2019; Winkler, Schrittwieser and Kroutil, 2021). The advances in enzyme engineering have facilitated the development and availability of tailor-made biocatalysts with the required activity, selectivity, and stability. This increased availability made it possible to replicate not only metabolic pathways existing in an organism but also design novel chemical compounds and pathways through the combination of enzymes from different organisms (Ardao, Hwang and Zeng, 2013; Sehl *et al.*, 2013; Honda *et al.*, 2017).

An example of the successful use of enzymes of different organisms is the work done by Molla *et al.* where a one-pot cascade reaction was designed using fructose-bisphosphate aldolase from rabbit muscle (RAMA), sn-glycerol 3-phosphate dehydrogenase (sn-G3PDH) and formate dehydrogenase from *Candida boidinii* (FDH) for the synthesis of optically pure d-glyceraldehyde 3-phosphate (d-GAP) and l-glycerol 3-phosphate (sn-G3P) (Molla, Wohlgemuth and Liese, 2016). The combination of enzymes from different organisms can also be used to modify and optimise existing pathways. Ye *et al*., alter a classical bacterial Embden-Meyerhof (EM) pathway for lactate production by substituting the enzymes glyceraldehyde-3-phosphate dehydrogenase (GAPDH) and phosphoglycerate kinase (PGK) with the archaeal non-phosphorylating glyceraldehyde-3-phosphate dehydrogenase (GAPN) (Ye *et al.*, 2012). The new synthetic pathway produced a stoichiometric amount of lactate from glucose with an overall ATP turnover number of 31. The results showcase the ability to combine highly selective and stable biocatalysts into artificial synthetic pathways for chemical manufacturing.

Hartkey *et al*. used enzyme immobilisation strategies to combine four enzymes in a one-pot cascade with in-situs ATP regeneration to produce dihydroxyacetone phosphate from glycerol (Hartley *et al.*, 2017). Co-factor recycling was achieved through fusion protein strategies that tethered the co-factor to the enzymes increasing the overall cascade efficiency. Having substrates and co-factors bound to enzymes makes their interaction more stable and protects them from reacting with other biocatalysts in the cascade (Singh *et al.*, 2013; Siedentop *et al.*, 2021).

In order to successfully develop one-pot cascades such as the ones mentioned so far, it is necessary to select the right biocatalysts capable of being optimised to work together towards the cascade goals. Selecting suitable enzymes and adjusting their concentration ratios based on their activity, selectivity and stability for the cascade requirements is crucial for the viability of the process. Finding the optimal operation window for the cascade where the conditions are suited for all catalytic steps is particularly important in chemoenzymatic cascade. Combining chemical and biocatalysts in a cascade is often challenging due to the incompatibility of reaction conditions, such as kinetic parameters, pHs, temperatures, and solvents. Furthermore,

the presence of chemical catalysts in the reaction media can affect the stability and activity of the enzymes.

One of the first examples of one-pot chemoenzymatic cascades was the combination of lipases with metal catalysts to achieve enantiopure products (Koh *et al.*, 1999). Due to their enantioselectivity and robust tolerance towards organic solvents and high temperatures, lipases have been frequently applied in the synthesis of optically pure alcohol and amines (Kourist, Brundiek and Bornscheuer, 2010). However, most enzymes in nature do not have this high tolerance to organic media, limiting the combination of chemical and biocatalysts in one-pot systems. This limitation motivated the development of several metalorganic catalysts capable of sustaining catalytic activity in aqueous environments and of enzymes with robust activity in the presence of transition metals and high solvent, temperature, and extreme pH tolerance compatible with optimum reaction conditions for chemical catalysts. Recently, García-Álvarez and González-Sabín combined the ruthenium catalysed isomerisation of allylic alcohols with asymmetric bioamination promoted by ω-transaminase (ω-TA) in a one-pot reaction under an aqueous medium at a moderate temperature of 50 °C (Rí os-Lombardí *et al.*, 2015). This combination was possible through a step-by-step approach, where each reaction step was individually optimised, considering each catalyst's stability and activity requirements in the cascade. Since enzymes are known to be inhibited by heavy metals, the concentration of the chemical catalyst in the batch had to be minimised, which led to an overall reduction in productivity.

One way to overcome this cross-contamination is to perform the reactions in a stepwise manner. Turner and co-workers demonstrated this concept by coupling two enzymatic reactions with a Suzuki–Miyaura reaction for the synthesis of optically pure L- and D-amino acids (Ahmed *et al*., 2015). First, two different enzymatic reactions catalysed by a phenyl ammonia lyase (PAL) and a D-amino acid dehydrogenase (DAADH) were used to generate both enantiomers of 4-bromophenylalanine. The enantiomers were subsequentially coupled with a panel of arylboronic acids to synthesise a range of N-protected nonnatural L- and D-biarylalanine derivatives. The chemical step required solvents and temperatures incompatible with the low reaction temperature required by the enzymes; therefore, the chemoenzymatic synthesis had to

be performed in sequential mode, instead of adding all the compounds to the same vessel simultaneously.

Conducting a cascade reaction in sequence allows for individual optimisation of reaction conditions for each reaction step, making it possible to combine reactions with different pHs and temperatures. Moreover, by performing each step sequentially, it is possible to minimise cross-inhibition and unwanted formation of side products by ensuring that the starting material from the preceding step is completely converted before initiating the following step. This separation of reaction steps can be further enhanced by compartmentalising each reaction step into different vessels or by physically separating each catalyst inside the same vessel. Continuous flow systems facilitate this compartmentalisation of reagents and catalysts and can therefore be a strategy to enable the use of different reaction conditions for each step, which ultimately allows for the development of multistep reaction sequences that would be incompatible otherwise.

1.4 Enzymatic and chemoenzymatic cascade reactions in continuous flow reactors

The modular configuration of continuous flow systems enables a spatial separation of each reaction step and catalyst, allowing each reaction to be conducted under the best possible conditions and preventing contamination from incompatible reaction steps. Furthermore, flow systems also facilitate faster parameter screening when optimising cascade reactions, which reduces the overall time and cost of the process.

The challenge of enzymatic cascades lies in matching reaction conditions and overcoming enzyme inhibitions caused by products and reactants in the solution. Gruber and co-workers developed a continuous flow system with free enzymes to characterise a two-step transketolase-ω-transaminase cascade for the synthesis of chiral amino alcohols (Gruber *et al.*, 2018). The flow setup consisted of two microreactors connected in-line and used to compartmentalise each reaction step (Figure 1.5). The separation of reactions in different microreactors enabled the combination of incompatible reaction steps and allowed for individual optimisation of reaction conditions, which resulted in complete conversion in a short period.

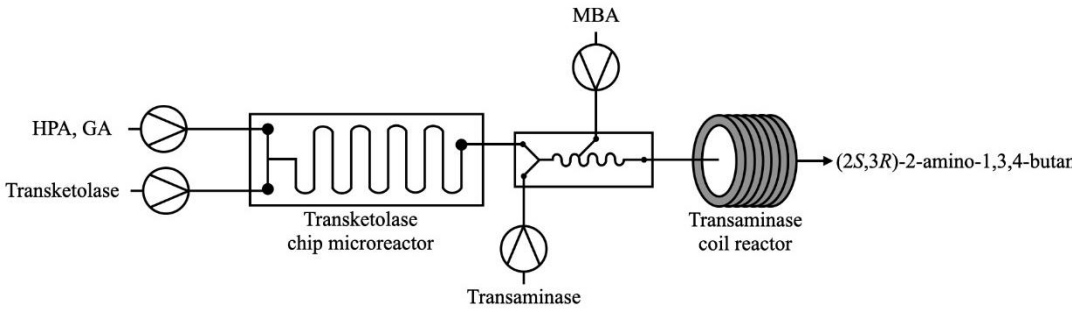

Figure 1.5: Scheme of the flow setup for the two-step transketolase-transaminase catalyzed synthesis of (2*S*,3*R*)-2-amino-1,3,4-butanetriol (ABT) developed by Gruber *et al.* (Gruber *et al.*, 2018).
Hydroxypyruvate (HPA) and glycolaldehyde (GA) were brought together in a chip microreactor with a transketolase (TK) solution. The product of the reaction, L-erythrulose, was fed into a micromixer where it was mixed with (S)-α-methylbenzyl-amine (MBA) and a transaminase (Tam) solution. Then Tam reaction took place in a coil reactor where (2*S*,3*R*)-2-amino-1,3,4-butanetriol was produced.

Recently, Flitsch and Cosgrove *et al*. designed a continuous flow system for the coupling of previously demonstrated incompatible enzyme reactions in batch (Mattey *et al*., 2021b). The combination of biocatalysts in flow was possible thanks to the compartmentalization of the enzymes in packed-bed reactors and reached as high as 98% yields, improving up to 58-fold space time yield in comparison the equivalent batch reactions.

Although incompatibility between reaction steps can be solved via reaction compartmentalisation in connected microreactors, the efficiency of a multi-enzyme cascade reaction is dependent on the functional and spatial orchestration of the biocatalysts in the cascade (Schmidt-Dannert and Lopez-Gallego, 2016). Wu *et al*. investigated the spatial positioning and mass transport regulating the kinetics of β-galactosidase (β-Gal)/glucose oxidase (GOx) cascade reaction. The enzymes were immobilised on two separated gold films patterned fitted in a microchannel with a controllable distance from 50 to 100 μm (Wu *et al*., 2016). The results showed that the reaction yield increases with decreasing distance between two enzymes and increasing substrate flow rate.

Another issue faced by enzymatic cascades is co-factors recycling. Several research groups have successfully developed ways to replenish and recycle co-factors in continuous flow systems in the last decade. Contente and Paradisi reported the biocatalytic synthesis of high-value primary aromatic alcohols from aromatic amines

using a continuous flow system with an in-line co-factor recycling step (Contente and Paradisi, 2018). The reaction was catalysed by ω-transaminase and alcohol dehydrogenase covalently immobilised onto epoxy resin used to pack two packed-bed reactors. The assembled continuous flow system enabled the integration of a closed-loop zero-waste system to recover by-products and recirculate the co-factor, increasing the system efficiency by over 20-fold compared with traditional batch methods. The products were recovered in excellent yields and in short times.

Hartley and co-workers developed a sophisticated protein engineering strategy to produce modular biocatalysts that retain and recycle their co-factors and allow orthogonal, site-specific covalent conjugation to a surface (Hartley *et al*., 2019). Each biocatalyst comprised a genetically encoded multi-enzyme fusion protein capable of retaining and recycling a tethered co-factor. The modular biocatalysts were immobilised on trifluoroketone (TFK)-activated agarose beads and packed into glass columns to produce three packed-bed reactors. The reactors were successfully connected in-line to and operated as a multi-step enzymatic continuous flow cascade to produce a pre-cursor of the antidiabetic drug D-fagomine.

In comparison with multi-enzymatic cascades, chemoenzymatic cascades are more complicated to engineer. This is due to incompatibility issues between biocatalysts and chemical catalysts, as they usually have different prefered reaction conditions, such as solvents, temperatures and pHs. Further issues are related to catalysts' mutual inhibition and poor matching of reaction kinetics. Compartmentalization of each type of catalyst in continuous flow systems may solve some of these incompatibility issues.

Luckarift and co-workers reported one of the first examples of a chemoenzymatic cascade in a continuous flow system for the synthesis of 2-aminophenoxyazin-3-one using three separate microreactors and achieving 18.9% yield (Luckarift *et al*., 2007a). Despite the low yield, the assembled flow system proved the advantages of compartmentalising catalysts to prevent enzyme inhibition. In another continuous flow system developed by Delville *et al*. a biocatalytic reaction in aqueous phase was combined with an organic phase chemical protection step through an in-line membrane-based phase separation module for the efficient synthesis of nine protected cyanohydrin derivatives (Mariëlle M.E. Delville *et al.*, 2015a) (Figure 1.6). More recently, Suveges *et al*. developed a seven-step continuous flow system combining

Novozyme 435 (Novo435) with several chemical catalysts with different optimal temperatures for the synthesis of a tenofovir pre-cursor (Suveges *et al*., 2018). Each catalyst was compartmentalized into a flow reactor allowing for individual reaction optimization and operation at different temperatures.

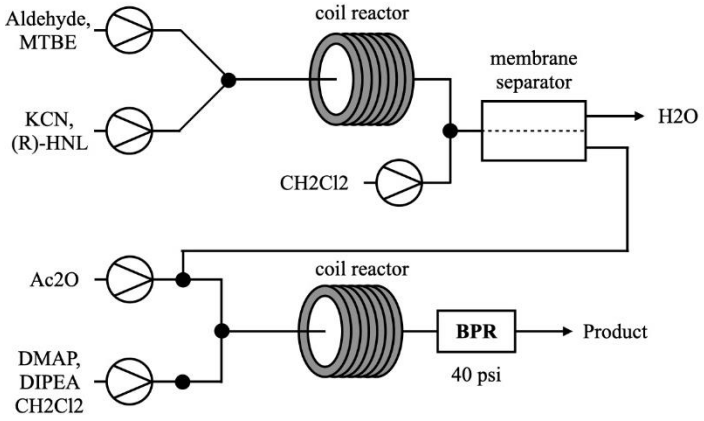

Figure 1.6: Schematic representation of the flow setup of the chemoenzymatic process developed by Delville *et al*. for synthesizing protected cyanohydrin derivatives using a membrane-based phase separation module (Mariëlle M. E. Delville *et al.*, 2015)**.**
A methyl tert-butyl ether (MTBE) solution of aldehyde substrates and a KCN and (R)-selective hydroxy nitrile lyase (HNL) crude cell lysate were mixed and then flowed through a coil reactor for the production of enantiopure cyanohydrins (98% ee). The coil reactor was connected to a polytetrafluoroethylene (PTFE) membrane-based phase separation module used to separate the organic phase and aqueous phase by feeding of dichloromethane. Protection of the hydroxyl function to produce protected cyanohydrins was achieved in the organic phase. Finally, the mandelonitriles in the remaining organic phase entered the last coil reactor for base-mediated acetylation, connected with a back pressure regulator (BPR) and affording enantiomerically pure cyanohydrin derivatives with yields up to 61%.

The compartmentalization approach is the easiest to implement and is, therefore, the most used. However, some research groups have reported successful continuous flow systems where the catalysts are all in the same vessel. For example, De Miranda *et al.* developed a chemoenzymatic continuous flow system for the dynamic kinetic resolution (DKR) of *rac*-1-phenylethanol using a single packed-bed reactor packed with *Candida antarctica* lipase B (CAL-B) and VOSO4 (De Miranda *et al*., 2017). The combination of catalysts was possible due to the use of toluene as the solvent media that proved compatible with CAL-B and VOSO4. The packed-bed reactor was filled with alternating layers of immobilised CAL-B and VOSO4, separated by a thin

cotton layer. The flow system enabled the synthesis of optically pure products with 90% *ee* and 82% yield in 2 hours.

Table 1.3 reports selected examples of biocatalytic cascades in continuous flow systems.

Table 1.3: Examples of multi-step enzymatic and chemoenzymatic cascade reactions in continuous flow reactors

Reaction	Continuous flow system	Comments	refs
Enzyme-enzyme			
Transketolase (TK)–Transaminase (TA) coupled reaction for synthesis of 2-amino-1,3,4-butanetriol (ABT)	Fluorinated ethylene propylene (FEP) tubular packed-bed reactor with a microfilter assembly at the end and packed with His-tagged TK and TA immobilised on Ni-NTA agarose beads	The coupled reaction reached approximately 83% conversion in 20 min and the turnover number kcat was reduced 3-fold compared to solution-phase TK and TAm reactions	(Abdul Halim, Szita and Baganz, 2013a)
	Microreactor-based reaction cascade with free enzymes: the fluidic path was created by connecting the transketolase PMMA microreactor, a micromixer and a transaminase PTFE coil	The continuous flow cascade reaction improved conversion yields significantly over free enzymes in one-pot systems and over immobilised enzymes in microfluidic systems. Full conversion was achieved, and issues, such as substrate and co-factor inhibition, were overcome	(Gruber *et al.*, 2018)

ω-Transaminase from *Halomonas elongata* (HEWT) coupled with horse liver alcohol dehydrogenase (HLADH) and coupled with ketoreductase from *Pichia glucozyma* (KRED1-Pglu) and a glucose dehydrogenase from *Bacillus megaterium* (BmGDH) for the preparation of primary and secondary aromatic alcohols from aromatic amines	Two packed-bed reactors in series packed with enzymes immobilised onto epoxy resin and with an in-line purification step (Quadrapure benzylamine (QP-BZA) column)	The continuous flow system was fully automated, with in-line recovery of benign by-products and recirculation of the aqueous media with the recycled co-factors in catalytic amounts, which increased the efficiency of the system by over 20-fold. The system enabled efficient and cost-effective synthesis of a large range of non-commercially available secondary alcohols with excellent yields (80 to >99%), in short reaction times	(Contente and Paradisi, 2018)
β-Galactosidase (β-Gal) and glucose oxidase (GOx) cascade reaction for the synthesis of H_2O_2 and gluconic acid from lactose	β-Gal and GOx were covalently bound to two separated gold films patterned in the channels of a polydimethylsiloxane (PDMS) chip microreactor	The reaction yield increased with decreased gap distance between enzymes at a fixed fluidic rate, i.e., about 5 times the reaction yield could be obtained if the gap distance decreased from 100 to 50 mm	(Wu *et al*., 2016)
Glycerol kinase (GK)/acetate kinase (AK) + glyceraldehyde-3-phosphate dehydrogenase(GAPDH)/NADH and oxidase (NOX) + fructose aldolase (FA) three step conversion of glycerol to a chiral D-fagomine	GK/AK and GPD/NOX were produced as modular biocatalysts that retain and recycle their co-factors as fusion proteins, to which co-factors were covalently tethered. The fusion proteins with conjugated co-factors were immobilised on chemically	The engineered biocatalysts were used to construct a three-step continuous-flow reactor system with superior yields of d-fagomine precursor compared to chemical syntheses, as well as high space-	(Hartley *et al*., 2019)

	trifluoroketone activated agarose beads and packed into three glass packed-bed reactor columns disposed in sequence	time yields and total turnover numbers (TTNs) for the catalysts and co-factors	
Lactate dehydrogenase (LDH) synthesis of lactate with *in situ* co-factor recycling with formate dehydrogenase (FDH)	Enzymes were immobilised via adsorption on carbon particles used to pack a glass packed bed reactor	100% conversion of pyruvate to lactate was achieved in a residence time of 30 min. The long-term stability of the biocatalytic reactor was also demonstrated, with full conversion maintained over more than 30 h of continuous operation	(Poznansky *et al*., 2020)
Combination of oxidases with aminating biocatalysts (transaminase/reductive aminase) with continuous *in situ* biocatalytic generation of amino donors for the reductive aminase	Several continuous flow systems were used including a multipoint injection microreactor (MPIR) and glass packed bed reactors; all biocatalysts used were immobilised	The yield of all examples could reach as high as 98% within 40 min; significant improvement were obtained up to 58-fold space-time-yield and 4-fold enzyme productivity, in contrast to the equivalent batch reactions	(Mattey *et al.*, 2021a)
Chemoenzymatic			
Synthesis of 2-aminophenoxazin-3-one from nitrobenzene	Three chip microrecators with zinc metal, silica-immobilised hydroxylaminobenzene mutase and silica-immobilised peroxidase in each microreactor	The overall conversion efficiency was reduced to 19% due to the reduction in the efficiency of the zinc conversion step at low flow rates suitable for the biocatalytic steps	(Luckarift *et al.*, 2007b)

(R)-Selective hydroxynitrile lyase ((R)-HNL) catalysed synthesis of the stereoisomers of various unstable cyanohydrins from aldehydes	Fluorinated ethylene propylene (FEP) tubular reactor with free (R)-HNL integrated with a commercially available FLLEX (Flow Liquid–Liquid Extraction) module utilizing a PTFE membrane	The ratio of enzyme:substrate solution in the reactor was 5:1, and the conversion was reported at 88 % in 12 min	(Mariëlle M.E. Delville *et al.*, 2015b)
Seven-step high-throughput synthesis of tenofovir ((*R*)-propylene carbonate)	NaAlO2, Pd/C, Novozyme 435 (Novo435) and NaHSO4.SiO2 were sequentially packed into the different packed-bed reactors with different volumes and under different temperatures, the system also included a tube-in-tube reactor and two coil reactors	The system resulted in 93% yield and increased selectivity (up to 98% *ee*) in comparison with the same reaction conditions in batch	(Suveges *et al.*, 2018)
Continuous flow dynamic kinetic resolution (DKR) of rac-1-phenylethanol catalyzed by immobilised *Candida antarctica* lipase B (CAL-B) and VOSO4	single glass packed-bed was packed with immobilised CAL-B and VOSO4·XH2O alternately resulting into 4 layers of enzyme and 3 layers of VOSO4·XH2O separated by thin cotton layers	An 82% yield of (R)-phenylethyl decanoate with 90% ee was obtained continuously from rac-1-phenylethanol in 2 h	(De Miranda *et al.*, 2017)
Continuous-flow dynamic kinetic resolution of racemic alcohols by lipase–oxovanadium co-catalysis	column reactor packed with a mixture of two solid cata-lysts, that is, CALB (commercial *Candida antarctica* lipase B im-mobilized on an acrylic resin) and VMPS4 (oxovanadium species immobilised on inner surface of mesoporous silica)	Optically pure esters were produced in 88–92 % yields	(Higashio *et al.*, 2020)

In this work, the promises and limitations of continuous flow systems to conduct biocatalytic cascades are explored in a multi-enzymatic cascade synthesis of a non-commercial glycolytic intermediate and a challenging chemoenzymatic cascade of broad relevance.

1.5 Thesis aims and structure

This thesis aims to demonstrate how the use of continuous flow systems at a micro-scale, combined with biocatalysis, can create powerful new process windows the synthesis of pharmaceutical intermediates. Cascade reactions offer several advantages over traditional multi-step reactions, including increased yield, improved selectivity, and reduced waste. These benefits can be further enhanced through microreactors that are designed to enable high-throughput chemical processing and process intensification. The high surface area to volume ratio of microreactors allows for faster reaction times and higher yields, and the precise control of reaction conditions is possible, leading to improved reaction selectivity and yield. In addition, the use of microreactors can reduce the amount of catalyst and other reagents needed for the reaction, as well as the amount of waste generated, leading to improved sustainability.

This thesis will investigate the ability of microreactors to enable biocatalytic process intensification through the application of continuous flow techniques to two biocatalytic cascades: a chemoenzymatic cascade and a multi-enzymatic cascade.

The biocatalytic cascade is introduced in Chapter 2 and deals with the integration of a Diels-Alder reaction with a transketolase reaction for the synthesis of 1-(3,4-dimethyl-3-cyclohexen-1-yl)-1,3-dihydroxypropan-2-one (DCDHP), a precursor of several antibiotics, such as thiamphenicol and chloramphenicol. The Diels–Alder cycloaddition reaction is among the most used chemical transformations to synthesise complex cyclic molecules efficiently. Combining the advantages of versatile reactivity of Diels-Alder reactions with the high selectivity of transketolase has numerous advantages over conventional organic chemistry, such as reducing the number of process steps, which makes the process more economical and environmentally sustainable. However, the combination of both catalysts is limited by incompatible reaction conditions, resulting in transketolase inhibition and low reaction yields. This chapter explores the ability of continuous microreactor systems to overcome these

incompatibility challenges by compartmentalising both reactions in different vessels, which saves time-consuming work-ups and allows for individual optimisation of reaction conditions.

The second biocatalytic cascade under study involves the coupling of three glycolytic enzymes to synthesise the only glycolytic metabolite non-commercially available, 1,3-biphosphoglycerate (1,3-BPG). Although some of the 1,3-biphosphoglycerate biological properties are known, such as the ability to control red cells' oxygen affinity, the full potential of this metabolite has not been completely assessed due to its complex synthesis and isolation. The strategies investigated to develop this enzymatic cascade with free enzymes in solution and overcome kinetic challenges are presented in Chapter 3. The chapter includes considerations on how to conduct the cascade in batch, and in a continuous flow system.

Possible process intensification strategies for the systems presented in Chapters 2 and 3 are presented in Chapter 4. In this chapter, the relationship between biocatalysis and continuous flow systems is further examined, focusing on the potential of continuous flow techniques to address common limitations of biocatalysis, such as co-factor regeneration issues, time-consuming downstream purifications, and difficult reaction scale-up. To this end, the advantages of flow systems were investigated in order to develop an in-situ substrate supply strategy and to implement product purification approaches through enzyme immobilization in a packed-bed reactor and integration with a micro-scale tangential flow filtration (TFF) downstream unit. Additionally, the feasibility of increasing the productivity of the processes by combining multiple microreactors in series and scaling out the reaction instead of scaling up was explored.

Each chapter includes an introduction section followed by a description of the materials and methods used, a results and discussion section, and ends with a summary of the findings. Finally, Chapter 5 concludes the studies and encourages further research.

As a whole, this thesis emphasizes the potential of biocatalysis for the synthesis of pharmaceutical intermediates and highlights the advantages of using continuous-flow systems over batch processes for chemoenzymatic and multi-enzymatic cascades. The overall objectives of the thesis were as follows:

- Identifying the optimal reaction conditions for a novel chemoenzymatic continuous flow cascade for the synthesis of a valuable pharmaceutical precursor.
- Developing a *de novo* enzymatic synthesis of a non-commercially available glycolytic metabolite.
- Exploring upstream and downstream process intensification strategies at a micro-scale for the continuous synthesis of pharmaceutical compounds.
- Comparing batch, fed-batch and continuous flow processes for biocatalysis.

2 Development of a Chemoenzymatic Cascade for the Synthesis of Chiral Intermediates in Continuous Flow

2.1 Introduction

Chemoenzymatic synthesis combines the chemo-, regio-, and stereoselectivity of biocatalysts with chemical catalysts' high productivity and versatility. Integrating both catalytic processes is therefore of interest for the synthesis of optically pure pharmaceutical intermediates. Although promising, combining chemical and biocatalysts requires the investigation of optimal compatibility windows. Most chemical reagents will have a toxic effect on the biocatalysts, and the presence of proteins may inhibit the chemical catalysts. Moreover, compatibility issues such as reaction rates, reagents concentrations, solvents, pH and reaction temperatures must be addressed to conduct a chemoenzymatic cascade successfully (Hailes, Dalby and Woodley, 2007; Xu *et al.*, 2021). The lack of compatible conditions leads to reactions being done in sequential batches instead of in one-pot with several intermediate downstream steps between batches to recover and purify products. These extra steps increase the processing time and cost and reduce the system's overall productivity.

Continuous flow systems may offer a solution to these incompatibility problems. The possibility of physically separating reaction steps into different compartments of a continuous flow reactor or in several reactors connected in flow minimises the need for purification steps, making flow systems ideal for developing chemoenzymatic reactions.

In this chapter, a chemoenzymatic cascade for the synthesis of a chiral pharmaceutical intermediate, 1-(3,4-dimethyl-3-cyclohexen-1-yl)-1,3-dihydroxypropan-2-one (DCDHP), will be investigated in a continuous flow system. The model chemoenzymatic reaction chosen is the combination of a Diels-Alder (DA) cycloaddition with a transketolase (TK) catalysed reaction. Figure 2.1 presents the chemoenzymatic reaction under study, where the product of both catalytic steps are valuable pharmaceutical precursors of 3,4-dimethylcyclohex-3-ene-2’-keto-1’,3’-propanediols.

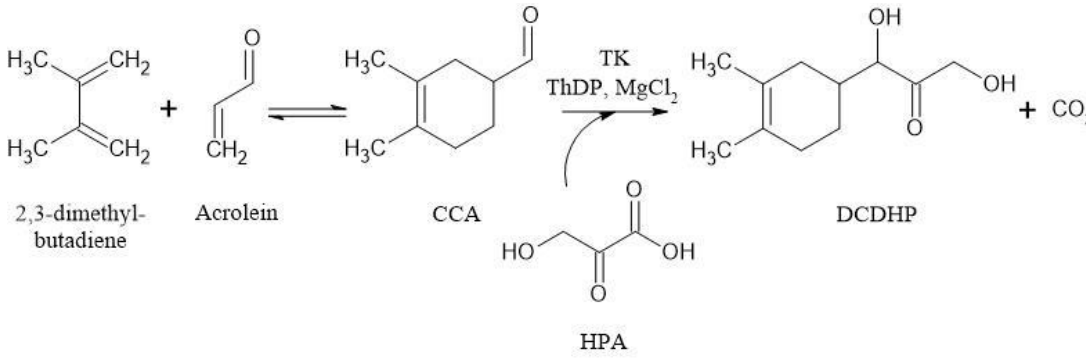

Figure 2.1: Diels-Alder – Transketolase chemoenzymatic cascade.
Transketolase (TK) catalyses the reaction between the product of the Diels-Alder reaction, 3,4-dimethyl-3-cyclohexene-1-carboxaldehyde (CCA) and hydroxypyruvate (HPA) for the synthesis of 1-(3,4-dimethyl-3-cyclohexen-1-yl)-1,3-dihydroxypropan-2-one (DCDHP). ThDP: thiamine diphosphate.

DCDHP is a chiral dihydroxyketone with synthetic potential for constructing keto sugars and keto sugar analogues, and it is also a non-aromatic analogue of the 1,3-dihydroxy-1-arylpropane-2-one motif, which is a precursor of the 2-amino-1-aryl-1,3-propanediol motif present in several antibiotics such as chloramphenicol and thiamphenicol (Smith *et al.*, 2006; Smithies *et al.*, 2009). Therefore, a chemoenzymatic synthesis of DCDHP is of interest.

Previous attempts at conducting this DA-TK reaction in one-pot without purification steps were not successful due to the incompatibility of reaction conditions. Initial experiments conducted by Lydia Coward as part of her doctoral thesis indicated that the DA solvent and catalyst led to the deactivation of the transketolase (Coward, 2014). To overcome this compatibility issue, a proof of concept for the DA-TK cascade in a continuous flow system was devised by Pia Gruber (Gruber, 2019). To avoid deactivation of the biocatalyst, each reaction step was conducted into two individual microreactors connected in-line. The chosen microreactors were a packed-bed reactor and a coil reactor. Aluminium chloride and acetonitrile were chosen as the catalyst and solvent combination for the DA reaction. The continuous flow setup led to the production of 3.5 mM of DCDHP in 200 min. The present work aims to increase the productivity of the DA-TK cascade in the continuous flow setup developed by Pia Gruber.

2.1.1 Diels-Alder reaction

The DA reaction was first discovered in 1928, by Otto Diels and Kurt Alder (Diels and Alder, 1959). Since then, it has become a powerful and versatile reaction for constructing cyclic and heterocyclic compounds. The DA reaction is a cycloaddition reaction between a conjugated diene and a dienophile to form a cyclohexene ring. The reaction can form six new stereocenters in a single step, with no by-product being formed. The DA reaction occurs between 1,3-butadiene, a conjugated diene, and ethane, a dienophile, to form cyclohexene (Figure 2.2).

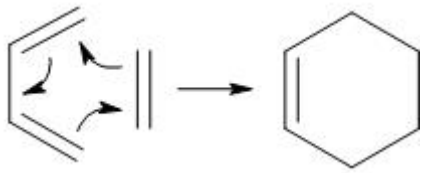

Figure 2.2: Diels-Alder cycloaddition reaction mechanism.

In this work, the diene used is 2,3-dimethyl-1,3-butadiene, and the dienophile is acrolein, forming the cyclohexene 3,4-dimethyl-3-cyclohexene-1-carboxaldehyde (CCA). Although there are several examples of successful catalytic DA reactions for the synthesis of CCA, most of the catalysts and solvent combinations used are not compatible with a subsequent enzymatic reaction (Abbott *et al.*, 2002; Cavill, Peters and Tomkinson, 2003; Chen, Young and Yu, 2004; Nakashima and Yamamoto, 2005; Taarning and Madsen, 2008; Stevens and Pagenkopf, 2010). Thus, an optimisation of the DA reaction is necessary to enable its integration with a transketolase catalysed reaction.

2.1.2 TK-catalysed reaction

Transketolase (E.C.2.2.1.1) is an essential and versatile enzyme in both the non-oxidative branch in the pentose phosphate pathway in animals and the Calvin Cycle of photosynthesis (Heinrich *et al.*, 1972). Its function in these pathways involves catalysing reversible reactions that facilitate the transfer of a two-carbon unit between specific molecules. In the pentose phosphate pathway, TK catalyses the reversible transfer of a two-carbon moiety from D-xylulose-5-phosphate to D-ribose-5-phosphate, generating, respectively, glyceraldehyde-3-phosphate and sedoheptulose-7-phosphate. Later in the same pathway, TK again transfers a two-carbon unit from D-xylulose-5-phosphate to erythrose-4-phosphate, affording, respectively,

glyceraldehyde-3-phosphate and fructose-6-phosphate (Figure 2.3). In the Calvin Cycle, transketolase catalyses the reverse reactions of those described in the pentose phosphate pathway.

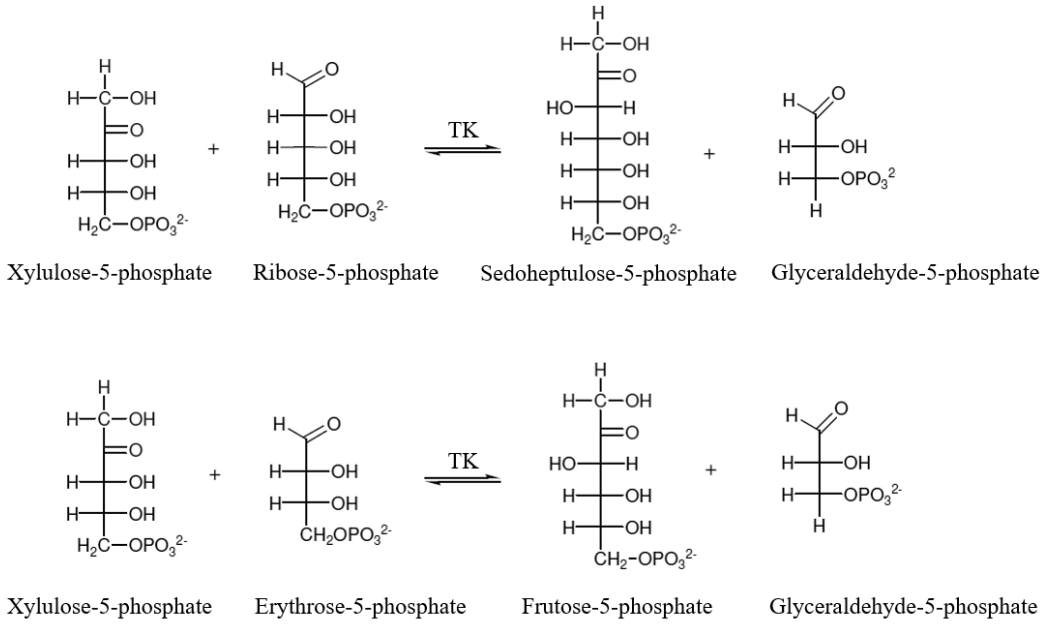

Figure 2.3: Natural substrates of TK.
From left to right, the TK-catalysed reactions in the pentose-phosphate pathway are represented.

TK is a transferase composed of of two identical subunits, each with a molecular mass of 74.2 kDa. TK is dependent on the cofactor thiamine pyrophosphate (ThDP) shown in Figure 2.4 and a bivalent metal ion (Ca^{2+}, Mg^{2+}, Co^{2+}, Mn^{2+}, Ni^{2+}) for enzymatic activity. Each monomer of TK contains three domains: N-terminus or PP- domain (residues 3-322); the middle section or Pyr-domain (residues 323-538), and the C-domain (539-680) (Figure 2.5). Although reports indicate that the first two domains are involved in the enzyme's catalytic profile and co-factor binding, the precise function of the C-domain remains unclear.

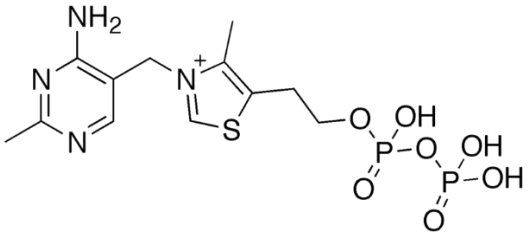

Figure 2.4: Thiamine pyrophosphate.

To form the holo-enzyme, ThDP and a bivalent metal ion bind within each of the two identical active-sites formed at the dimer interface. The transition between apo-TK and holo-TK is a complex mechanism. First, ThDP binds to the holo-TK. In this state, the C2 atom within the thiazolium ring of ThDP undergoes deprotonation, creating a carbanion. This carbanion serves as a nucleophile, initiating a nucleophilic attack on the carbonyl group of the ketol donor substrate. This attack removes a two-carbon moiety from the donor substrate and cleavage of the adjacent C-C bond, forming the first product. The two-carbon fragment remains attached to the enzyme-substrate complex, generating a new carbanion.

Subsequently, the newly formed C2 carbanion carries out another nucleophilic attack, targeting the aldehyde carbon of the aldehyde acceptor substrate. This nucleophilic interaction leads to the formation of the second product, which is then released from the enzyme. This entire process regenerates the enzyme's active form, allowing it to participate in further catalytic reactions.

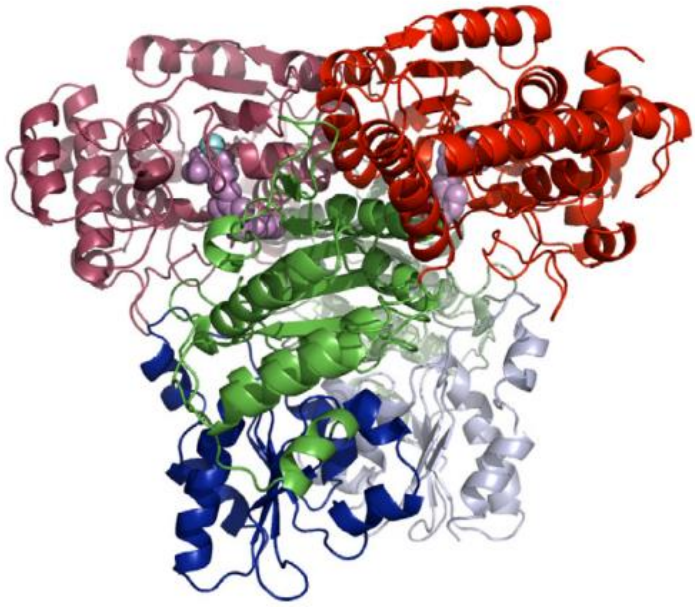

Figure 2.5: Structure of *E. coli* holo-TK.
The PP-domain is represented in dark and light red; the Pyr-domain are highlighted in a dark and light green and the C-terminal domain in blue. The two magnesium ions are represented as cyan spheres, and the ThDP co-factor as violet spheres. This image was obtained from Jahromi *et al.*, 2011.

The reaction mechanism of TK makes it an attractive enzyme for industrial biocatalysis. The ThDP co-factor is regenerated at each reaction cycle, reducing the costs usually associated with co-factors or co-factor recycling mechanisms. Additionally, using hydroxypyruvate (HPA) as the ketol donor makes the reaction irreversible due to the release of CO_2 as a side product, thereby increasing the atom efficiency of the reaction. Additionally, TK catalyses the stereoselective transfer of a two-carbon ketol group to an aldose sugar to form a new asymmetric carbon–carbon bond in a single step which is of great interest in synthetic chemistry.

In this chapter the TK used in the chemoenzymatic reaction, is a one-point mutant of the wild type TK in which the aspartic acid (D) in position 469 was replaced with a threonine (T) (D469T). This mutation allows TK to accept cyclic substrates like CCA. The mutant was selected based on Daniel Pais's (Pais, 2013) and Lydia Coward's (Coward, 2014) research work where the wild type, the D469T mutant and a three-point mutant were screened for this reaction.

2.2 Materials and Methods

Unless otherwise stated, all chemicals and reagents used were of analytical grade, purchased from Sigma-Aldrich (Gillingham, UK), and used without further purification. All continuous flow reactions were conducted using glass syringes (Hamilton Bonaduz, Switzerland) and a Nemesys syringe pump (290N Nemesys, Cetoni GmbH, De).

2.2.1 Synthesis of CCA enantiomers

To prepare S-3,4-dimethyl-3-cyclohexene-1-carboxaldehyde (S-CCA), 0.257 g of the chiral catalyst (0.87 mmol), (5R)-5-(1H-indol-3-ylmethyl)-2,2,3,-trimethyl-4-imidazolidinone monohydrochloride, were dissolved in a mixture of water (0.05 mL) and methanol (0.8 mL) and cooled in an ice bath. Then, 1.16 mL of acrolein (0.017 mol) were added dropwise to avoid extreme reaction heating to the catalyst solution and stirred for 2 minutes. Finally, 3.25 mL of 2,3-Dimethyl-1,3-butadiene (0.029 mol) were added, and the reaction was left stirred at room temperature for 3 days.

For the synthesis of the R enantiomer (R-CCA) the same procedure was followed. 813 µL of 2,3-dimethyl-1,3-butadiene (7.3 mmol) and of 290 µL acrolein (4.2 mmol) were stirred in water (12.5 µL) and methanol (200 µL) with 0.065 g of (5S)-5-(1H-indol-3-ylmethyl)-2,2,3,-trimethyl-4-imidazolidinone monohydrochloride for 3 days.

After 3 days, 50 mL (total volume) trifluoroacetic acid:water:chloroform 1:1:2 were added to each reaction for 10 minutes under stirring. Diethyl-ether (30 mL) was added creating two immiscible phases (Figure 2.6), and the aqueous phase was extracted at least three times, dried over magnesium sulphate and filtered. The solvent was evaporated on a rotary evaporator (Buchi R-114 Rotary Vap System) and the residue containing the enantiomers was dry loaded onto a silica column and eluted with ethyl acetate:hexane (3:1). The eluted fractions were analysed by GC-FID and the fractions presenting CCA were combined and dried again on the rotary evaporator.

a) b) c)

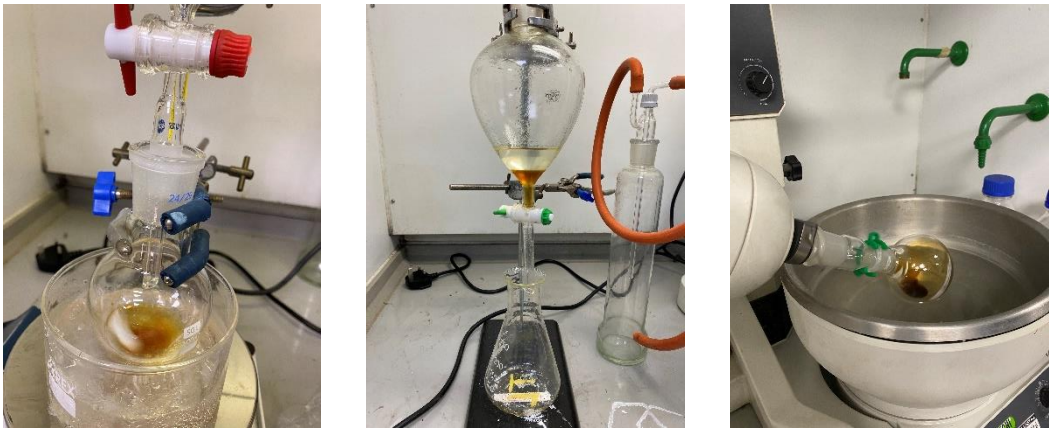

Figure 2.6: Synthesis of R- and S- 3,4-dimethyl-3-cyclohexene-1-carboxaldehyde a) Reaction mixture containing the substrates and the organocatalyst in a solution of water and methanol being stirred in an iced bath; b) Extraction of the CCA enantiomer with diethyl-ether; c) Evaporation of the extraction solvent on a rotary evaporator.

2.2.2 DA aluminium chloride packed-bed reactor

The DA reaction was conducted in a packed-bed reactor previously constructed by Pia Gruber (Gruber, 2019) whereby a blank HPLC column with an internal diameter of 0.46 cm and length of 15 cm (Sigma Aldrich, Gillingham, UK) was cut down to a length of 3.5 cm. This led to a reactor volume of approximately 600 µL (Figure 2.7). Aluminium chloride immobilised on silica gel (particle size 40-63 µm) was used to pack the column, under nitrogen atmosphere. After packed with the catalyst the volume of the packed bed reactor was determined to be 490 µL, by measuring the residence time of an acetonitrile solution pumped through the reactor at a flow rate of 10 $\mu L.min^{-1}$. Acetonitrile was pumped through the packed-bed reactor for 10 column volumes to wash all the unbound catalyst before running the Diels-Alder reaction. Efficiency of the assembled packed-bed reactor was verified by pumping through an equimolar solution of 100 mM of acrolein and 2,3-dimethylbutadiene in acetonitrile at different flow rates between 4 and 80 $\mu L.min^{-1}$. Samples collected from the outlet of the reactor were treated and analysed by GC-FID for CCA production.

Figure 2.7: Diels-Alder packed-bed reaction with aluminium chloride immobilised on silica gel.

2.2.3 Biocatalyst production

2.2.3.1 Strain and plasmid

The D469T transketolase (TK) mutant was produced in house by fermentation of glycerol stocks of *Escherichia coli* BL21gold previously transformed with the expression vector pQR791 by Prof. John Ward's group, from the Department of Biochemistry and Molecular Biology, UCL. Further information about cloned mutant into the expression vector pQR791 can be found in Payongsri *et al.* (Payongsri *et al.*, 2012).

2.2.3.2 LB-agar plates

LB-agar plates were prepared by mixing 10 $g.L^{-1}$ LB media with 15 $g.L^{-1}$ agar in water. The solution was autoclaved and once cooled 0.15 $g.L^{-1}$ of an ampicillin solution was added. After gentle mixing, 20 mL of the media was poured into standard-sized petri dishes. The LB-agar plates were then streaked with *E.coli* cells (BL21 pQR791) from glycerol stocks previously prepared in 50% (v/v) glycerol and incubated for approximately 16 hours at 37°C.

2.2.3.3 Shake flasks fermentation

Single colonies, from the LB-agar plates, were used to inoculate 50 mL Falcon tubes containing 20 mL of 10 $g.L^{-1}$ LB media supplemented with 10 $g.L^{-1}$ glycerol and 0.15 $g.L^{-1}$ ampicillin. The inoculums were left overnight in a shaker incubator at 37°C and 250 rpm.

The overnight culture was used to inoculate 2 L shake flasks with 500 mL of the same media and shaken for approximately 9 hours at 37 °C and 250 rpm. The fermentation

was monitored by OD600nm in using a Unicam UV2 UV/vis spectrometer (Cambridge, UK) until growth reached stationary phase.

2.2.3.4 Glycerol stocks

Glycerol stocks were prepared by adding 50% (v/v) filter-sterilized glycerol to the overnight culture in a 1:1 ratio and stored at -80°C. A cell bank was kept at -80°C and used for plate streaking when needed.

2.2.3.5 Cell harvest

Cells were harvested by centrifugation at 4,000 rpm for 20 minutes at 4 °C (Beckman Coulter, Avanti J6-MI, Indianapolis, USA). The cell pellet was re-suspended in 50 mM Tris-HCl buffer pH 7 (4 mL of buffer per gram of pellet) and lysed through sonication (Soniprep 150, MSE Sanyo, Japan). Cell pellets were kept on an ice jacket for 10 cycles of 10 s sonication followed by 10 s pause. Clarification of the lysate was achieved by centrifugation at 7,000 rpm for 6 minutes at 4°C and stored at −20°C.

2.2.4 Biocatalysis quantification

2.2.4.1 Quantification of protein concentration

A Bradford assay was used to quantify total protein concentration. A protein assay kit was used (Bio-Rad Labs Inc., UK) and protein concentration was calibrated with bovine serum albumin (BSA, Sigma-Aldrich, Gillingham, UK) standard. Absorbance was measured at 595 nm using a UV/Vis spectrophotometer. The Beer-Lambert law was used to determine protein concentrations from absorbance measurements, considering an extinction coefficient of 93,905 M. cm^{-1} for transketolase.

After determination of total protein concentration, 25 µg of lysate was diluted in Laemelli Buffer (containing 4% SDS, 20% glycerol, 10% 2-mercaptoethanol, 0.004% bromophenol blue and 0.125 M Tris HCl, pH approx. 6.8.) and denatured at 85 ^{o}C for 10 minutes, using a Thermal Cycler (Techne, Techgene). After denaturation, 20 µL of the lysate mixture was loaded into the gel (NuPAGE 4-12% Bis-Tris Protein Gels, 1.0 mm, 12-well-10 gels, Thermo Fisher Scientific). In order to identify the molecular weight of the proteins, a protein ladder (Precision Plus Protein Dual Color Standards, Bio-Rad Laboratories) was also added to the gel. The electrophoresis was carried in a Bio-Rad Power Pac 300 system in a Tris-Tricine buffer, with a constant voltage of

180V for 90 minutes. The gel was then rinsed with RO water and stained with SimplyBlue SafeStain for 1 h at room temperature. After 1 h, the gel was left in RO water overnight. Gels were then visualized and analysed on a gel imaging system.

2.2.4.2 D469T Transketolase activity assay

Co-factor stock solution of thiamine pyrophosphate (ThDP) magnesium chloride ($MgCl_2$) were made 10 times more concentrated, 24mM and 96mM, respectively, in a 25 mM Tris-HCL adjusted to pH 7 with NaOH whilst stirring.

Substrate stocks solutions were prepared fresh before each reaction as a mixture of 50 mM lithium hydroxypyruvate (HPA) and 3-formylbenzoic acid (3-FBA) in 25 mM Tris–HCl pH 7.

The D469T mutant was pre-incubated with co-factor solution (ThDP 2.4 mM, and $MgCl_2$ 9.6 mM) for half an hour in a 1.5 mL Eppendorf. Substrates HPA and 3-FBA (50 mM each) solution was added to the mixture to initiate the reaction. Samples were taken every minute for 3 minutes, quenched with 0.1% Trifluoroacetic acid (TFA) and analysed by HPLC for HPA and 3-FBA depletion. One transketolase unit (U) was defined as the amount of transketolase which catalysed the conversion of 1 μmol of substrate per minute at pH 7 and room temperature.

2.2.4.3 Transketolase selectivity assay

A 5 mM solution of each CCA enantiomer previously produced were stirred for six hours with 5 mM hydroxypyruvate (HPA) and a 1.14 $U.mL^{-1}$ transketolase solution previously incubated with co-factors (ThDP 2.4 mM, and MgCl2 9.6 mM) for 30 min in 50 mM Tris-HCl buffer pH 7. The enzyme was removed by centrifugation and silica was added and the reaction mixture concentrated to dryness was dry loaded onto a flash silica gel column to isolate DCDHP for posterior analysis via mass spectrometry. The presence of DCDHP in the reaction mixture was also verified by TLC.

2.2.5 Effect of acetonitrile on TK activity

Transketolase was incubated for half an hour with a co-factors solution (2.4 mM ThDP and 9.6 mM MgCl2) in 25mM Tris-HCl at pH 7, for a final enzyme concentration of 1.14 $U.mL^{-1}$. TK batch reaction was initiated with the addition of HPA and racemic CCA, for a final concentration of 5mM and 10mM, respectively. The CCA added was

either commercially bought or produced by the Diels-Alder reaction conducted in the packed bed reactor. The use of CCA from the Diels-Alder reaction added to the batch reaction mixture 10% of acetonitrile. Samples from both reaction systems were taken every 15 minutes, quenched via a 1:10 dilution with 0.1% trifluoroacetic acid, analysed by HPLC for HPA depletion and by colorimetric assay for DCDHP formation. Production of DCDHP was also confirmed by TLC analysis.

2.2.6 DA-TK cascade assembly in continuous flow

The DA-TK continuous flow setup followed the designed proposed by Pia Gruber (Gruber, 2019), in which the DA packed-bed reactor was connected to a coil reactor (PTFE, ID 0.75 mm, VWR International Ltd, Lutterworth, UK) for the TK reaction using a four-way connector (Figure 2.8). An equimolar mixture of 100 mM of 2,3-dimethyl 1,3-butadiene and acrolein in acetonitrile was pumped through the packed bed reactor at a flow rate of 4 $\mu L.min^{-1}$. The resulting flow was then diluted with 50 mM HPA in 25 mM Tris-HCl buffer pH 7 at 4 $\mu L.min^{-1}$ and a transketolase solution of 1.43 $U.mL^{-1}$, previously incubated for 30 minutes with co-factors, at a flow rate of 32 $\mu L.min^{-1}$. Total flow rate entering the coil reactor was 40 $\mu L.min^{-1}$. Several coil reactors were used to accommodate residence times from 15 min to 75 min to obtain a flow reaction profile.

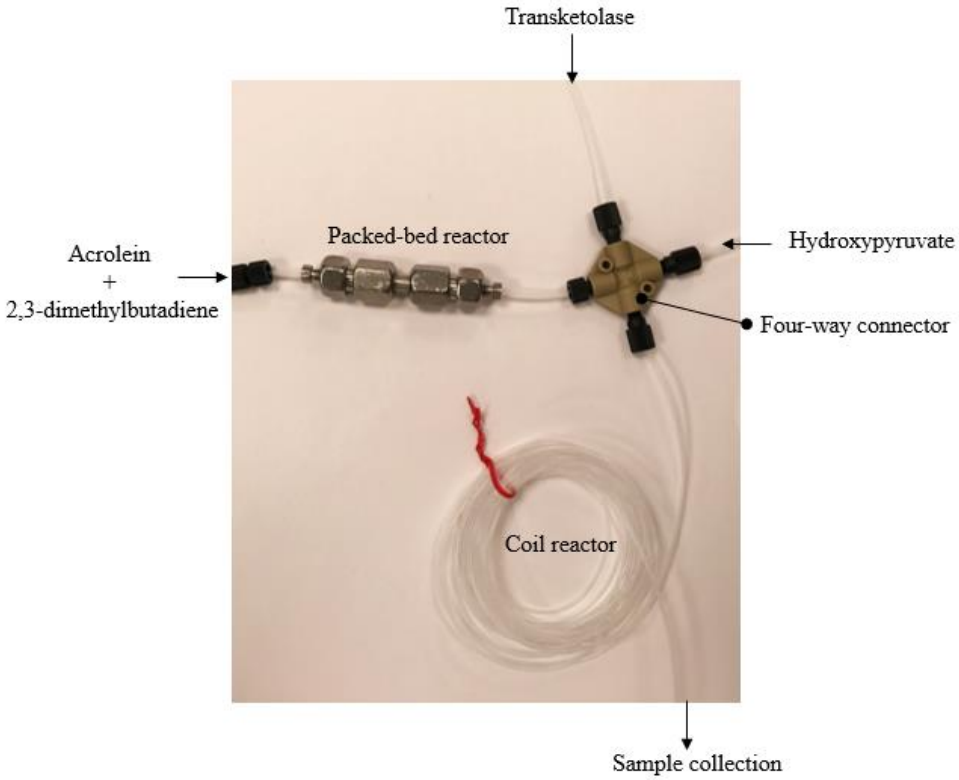

Figure 2.8: Diels-Alder-transketolase continuous flow setup.

Samples from the coil reactor were taken and quenched via a 1:10 dilution with 0.1% trifluoroacetic acid, analysed by HPLC for HPA depletion and by colorimetric assay for DCDHP formation. The production of DCDHP was confirmed through TLC analysis of the product stream, which showed a clear spot at the same R_f value as the DCDHP standard.

2.2.7 Detection and quantification methods

2.2.7.1 Sample preparation

Samples containing enzyme lysate were always quenched via a 1:10 dilution with 0.1% trifluoroacetic acid and centrifuged for 3 minutes at 1,4000 rpm before analysis via HPLC.

2.2.7.2 HPLC assay for 3-FBA and HPA

Chromatographic separation of hydroxypyruvate (HPA) was achieved on an Aminex HPX-87H column (300 mm x 7.8 mm; Bio Rad, UK) at 60 ºC with a 0.6 $mL.min^{-1}$

isocratic elution of 0.1% (v/v) TFA for 15 minutes. HPA was detected via a UV detector at 210 nm.

3-formylbenzoic acid (3-FBA) was quantified with an ACE 5 C18 RP column (150 mm x 4.6 mm, 5 μm particle size, Advance Chromatography Technologies, UK) with a 1.0 mL.min-1 mobile phase comprised of 0.1% (v/v) TFA and a gradient of acetonitrile from 15% to 72% over 9 min, followed by a 2 min equilibration. Detection was via a UV detector at 254 nm. Concentrations were determined using calibrations curves of HPA and 3-FBA standards in 25 mM Tris-HCL pH 7.

2.2.7.3 GC-FID analysis

3,4-dimethyl-3-cyclo-hexene-1-carboxaldehyde (CCA) was quantified using a ThermoScientific Trace 1300 flame ionization detector gas chromatograph (GC-FID) with a Rxi® 5 Sil MS column (30 metres, 0.25 mm ID, 0.5 μm df, Sigma Aldrich, Gillingham, UK). Analysis was conducted in split-flow mode with a temperature gradient from 40 °C to 140 °C for 25 min, followed by an increase from 140 °C to 180 °C in 3 min. CCA was detected at a retention time of 18.5 min.

2.2.7.4 Flash chromatography

Flash silica chromatography was carried out using silica gel (BDH silica 40-63 μm) to load the column. The column was equilibrated with mobile phase of ethyl acetate and n-hexane (1:1) before loading the reaction mixtures absorbed onto silica and previously dried on a rotary evaporator. After dry loading the column, elution of compounds was achieved with ethyl acetate and n-hexane (1:1) and the presence of CCA and DCDHP in the eluted fractions verified by thin layer chromatography (TLC). Fractions containing products of interest were combined and dried on a rotary evaporator for further use and analysis.

2.2.7.5 Thin layer chromatography

A TLC assay was used as an initial detection method to validate the production of DCDHP by transketolase. Aluminium silica gel TLC plates, coated with fluorescent indicator F254, were used as stationary phase. Samples were spotted on the TLC plates using 5 μL glass capillaries. Mobile phase solvents system consisted of a 1:1 ratio of ethyl acetate and n-hexane. TLC plates were developed using a 10% phosphomolybdic

acid stain in ethanol and placed over a hot plate to evaporate the solution. During heating, all CCA and DCDHP spots gradually became visible. The retention factor (Rf) for CCA was around 0.90 and 0.50 for DCDHP, under these conditions. The retention factor of a compound is equal to the distance travelled by the compound divided by the distance travelled by the solvent front measured from the origin.

$$R_f = \frac{\text{distance traveled by solute}}{\text{distance traveled by solvent}} \qquad 2.1$$

2.2.7.6 Colorimetric assay

Detection of DCDHP in the transketolase catalysed reactions was achieved through a colorimetric assay adapted from Smith *et al* (Mark E.B. Smith *et al.*, 2006). 50 µL of reaction sample were mixed with 20 µL tetrazolium red solution (0.2% 2,3,5-tripheyltetrazolium chloride in methanol) and 10 µL 3 M NaOH (aq). Followed by immediate measurement by FLUOstar Optima plate reader (BMG Labtechnologies GmbH) at OD485nm. Standard solutions of DCDHP, enzymatically synthesized at Sigma Aldrich (Steinheim, Germany), were used to generate a calibration curve (appendix Figure 6.4)

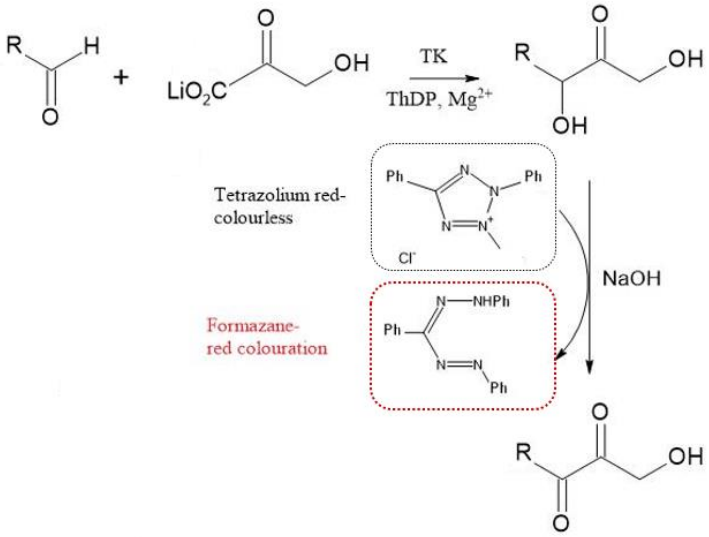

Figure 2.9: Colorimetric assay mechanism.
The colorimetric assay utilises the reduction of colourless tetrazolium red in the presence of non-α-hydroxyaldehydes forming red coloured compound formazane.

2.2.7.7 Accurate mass spectrometry

Mass measurements were performed in UCL Chemistry Mass Spectrometry Facility using a Waters 2720 autosampler connected to the LCT Premier XE Q-TOF mass spectrometer. Briefly, 5 µL of the sample was injected through the autosampler into the QTOF using a six-valve loop. The analysis time was 2 min. The mass spectrometer operated in positive and negative ionisation ESI with full MS scan with mass range from 100 to 2,000 m/z. The LCT Premier XE mass spectrometer was operated in W-mode with the source capillary at 2,500 V, sample cone at 30 V, desolvation temperature set at 400°C, source temperature of 80°C, cone gas flow 50, and desolvation gas flow of 450 $L.h^{-1}$. The Q-TOF was calibrated with sulfadimethyhoxidne [M]+ (m/z 311.0814) and leucine encephalin [M]+ (m/z 556.2771).

2.3 Results and Discussion

2.3.1 TK quantification

To catalyse the conversion of CCA to DCDHP, a TK mutant, in which a threonine replaced the aspartic acid in position 469 (D469T), was chosen. This mutation was previously explored in Daniel Pais's (Pais, 2013) and Lydia Coward's (Coward, 2014) research work and enables transketolase acceptance of cyclic substrates like CCA.

The D469T TK mutant was produced in-house by fermentation of transformed *E.coli* cells containing the TK gene. A Bradford assay determined total protein concentration in the obtained clarified lysate, and an SDS-PAGE gel was conducted to verify the presence of transketolase amongst the proteins. Figure 2.10 shows a typical SDS-PAGE gel with a protein ladder verifying the TK bands' presence below 75 kDa, which corresponds to the molecular weight of the transketolase monomers around 73 kDa (Sprenger *et al.*, 1995).

Differences in the over-expression levels of the TK mutant can be observed in Figure 2.10 among the cell lysates obtained from various fermentation processes. Additionally, the figure highlights the presence of several other proteins in the lysate, expressed at levels similar to that of the TK mutant. This co-expression of proteins suggests the presence of a complex protein mixture within the lysate, which could impact the reaction efficiency and subsequent purification and analysis processes. To address the complexity introduced by co-expressed proteins and to enhance the purity of the TK mutant, a viable approach would be to purify the expressed TK mutant by passing the cell lysate through a Ni-NTA column. Notably, the TK mutant used in this study contained a His-tag, which facilitates its purification through affinity chromatography.

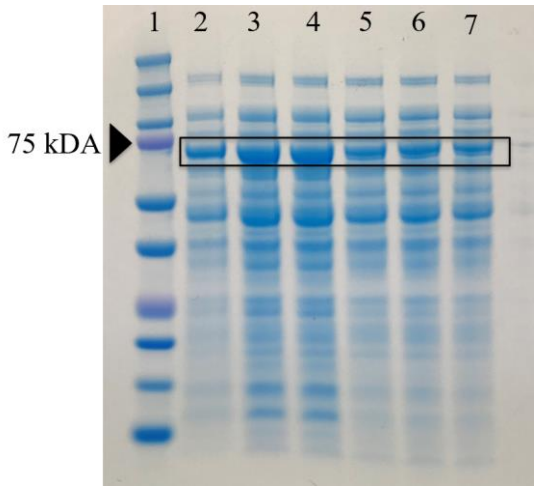

Figure 2.10: SDS-PAGE gel with TK lysates.
SDS-PAGE gel with a protein ladder (lane 1) verifying the TK bands' presence below 75 kDa, which corresponds to the molecular weight of the transketolase monomers around 73 kDa (Sprenger *et al.*, 1995).

To ensure that the concentration of transketolase in the various experiments was kept the same, TK activity in each clarified lysate was determined. Figure 2.11 shows the model reaction used to measure the activity of the D469T TK mutants.

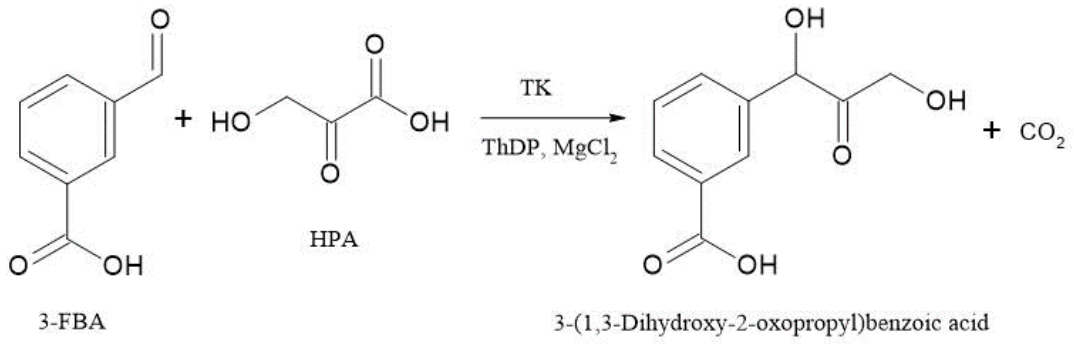

Figure 2.11: Reaction scheme for the transketolase-catalysed reaction between 3-FBA and HPA to produce 3-(1,3-Dihydroxy-2-oxopropyl)benzoic acid and CO_2.

Activities assays were conducted in batch at room temperature with HPA and 3-FBA as described in section 2.2.4.3. Enzymatic activity (U) was defined as the amount of transketolase which catalysed the conversion of 1 µmol of hydroxylamine per minute. The TK lysates were pre-incubated with a co-factor solution (ThDP 2.4 mM, and $MgCl_2$ 9.6 mM) for half an hour prior to adding an equimolar solution of 50 mM of HPA and 3-FBA. The reaction was followed for 3 min, and TK activity was determined from the slope of a fitted line. Figure 2.12 presents the activity assay data

obtained from 4 different D469T TK lysates obtained from 4 different *E.coli* fermentations.

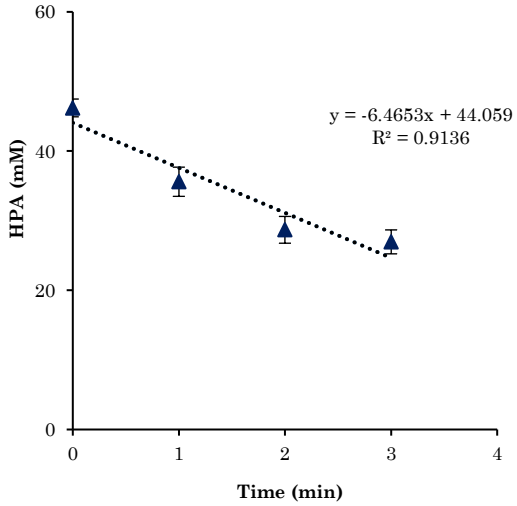

Figure 2.12: D469T TK mutant activity assay.
Results are shown for 4 different D469T TK lysates obtained from 4 different *E.coli* fermentations (n=4). Error bars represent mean ±SD.
.

2.3.2 Determination of TK substrate selectivity

The synthesis of 3,4-dimethylcyclohex-3-ene-2'-keto-1',3'-propanediols, which contain two chiral centers, can be envisioned to be constructed from the corresponding (R)- or (S)-enantiomer of 3,4-dimethyl-3-cyclo-hexene-1-carboxaldehyde by a transketolase-catalysed two-carbon chain elongation using HPA as C2-donor (Figure 2.13).

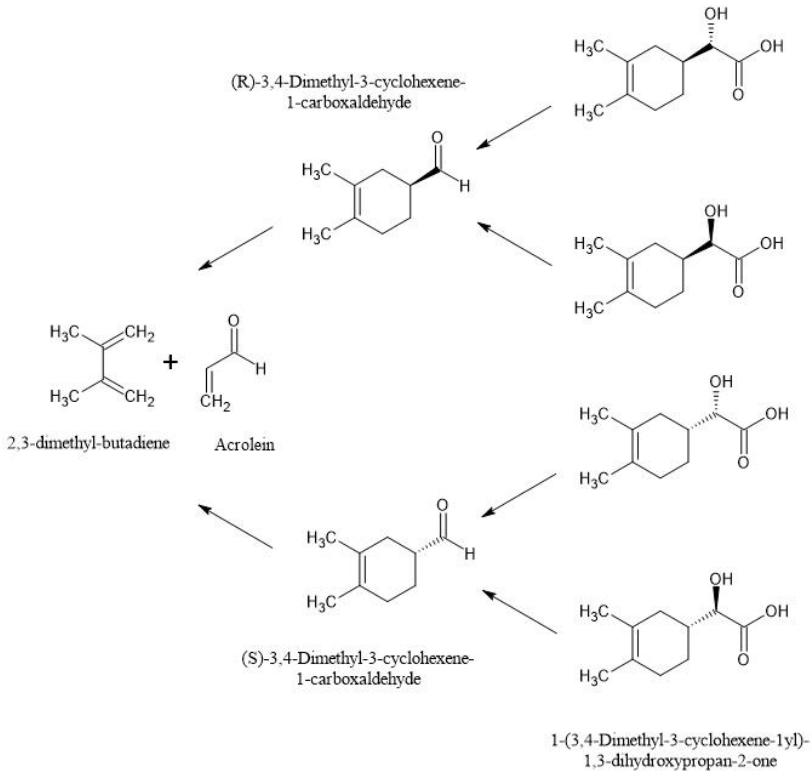

Figure 2.13: Retrosynthetic analysis of 1-(3,4-dimethyl-3-cyclohexen-1-yl)-1,3-dihydroxypropan-2-one

The enantioselectivity of D469T TK was determined via preparation of the (R)- and (S)-enantiomer of CCA in an asymmetric Diels-Alder reaction catalysed by enantiocomplemetary organocatalysts, (5R)- and (5S)-5-((1H-indol-3-yl)methyl)-2,2,3-trimethylimidazolidin-4-one hydrochloride produced at Sigma Aldrich (Figure 2.14).

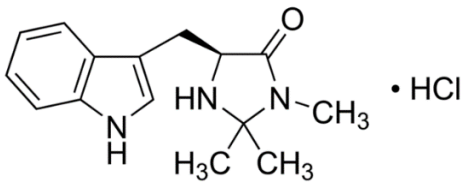

Figure 2.14: Structure of the organocatalysts used to selectively produce CCA enantiomers.

Both reactions were conducted for 3 days and the CCA enantiomers were purified via silica column chromatography. The eluted fractions were analysed by GC-FID and the fractions presenting CCA were combined, dried on a rotary evaporator, and analysed by GC-FID again for CCA quantification. The asymmetric DA reactions resulted in 80 mM of (S)-CCA and 10 mM of (R)-CCA. The selectively produced CCA

enantiomers were then used in TK-catalysed reactions with HPA. After six hours, the reactions were centrifuged to remove the enzyme, and the reaction product was purified in a silica chromatography column and analysed via mass spectrometry.

The analysed samples from the batch performed with the R-enantiomer showed a clear mass peak at 199 m/z, corresponding to 1-(3,4-dimethyl-3-cyclohexen-1-yl)-1,3-dihydroxypropan-2-one (DCDHP) (Figure 2.15).

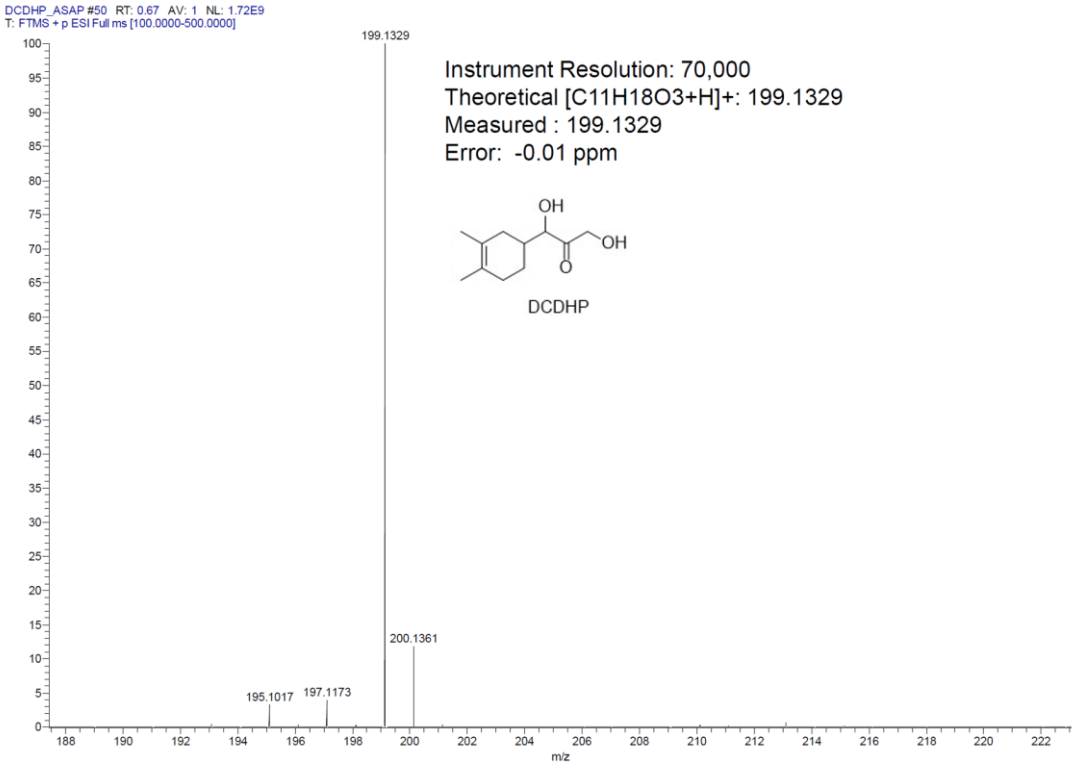

Figure 2.15: MS analysis of TK reaction with (R)-CCA and HPA.
Accurate mass performed on a LCT Premier XE mass spectrometer; the theoretical mass of DCDHP and the measured mass were the same 199.1329 m/z.

Confirmation of DCDHP production in the batch reaction with R-enantiomer was further confirmed by TLC analysis as shown below in Figure 2.16.

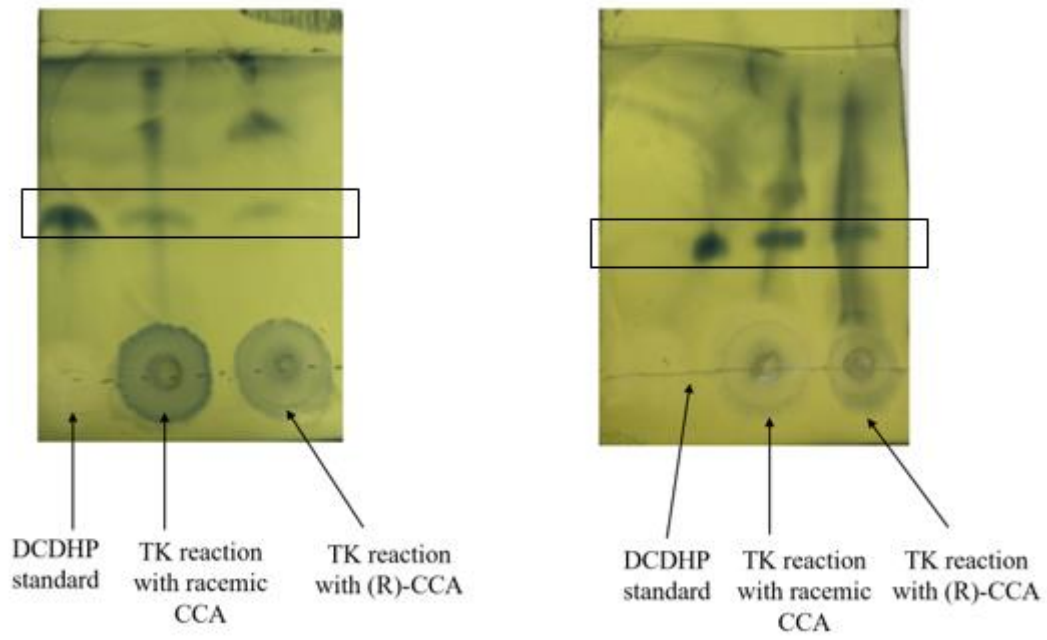

Figure 2.16: TLC plates confirming TK selectivity towards (R)-CCA.
Both TLC plates show the DCDHP standard in the first lane, a sample from a TK batch reaction with racemic CCA in the second lane and in the third lane a sample from the TK batch reaction with (R)-CCA. There is a clear DCDHP spot in the third lane of both TLC plates, indicating TK selectivity towards the (R)-enantiomer.

In both analytical methods, no DCDHP was detected in the batch conducted with the S-enantiomer. Since substrate conversion and presence of the reaction product were only verified in the batch containing the (R)-enantiomer it was possible to conclude that D469T TK is specific towards the R-enantiomer of CCA.

While these organic catalysts were essential for the individual enantiomers' production, with reaction time of 3 days the catalysed reactions were too slow for a viable flow system. Nevertheless, this approach allowed for the determination of transketolase enantioselectivity.

2.3.3 DA flow reaction

The optimisation of the DA-TK cascade started before the beginning of this thesis. Previous work included the early stages of the optimisation of the Diels-Alder reaction by Pia Gruber (Gruber, 2019). In the work undertaken by Pia Gruber, four catalysts,

zinc chloride, scandium triflate, aluminium chloride and (5S)-5-(1H-indol-3-ylmethyl)-2,2,3,-trimethyl-4-imidazolidinone monohydrochloride, were screened for the DA synthesis of CCA in combination with four different solvents, acetonitrile, methanol, ethanol and isopropanol. The chosen solvents were previously tested for compatibility with a TK catalysed reaction with no enzyme deactivation up to a 10% (v/v) concentration in the reaction media. The reactions were conducted in batches for 2 hours with a substrate solution of 200 mM acrolein and 2,3-dimethylbutadiene. The combination of acetonitrile and aluminium chloride (AlCl3), led to the highest conversion achieved, corresponding to a 37.5% conversion. Furthermore, aluminium chloride is not soluble in acetonitrile, making this an ideal solvent and catalyst combination to attempt an immobilization approach. For these reasons, aluminium chloride and acetonitrile were used for all further DA experiments undertaken as part of this thesis.

To immobilize the chemical catalyst a continuous flow packed-bed reactor previously created by Pia Gruber from a blank HPLC column was used. After being filled with aluminium chloride, the volume of the packed bed reactor was determined to be 490 µL, by measuring the residence time of an acetonitrile solution pumped through the reactor at a flow rate of 10 $\mu L.min^{-1}$.

Each DA flow reaction was conducted with fresh catalyst and every time after packed, the column was flushed with acetonitrile for 3 h at a flow rate of 50 $\mu L.min^{-1}$. This allowed flushing of the catalyst that was not completely immobilised inside the column. Figure 2.17 shows the catalyst, in red colour, leave the column during this period. After 3 h the stream ran clear, although some additional colour-less catalyst may still be present.

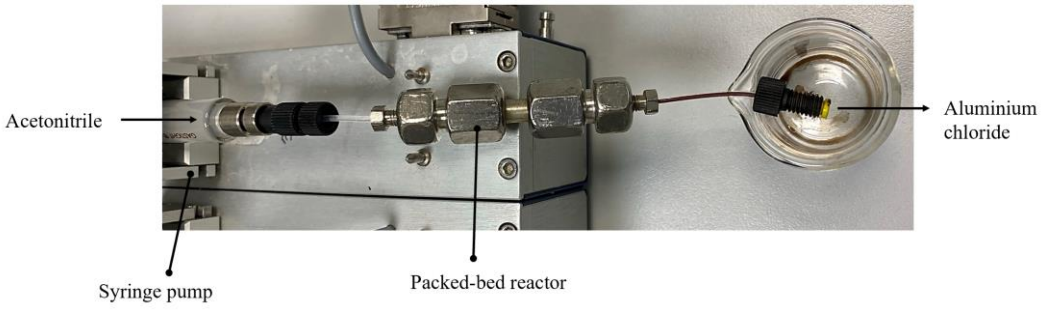

Figure 2.17: Aluminium chloride being flushed out of the packed-bed reactor with acetonitrile.

In order to determine the residence time necessary to achieve complete substrate conversion, a solution of 100mM butadiene and 100mM acrolein in acetonitrile was pumped through the column at several flow rates (from 4-80 µL.min^{-1}). Complete substrate conversion into 100mM of racemic CCA was achieved at a flow rate of 4 µL.min^{-1}, which corresponds to a residence time of 2 h in the packed-bed reactor (Figure 2.18). CCA production was confirmed via GC analysis.

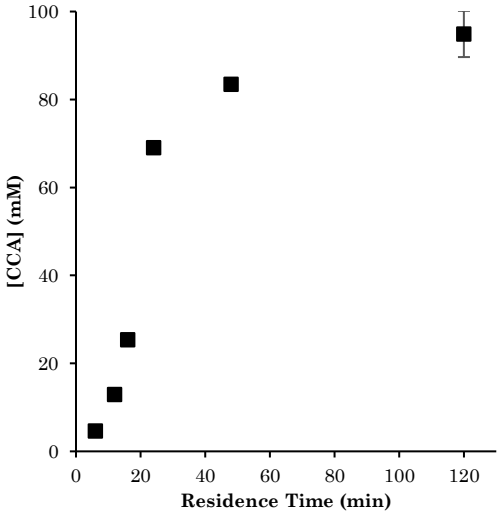

Figure 2.18: Diels-Alder reaction in the packed-bed reactor at different flow rates.
Full substrate conversion occurs at a residence time of 2 h, at a flow rate of 4 µL.min^{-1}, resulting in 94.9 ± 4.29 mM of racemic CCA. Error bars represent mean ±SD (n=6).

2.3.4 Influence of the organic solvent on TK activity

Having optimised the DA reaction, the next step was to confirm the compatibility of the DA product with the D469T TK mutant (Figure 2.19).

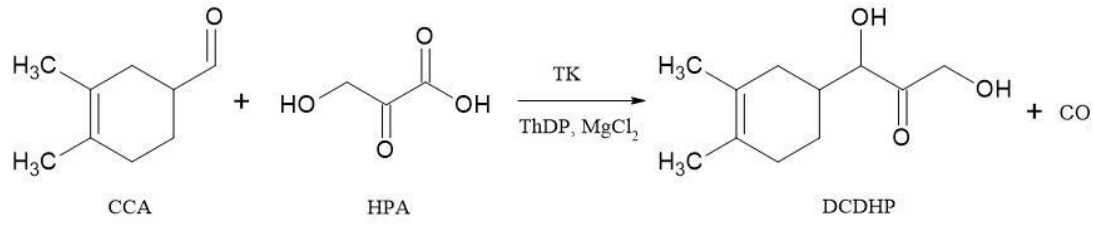

Figure 2.19:Transketolase catalyse reaction under study.
Transketolase catalysed reaction using hydroxypyruvate (HPA) and 3,4-dimethyl-3-cyclo-hexene-1-carboxaldehyde (CCA) to form 1-(3,4-dimethyl-3-cyclohexen-1-yl)-1,3-dihydroxypropan-2-one (DCDHP), in the presence of Thiamine pyrophosphate (ThDP) and Magnesium ions ($MgCl_2$).

The ability of the TK mutant to convert CCA was evaluated in batch reactions with commercial CCA and with 100 µL of the outlet stream of the DA packed-bed reactor containing 100 mM of CCA. Both batch reactions contained 10 mM racemic CCA, 5 mM HPA and 1.14 U.mL-1 TK in 25 mM tris buffer at pH 7, and the batch with the product from the DA flow reaction contained 10% (v/v) of acetonitrile. Samples were taken in regular intervals and analysed for HPA depletion by HPLC. Figure 2.20 shows obtained time-course reaction profiles for TK batches conducted with commercial CCA and with CCA synthesised in the DA packed-bed reactor. Both reactions appear to reach complete HPA conversion in 20 minutes, which corresponds to a production of 5 mM of DCDHP. The results also suggest that the activity of TK is not affected by the presence of 10% (v/v) of acetonitrile.

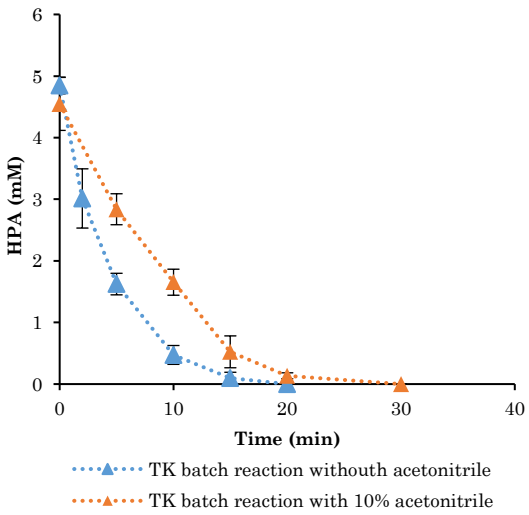

Figure 2.20: Comparison between TK batch reaction with commercial CCA and synthetised CCA.
Full conversion of HPA happens in 20 min in the TK batch reactions with and without 10 % (v/v) acetonitrile, confirming that the TK activity is not affected by the presence of the organic solvent up to a 10 % (v/v); no statistical difference was found between the two sets of data; Error bars represent mean ±SD (n=3).

The synthesis of DCDHP was further confirmed by TLC (Figure 2.22) and quantified by a colorimetric assay using tetrazolium red salt. Tetrazolium red oxidizes the hydroxyl groups of DCDHP to a ketone that is reduced to a formazan dye of pink colour. By measuring the formazan absorbance at 485 nm it was possible to determine the amount of DCDHP present in the samples. However, since HPA also reacts with tetrazolium salt, the samples were first analysed by HPLC for HPA quantification. Figure 2.21 presents the concentration profiles of HPA and DCDHP on samples from

TK batch reaction with the product from DA flow reaction. Product formation was found to quantitatively correlate with HPLC data obtained for HPA depletion.

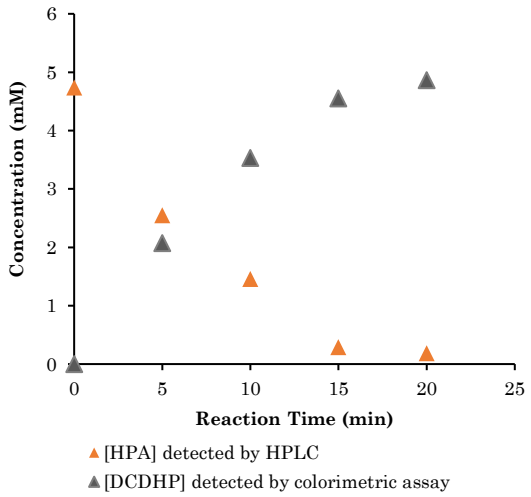

Figure 2.21: Profile of HPA depletion and DCDHP formation in a TK batch reaction.
HPA depletion profile was monitored by HPLC and DCDHP formation by colorimetric assay (n=1).

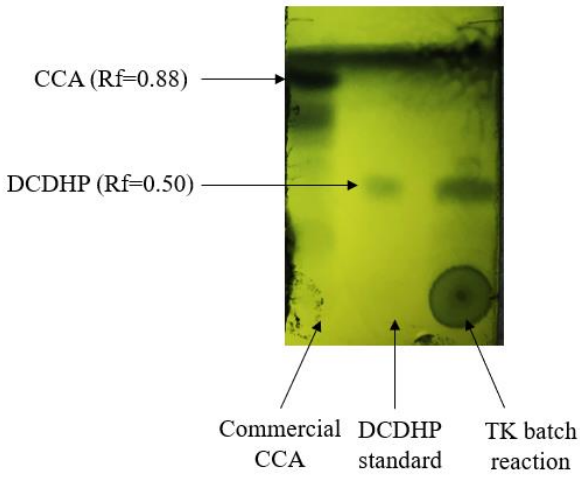

Figure 2.22: TLC plate analysis of a TK batch reaction with synthetised CCA and HPA.
The TLC plate shows commercial CCA in the first lane with a Rf=0.88; the second lane shows a sample of DCDHP with a Rf=0.50 and the third lane show a clear DCDHP spot confirming the presence of DCDHP in the TK batch reaction conducted with CCA produced in the DA packed-bed reactor and 10% (v/v) of acetonitrile.

2.3.5 Chemoenzymatic continuous flow reaction

In order to combine the DA reaction with the TK-catalysed reaction in a continuous flow system, the packed-bed reactor was connected to a coil reactor (PTFE, ID 0.75 mm) using a four-way connector. Figure 2.23 presents a scheme of the assembled continuous-flow setup. The DA-TK flow cascade was initiated by pumping through the DA packed-bed reactor a 100 mM mixture of 2,3-dimethyl-1,3-butadiene and acrolein in acetonitrile at a flow rate of 4 $\mu L.min^{-1}$. The exiting flow stream containing 100 mM of racemic CCA was then diluted ten times in a four-way connector before entering the coil reactor. By diluting the flow ten times the percentage of acetonitrile in the TK reaction medium is kept at 10%(v/v). A TK solution previously incubated with co-factors for 30 min was brought together with the substrates in the four-way connector. At the point of confluence, the exit stream of the packed-bed reactor was mixed with a 50 mM HPA solution pumped at 4 $\mu L.min^{-1}$ and a transketolase solution introduced through another inlet at a flow rate of 32 $\mu L.min^{-1}$. Since the TK mutant used was previously shown to be selective toward the R- enantiomer of CCA, only half of the concentration of HPA related to CCA was added to the reaction system. The TK reaction in the coil reactor starts with 5 mM HPA, 10 mM racemic CCA and 1.14 $U.min^{-1}$ transketolase lysate in Tris-HCl buffer pH 7 with 10% (v/v) acetonitrile. The length of the coil reactor varied to accommodate different residence times.

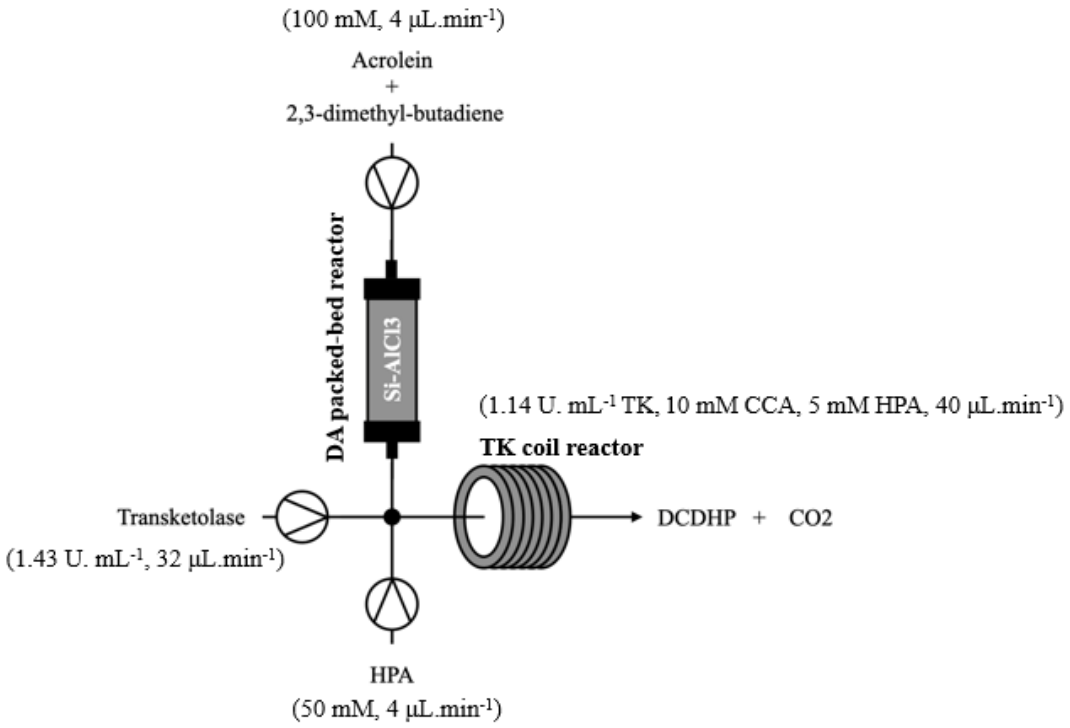

Figure 2.23: Schematic of the continuous-flow setup for the chemoenzymatic cascade reaction.

Samples were taken after each residence time and analysed by HPLC for HPA depletion. The production of DCDHP in the cascade was confirmed by TLC analysis. Figure 2.24 shows the product stream's TLC analysis, showing a clear spot at the same Rf value as the DCDHP standard. A colorimetric assay further determined the DCDHP concentration in the samples at 485 nm. Figure 2.25 presents the concentrations of DCDHP accordingly with different residence times inside the coil reactor. At a residence time of 75 min, a

concentration of 5 mM DCDHP was detected, which matched the initial concentration of HPA in the reaction, indicating that complete substrate conversion had been achieved.

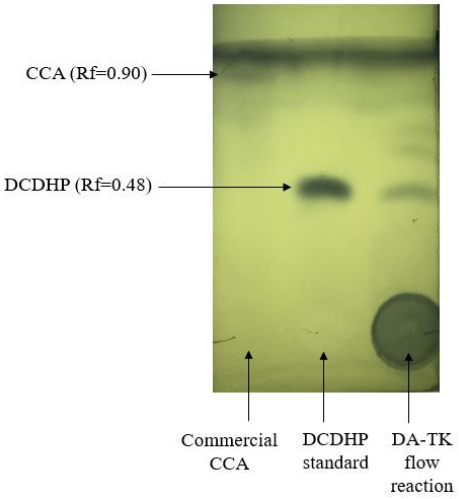

Figure 2.24: TLC plate analysis of a DA-TK flow reaction.
The TLC plate shows commercial CCA in the first lane with a Rf=0.90; the second lane shows a sample of DCDHP with a Rf=0.48 and the third lane show a clear DCDHP spot confirming the presence of DCDHP in the DA-TK continuous flow reaction.

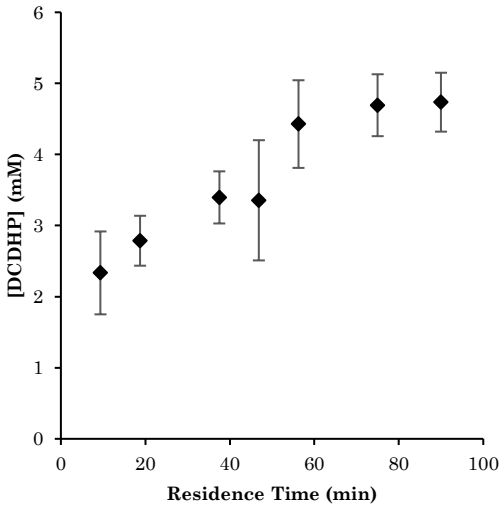

Figure 2.25: Chemoenzymatic flow reaction – production of DCDHP.
Endpoint DCDHP concentrations on the exit flow streams of TK coil reactors with different volumes connected in-line with the DA packed-bed reactor; full HPA conversion occurs at a residence time of 75 min which corresponds to a coil volume of 3 mL; Error bars represent mean ±SD (n=3).

2.3.6 Transketolase batch vs continuous flow reaction

To compare the transketolase catalysed reaction in batch and in continuous-flow the residence times were normalised according to Marques *et al*. (Marques *et al.*, 2012), as explained on section 1.2 by the equations 1.2 and 1.3.

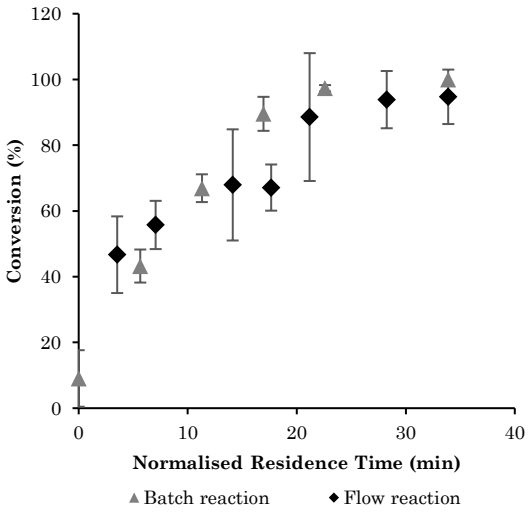

Figure 2.26: Comparison of performance of batch and continuous-flow reactions based on normalization of residence time.
Error bars represent mean ±SD (n=3).

Flow biocatalysis has been shown to outperform conventional batch systems (Bras *et al.*, 2021). However, looking at Figure 2.26 one may conclude that the transketolase reaction profile is similar for batch and continuous operation modes. This comparison is based on the enzyme activity and the scale. The TK batch reactions were conducted in a 1 mL Eppendorf which is a relatively small volume. Considering this normalization, if the batch reactor's volume increases at the same enzyme concentration, the difference between the batch and flow's reaction profile will become more significant. TK batch reactions were conducted with the DA flow reaction's product. Therefore, the enzyme was never exposed to the chemical catalyst, which could affect its activity. The TK reaction step benefits from doing the DA reaction in flow with an immobilised catalyst; otherwise, an extra step would be required to separate the catalyst from the product. Furthermore, continuous flow makes adjusting reaction conditions and limiting the amount of organic solvent present in the TK step from the chemical reaction easier. Hence doing the whole chemoenzymatic reaction in flow has advantages over a batch process.

2.4 Conclusion

In this chapter, a Diels-Alder-transketolase chemoenzymatic cascade for the synthesis of DCDHP was successfully demonstrated in a continuous flow system, with complete substrate conversion and without the need for intermediate purification steps. The coupling of both reaction steps in a single flow system was possible by immobilising the chemical catalyst in a packed-bed reactor and by playing with the operational flows to minimise the impact of the organic solvent on the TK activity.

The selected TK mutant demonstrated high enantio- and stereoselectivity towards the DA product, CCA, facilitating the coupling of the reactions in flow for the efficient synthesis of DCDHP. The enantioselectivity of the TK mutant towards the CCA enantiomers was investigated in batch reactions with (S)- and (R)-CCA produced from asymmetric DA reactions with organocatalysts. Only the batch reaction with (R)-CCA enabled the production of DCDHP, and therefore the TK mutant was determined to be specific to the (R)-enantiomer of the DA reaction product.

The DA reaction was conducted with simple non-chiral starting compounds acrolein and 2,3-dimethyl-1,3-butadiene using aluminium chloride immobilised on silica gel as a catalyst and acetonitrile as a solvent. The reaction was conducted in flow in a packed-bd reactor, resulting in the complete conversion of an equimolar 100 mM solution of acrolein and butadiene in 2 hours. The packed-bed reactor was linked to a coil reactor using a four-way micromixer with inlets for the transketolase solution and for the enzyme co-substrate HPA, which renders the reaction irreversible due to the release of carbon dioxide as a side product. Experiments conducted in batch demonstrated that transketolase could withstand 10% (v/v) of acetonitrile without losing significant activity. Therefore, the acetonitrile concentration was diluted to 10%(v/v) in the micromixer before initiating the enzymatic reaction in the coil reactor. The DA-TK continuous flow setup resulted in the complete conversion of the substrates and a production of 5 mM DCDHP in 195 minutes.

Despite achieving full conversion of the substrates, further improvement of the cascade reaction could be attained by employing purified TK. The presence of other proteins in the lysate may lead to side reactions and potentially reduce the overall efficiency of the reaction cascade.

In previous preliminary experiments by Pia Gruber using the same setup, 3.5 mM of DCDHP was produced in 200 minutes from a starting concentration of 200 mM acrolein and 2,3-dimethyl-1,3-butadiene. Thus, the current experiment showed an increase in productivity of 43% by using half the concentration of the DA substrates.

Overall, this chapter showcases the advantages of combining chemical and biocatalysts and how continuous flow systems can accelerate their applicability to organic synthesis. The use of a biocatalyst simplified the synthesis of chiral 3,4-dimethylcyclohex-3-ene-2'-keto-1',3'-propanediols, by reducing the number of steps and avoiding by-product formation. Furthermore, performing this chemoenzymatic synthesis in continuous flow allowed for overcoming typical problems related to the integration of enzymes with chemical steps, such as solvent compatibility, differing reaction rates, and mismatch of pH.

3 Development of an Enzymatic Cascade Reaction for the Synthesis of 1,3-Biphosphoglycerate

3.1 Introduction

Discovered nearly a century ago by Warburg and Christian, 1,3-biphosphoglycerate is a glycolytic metabolite involved in the control of cellular metabolism, oxygen affinity of red cells and other cellular functions. In the glycolysis pathway, 1,3-biphosphoglycerate is synthesised from glyceraldehyde-3-phosphate (GAP) oxidation by glyceraldehyde 3-phosphate dehydrogenase (GAPDH) (Warburg and Christian, 1942). This enzymatic step also involves the reduction of NAD+ to NADH and the transference of inorganic phosphate to the carboxyl group, which gives 1,3-biphosphoglycerate a high phosphoryl-transfer potential that will be used in the next step to produce ATP (Wolfson-Stofko, Hadi and Blanchard, 2013; Sirover, 2014). In the next step of the glycolysis, phosphoglycerate kinase catalyses the transfer of the phosphoryl group from the acyl phosphate of 1,3-bisphosphoglycerate to ADP, making a molecule of ATP and turning into 3-phosphoglycerate (3-PGA), a carboxylic acid, in the process (Hanson, 1981). In the Calvin cycle during photosynthesis, the same set of reactions occur but in reverse order. In this reverse glycolysis pathway, the enzyme phosphoglycerate kinase catalyses the phosphorylation of 3-PGA by ATP, resulting into 1,3-biphosphoglycerate and ADP. GAPDH then catalyses the reduction of 1,3-biphosphoglycerate by NADPH, GAP is produced, and NADPH is oxidised to NADP+.

1,3-Biphosphoglycerate also plays a pivotal role in gluconeogenesis. In this pathway, 1,3-bisphosphoglycerate serves as an intermediate metabolite that helps channel carbon atoms' flow towards glucose production. In gluconeogenesis, the conversion of 1,3-bisphosphoglycerate to GAP is facilitated by the enzyme phosphoglycerate kinase, which catalyses the reverse of the glycolytic reaction. This step involves the phosphorylation of 3-PGA using ATP to form 1,3-bisphosphoglycerate. This conversion is essential for reversing the glycolytic pathway, allowing the cell to generate glucose from sources other than carbohydrates. By participating in this step, 1,3-bisphosphoglycerate contributes to forming glucose molecules, enabling stable blood glucose levels.

This metabolite is also present in the Rapaport-Leubering cycle, a supplementary pathway to glycolysis in the erythrocytes responsible for 15 to 25 % of the glucose converted to lactate. In this pathway, 1,3-biphosphoglycerate is catalysed by the enzyme biphosphoglycerate mutase (BPGM) to synthesise 2,3-biphosphoglycerate (2,3-BPG). 2,3-BPG is then hydrolysed to 3-PGA by 2,3-BPG phosphate allowing the glycolysis pathway to proceed without ATP production. The synthesis of 2,3-BPG from 1,3-biphosphoglycerate is also used as a control mechanism in the affinity of haemoglobin to oxygen. By binding with haemoglobin, 2,3-BPG stabilises the deoxygenated form of haemoglobin, thereby releasing oxygen to tissues. Usually, in hypoxic situations, caused by high altitudes or health conditions such as hypoxemia, chronic lung disease, anaemia, congestive heart failure, and others, low levels of oxygen will trigger a rise in 1,3-biphosphoglycerate concentration, which in turn, leads to increased levels of 2,3-BPG enhancing the release of oxygen from haemoglobin to tissues (Sasaki and Chiba, 1983).

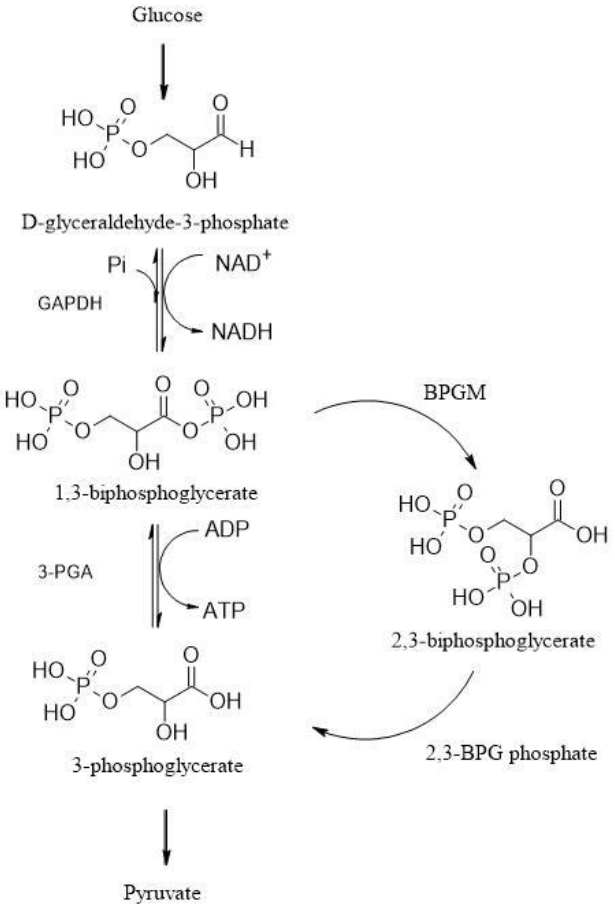

Figure 3.1: 1,3-biphosphoglycerate synthesis and competing reactions in metabolism.

Despite being involved in several essential pathways, studies on the role of 1,3-biphosphoglycerate in the metabolism and cell pathologies have been limited due to the lack of commercial availability. The acyl phosphate group of 1,3-biphosphoglycerate makes the metabolite extremely unstable and particularly sensitive to spontaneous hydrolysis or isomerization to 3-PGA and 2,3-bisphosphoglycerate (2,3-BPG), respectively. Furthermore, in the course of metabolism, 1,3-biphosphoglycerate can also be enzymatically converted into 3-PGA and 2,3-BPG, which makes the isolation and analysis of this group of connected metabolites challenging (Figure 3.1). To date no conditions are known under which 1,3-biphosphoglycerate is stable for long-periods of time. A study in the sixties was able to report that 1,3-biphosphoglycerate decomposition rate depends on the temperature and pH of the solution (Negelein, 1965). 1,3-biphosphoglycerate was the most stable when frozen in an alkaline solution, above pH 7 until pH 9. It was discovered that the compound is not stable in the dry state and that hydrolysis is accelerated when in an acid solution. However, until now, no conditions are known under which 1,3-biphosphoglycerate is stable for a long time, so standard metabolomic methods can't correctly access its potential.

In an attempt to isolate 1,3-biphosphoglycerate and prevent unwanted spontaneous chemical transformations that occur during sample preparation and conventional mass spectrometric analysis, Chang and co-workers took advantage of the reactive acylphosphate group in 1,3-BPG to chemically trap the metabolite with hydroxylamine and enable quantitative analysis of the metabolite by LC−MS/MS (Chang et al., 2016). Here, 1,3-biphosphoglycerate was produced *in vitro* by incubating human GAPDH (0.1 $mg.mL^{-1}$) with GAP (2 mM) and NAD+ (0.4 mM). The reactions were run for 1 hour before adding an equal volume of a solution of hydroxylamine. Hydroxylamine reacted with the metabolite to form a stable hydroxamic acid (3PGha) with a mass of 199.98 Da detected by targeted LC−MS/MS (Figure 3.2). This approach has also enabled specific detection of 1,3-biphosphoglycerate instead of the 2,3-BPG isomer in the cellular metabolome for the first time.

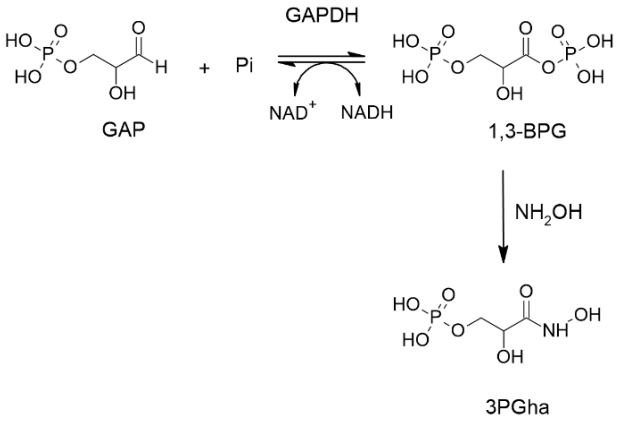

Figure 3.2: Chemical entrapment of 1,3-biphosphoglycerate with hydroxylamine.

Although applicable to confirm the presence of 1,3-biphosphoglycerate in reaction samples, the hydroxylamine chemical entrapment developed by Chang and co-workers is not reversible. Thus, hydroxylamine cannot be used as a stabilisation reagent if the goal is to use 1,3-biphosphoglycerate as a substrate.

Moellering and Cravatt reported in 2013, the discovery of a new functional lysine modification facilitated by 1,3-biphosphoglycerate. Accordingly, to their findings, 1,3-biphosphoglycerate reacts with specific lysine residues in proteins to form 3-phosphoglyceryl-lysine (pgK) (Moellering and Cravatt, 2013b). These pgK modifications were found to inhibit glycolytic enzymes' activity, acting as a feedback mechanism by which 1,3-biphosphoglycerate regulates the build-up and redirection of glycolytic intermediates across pathways in response to changes in the metabolism. Since 1,3-biphosphoglycerate is not commercially available, to conduct this study, Moellering and co-workers produced the metabolite *in situ* by incubating purified human GAPDH (0.1 mg.mL^{-1}) with GAP (2 mM) and NAD+ (0.4 mM) in PBS buffer for 12 hours at 30°C. Reactions were monitored for NADH production (340 nm absorbance), confirming the synthesis of 1,3-biphosphoglycerate and GAPDH was trypsinized and analysed by LC-MS/MS where several pgK-modified GAPDH peptides were identified.

In a recent study, Oslund *et al* (Oslund *et al.*, 2017) showed that 1,3-biphosphoglycerate can directly phosphorylate phosphoglycerate mutase 1 (PGAM1), supporting normal glycolytic and cellular growth rate in the absence of

bisphosphoglycerate mutase (BPGM) activity. Here 1,3-biphosphoglycerate was enzymatically produced in vitro using a GAPDH and LDH coupled reaction. GAPDH was used to convert GAP and NAD+ into 1,3-biphosphoglycerate and NADH, which was recycled to NAD+ by lactate dehydrogenase (LDH) catalysed reduction of pyruvate. The reaction mixture contained 25 mM Tris pH 8.0, 50 mM NaCl, 1 mM MgCl2, 10 mM KH2PO4, 0.4 mM NAD+, 1 mM GAP, 3.3 mM pyruvate, 1 unit/mL GAPDH, 0.1 mg/mL BSA and 16.7 units/mL LDH. After 30 minutes, the reaction was quenched with 50% methanol, and purification of 1,3-biphosphoglycerate was achieved by HPLC. Due to the low reaction yields several samples were purified and the fractions containing 1,3-biphosphoglycerate were collected and further concentrated for analysed by LC-MS. The presence of 1,3-biphosphoglycerate was verified using a phosphoglycerate kinase (PGK) assay. In the presence of both PGK and ADP, 1,3-biphosphoglycerate was consumed indicating that the metabolite was successfully prepared.

In both the research studies mentioned above, 1,3-biphosphoglycerate was enzymatically produced by GAPDH in the presence of GAP and NAD+. This reaction seems to be the preferred route since early studies on the conversion of 3-PGA into 1,3-biphosphoglycerate by PGK (Figure 3.3), concluded that the equilibrium of the PGK reaction strongly favours the formation of 3-PGA and ATP from 1,3-biphosphoglycerate and ADP (Krimsky, 1958). However, several studies have reported on GAP instability (Richard, 1984; Slaughter *et al.*, 1993), particularly under alkaline conditions (Shaeri *et al.*, 2008).

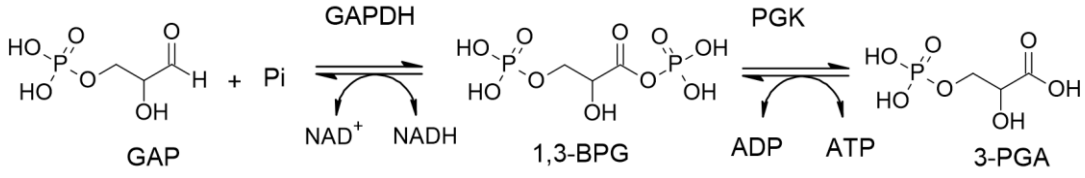

Figure 3.3: Reaction scheme of the enzymatic synthesis of 1,3-biphosphoglycerate by GAPDH and PGK.

This chapter aims to present a de novo enzymatic cascade compromising three glycolytic enzymes for the synthesis of 1,3-biphosphoglycerate for posterior isolation and use in research. The enzymatic cascade starts with dihydroxyacetone phosphate (DHAP) conversion into GAP by triosephosphate isomerase (TPI), followed by a

GAPDH catalysed conversion of GAP using NAD+ to produce 1,3-bisphosphoglycerate and NADH. These two sugars, DHAP and GAP, are isomers of each other and can be interconverted by TPI. The thermodynamic equilibrium of this reaction favours DHAP formation 20:1 over GAP production. However, in glycolysis, the use of GAP in the subsequent steps of the pathway drives the reaction towards GAP production (Davenport *et al*., 1991; Harris, Abeygunawardana and Mildvan, 1997; Harris *et al*., 1998; Venkatesan *et al*., 2011). Here, in an attempt to emulate the glycolysis pathway to design this cascade, TPI and GAPDH were coupled in solution to produce 1,3-biphosphoglycerate from the starting substrate DHAP. To regenerate the GAPDH co-factor NAD+ in situ a lactate dehydrogenase (LDH) was added to the cascade (Figure 3.4). LDH catalyses the reduction of pyruvate with concomitant oxidation of NADH to lactate (Kr, And and Wsttestdes, 1989).

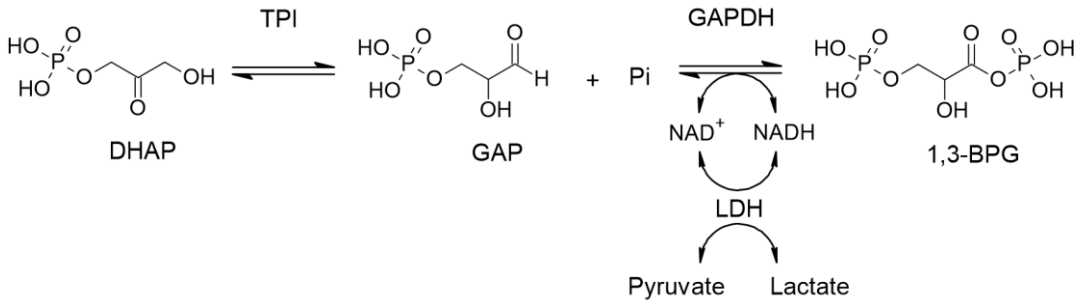

Figure 3.4: TPI-GAPDH-LDH cascade reaction for the synthesis of 1,3-biphosphoglycerate.

Given the instability of the metabolites involved in this reaction cascade and considering the improvements in yield achieved with continuous flow microreactors in the previous chapter (Chapter 2), this chapter explores whether a microreactor would facilitate the production of 1,3-biphosphoglycerate over a batch process.

Using a microreactor for such reactions provides improved mass transfer rates which may ensure that the reaction operates close to intrinsic kinetics. Furthermore, the versatility of flow systems allows for faster screening of reaction conditions, requiring minor input of solvents, enzymes, and substrates, which makes the overall process more sustainable.

3.2 Materials and methods

Unless otherwise stated, the reactions were carried out at room temperature and all the chemicals were purchased from Sigma-Aldrich (Gillingham, UK), and used without further purification. The enzymes used in this chapter are listed in Table 3.1.

Changes in absorbance due to the reduction of NAD+ to NADH were measured in a FLUOstar Optima plate reader (BMG Labtechnologies GmbH). The reduced form (NADH) absorbs at 340 nm with an extinction coefficient of 6.22 $mM^{-1}cm^{-1}$, whereas the oxidized form (NAD+) has no absorbance at 340 nm.

Table 3.1:Origin and activity of the enzymes used.

Enzyme	Origin	Formulation	Foreign Activity	Activity (units/mg protein)
TPI	Baker's yeast, *Saccharomyces cerevisiae*	Ammonium sulfate suspension	Pyruvate kinase, lactic dehydrogenase, 3-phosphoglyceric phosphokinase, phosphoglucose isomerase, α-glycerophosphate dehydrogenase, aldolase, and glyceraldehyde-3-phosphate dehydrogenase <0.01%	~ 10,000
GAPDH	Rabbit muscle	Lyophilized powder	3-Phosphoglyceric phosphokinase ≤0.05%, lactic dehydrogenase,	≥ 75

			myokinase, and pyruvate kinase ≤0.01%, triosephosphate isomerase ≤0.1%	
LDH	Rabbit muscle	Lyophilized powder	Pyruvate kinase, myokinase, malic dehydrogenase, glutamic-pyruvic transaminase, glutamic-oxalacetic transaminase and α-glycerophosphate dehydrogenase ≤0.01%	25,000
PGK	Baker's yeast, *Saccharomyces cerevisiae*	Ammonium sulfate suspension	Glyceraldehyde-3-phosphate dehydrogenase ≤0.1%	5,000

3.2.1 Buffer optimisation and effect of pH on the activity of GAPDH and TPI-GAPDH forward reactions

To optimise the forward reactions for GAPDH and TPI-GAPDH, activity assays were performed with two different buffers at different pH conditions (7-8.5). The composition of the buffers tested is indicated in Table 3.2.

GAPDH individual activity in the buffers was followed in a reaction mixture containing 0.4 mM NAD+, 1 mM glyceraldehyde-3-phosphate (GAP), and 1 $U.mL^{-1}$ GAPDH (calculated from product certificate). Whereas, the coupled TPI-GAPDH reaction was conducted with 10 mM dihydroxyacetone phosphate (DHAP), 0.4 mM NAD+ and 1 $U.mL^{-1}$ of TPI and GAPDH. The rates of these reactions were measured

as changes in absorbance due to reduction of NAD+ to NADH at 340 nm in 96-well microplates using plate reader for 15 min.

Table 3.2: Compositions of reaction buffers screened for GAPDH and coupled TPI-GAPDH forward reactions.

Buffer	Composition
A	25 mM Tris, 50 mM NaCl, 1 mM $MgCl_2$, 10 mM KH_2PO_4
B	50 mM glycine, 50 mM sodium monophosphate

3.2.2 GAPDH and TPI-GAPDH reactions and activity assays

GAPDH was dissolved in 50 mM glycine-phosphate buffer pH 8.5 to a concentration of 1 $U.mL^{-1}$ with 0.4 NAD+ and 1 mM GAP. Reactions were run for 15 min and monitored for NADH production (340 nm absorbance). To validate the assumption that GAPDH required both NAD+ and GAP to produce 1,3-biphosphoglycerate, GAPDH reactions were performed as above but in the absence of NAD+ co-factor or GAP.

To verify the capacity of TPI-GAPDH reaction to produce 1,3-biphosphoglycerate TPI and GAPDH were dissolved in 50 mM glycine-phosphate buffer pH 8.5 to a concentration of 1 $U.mL^{-1}$ with 0.4 NAD+ and 10 mM DHAP. Reactions were run for 15 min and monitored for NADH production (340 nm absorbance) and compared with TPI reaction performed as above but in the absence of GAPDH and NAD+ or DHAP.

Michaelis-Menten kinetic assays were performed with the GAPDH alone in solution and TPI activity was measured by means of a coupled reaction with GAPDH. The reactions were supplemented with constant NAD+ (0.4 mM) and with GAP concentrations varying from 1 to 0.31 mM and DHAP concentrations from 10 to 0.25 mM. Measurements of activity were determined from slopes taken from within the linear range and Michaelis constant (Km) and maximum reaction velocity (Vmax) of GAPDH and TPI were determined according to double-reciprocal Lineweaver–Burk plots (appendix Figure 6.22)

3.2.3 Influence of GAPDH concentration on conversion

To investigate if higher concentrations of GAPDH in relation to TPI would result into higher conversion rates, batch reactions with 1 $U.ml^{-1}$ TPI: 10 $U.ml^{-1}$ GAPDH were carried out with 10 mM of DHAP and 0.4 mM NAD+ in 50 mM glycine-phosphate buffer pH 8.5. The reactions were monitor at 340 nm in 96-well microplates using a FLUOstar Optima plate reader (BMG Labtechnologies GmbH) (appendix Figure 6.23).

3.2.4 Co-factor regeneration system

L-Lactic Dehydrogenase (LDH) from rabbit muscle was coupled in solution with GAPDH and the TPI-GAPDH cascade reaction, to catalyse the *in situ* regeneration of NADH. The reactions were carried out in 50 mM glycine-phosphate buffer at pH 8.5 with the reagents and concentrations indicated in Table 3.3. All the reactions were incubated in batch for 30 minutes and samples were collected, quenched, and analysed by HPLC for pyruvate consumption.

Table 3.3: Enzyme reaction mixes in solution for GAPDH-LDH and TPI-GAPDH-LDH reactions.

Coupled reaction	Enzymes and reagents	Final concentrations
GAPDH-LDH	GAP	1 mM
	NAD+	0.4 mM
	Pyruvate	3.3 mM
	GAPDH	1 $U.ml^{-1}$
	LDH	16.7 $U.ml^{-1}$
TPI-GAPDH-LDH	DHAP	10 mM
	NAD+	0.4 mM
	Pyruvate	3.3 mM
	TPI	1 $U.ml^{-1}$
	GAPDH	1 $U.ml^{-1}$
	LDH	16.7 $U.ml^{-1}$

3.2.5 TPI-GAPDH-LDH continuous flow cascade

Having optimised reaction conditions in batch for the TPI-GAPDH-LDH cascade reaction, 1,3-BPG production was attempted in continuous flow. The setup comprised one syringe pump (290N neMESYS, Cetoni GmbH, De) with two glass syringes (Hamilton Bonaduz, Switzerland), one for the substrates and another for the enzyme's solution. The flow streams from the syringes were brough together through an Upchurch® PEEK T-shape micromixer (Upchurch Scientific, through VWR, Pennsylvania, USA) connected to a coil reactor (PTFE, ID 0.75 mm, VWR International Ltd, Lutterworth, UK) with a volume of 135 µL.

The TPI-GAPDH-LDH cascade reactions were carried out under identical conditions as previously optimised for batch. The substrates syringe contained 20 mM DHAP, 0.8 mM NAD+ and 6.6 mM pyruvate in 50 mM glycine-phosphate buffer pH 8.5; while the enzymes syringe contained: 2 $U.ml^{-1}$ TPI, 2 $U.ml^{-1}$ GAPDH and 33.4 $U.ml^{-1}$ LDH dissolved in 50 mM glycine-phosphate buffer pH 8.5. Solutions were pumped at the same flow rate, in the range of 3 to 27 $\mu L.min^{-1}$, into a T-shape micromixer connected to the coil reactor as shown in Figure 3.5. Final concentrations in the coil reactor were: 10 mM DHAP, 0.4 mM NAD+, 3.3 mM pyruvate, 1 $U.ml^{-1}$ TPI, 1 $U.ml^{-1}$ GAPDH and 16.7 $U.ml^{-1}$ LDH. Samples were collected at the outlet of the coil, after three residence times, quenched and analysed by HPLC. Residence times were calculated by dividing the reactor volume by the flow rate.

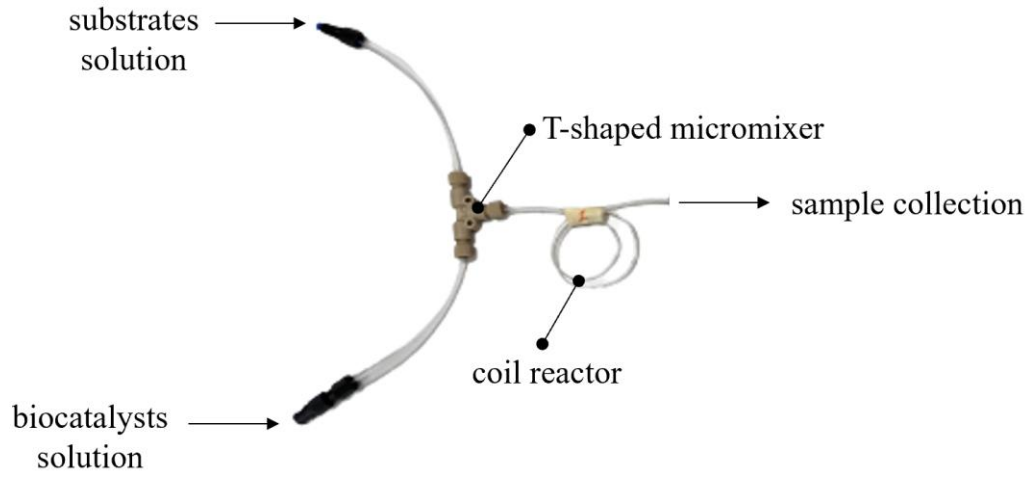

Figure 3.5: Schematic of the continuous flow setup compromising a T-shaped micromixer and a coil reactor for the production of 1,3-biphosphoglycerate.

3.2.6 Confirmation of the enzymatic production of 1,3-biphosphoglycerate

In order to confirm the presence of 1,3-biphosphoglycerate in reaction medias, 50 % (v/v) of the supernatant of the enzymatic reactions used to make 1,3-biphosphoglycerate were mixed with 1 mM ADP and 3.7 $U.mL^{-1}$ of phosphoglycerate kinase (PGK) in 50 mM Tris pH 7.5 with 5 mM $MgCl_2$. The reaction was carried out at in 1 mL Eppendorf at room temperature for 30 min, samples were taken in regular intervals of time quenched and analysed by HPLC and LC-MS for ATP production.

3.2.7 Detection and quantification methods

All reaction samples were quenched with equal volume of 80 % (v/v) MeOH/water, centrifuged (5000 rpm, 5 min) and the supernatant analysed by HPLC. Samples analysed by LC-MS were further purified in a speed vacuum.

3.2.7.1 HPLC analysis

Reaction samples were analysed on a Synergy Hydro-RP column (150 mm × 2 mm, 4 μm particle size, Phenomenex, UK) using a gradient of solvent A (3% (v/v) MeOH/water supplemented with 10 mM tributylamine and 15 mM acetic acid), and solvent B (100% MeOH). The gradient was 0 min, 0% B; 5 min, 0% B; 10 min, 20% B; 20 min, 20% B; 35 min, 65% B; 38 min, 95% B; 42 min, 95% B; 43 min, 0% B; 50 min, 0% B. The flow rate was 200 $\mu L.min^{-1}$. Injection volume was 10 μL and column temperature 25 °C.

Calibration curves for DHAP and GAP in 15 mM Tris buffer pH 7.6 were obtained on an Aminex HPX-87H column (300 mm x 7.8 mm; Bio Rad, UK) with 0.4 $mL.min^{-1}$ isocratic elution of 0.1% (v/v) TFA at 55 ºC, using a refractive index detector at 40ºC.

3.2.8 Statistical analysis

Statistical analysis was performed using Excel v2211. The experimental data means were compared using the student's t-test. Depending on the assumptions and hypotheses required for each experiment a paired t-test or an unpaired t-test was used. Differences were considered significant at p-values < 0.05 and very significant at p-values < 0.01.

3.3 Results and discussion

3.3.1 Optimisation of reaction buffers for GAPDH and TPI-GAPDH forward reactions

The first challenge of multi-enzymatic reactions lies in matching reaction media conditions. Therefore, to combine TPI and GAPDH in solution, different buffer conditions were explored to guarantee optimal activity of both enzymes and stability of substrates and co-factor.

A previous study on GAP stability concluded that the substrate is stable for long periods in a Tris buffer compared with a phosphate-based buffer (Molla, Wohlgemuth and Liese, 2016). In another study, phosphate ions were reported to inhibit TPI activity by binding into the enzyme's active site (Wierenga *et al.*, 1987). However, the synthesis of 1,3-biphosphoglycerate by GAPDH requires inorganic phosphate to happen and thus, the inclusion of phosphate in the reaction media is necessary. Therefore, two reaction buffers with phosphate ions, previously used in studies with GAPDH and TPI, were tested. These buffers were a Tris buffer (25 mM Tris, 50 mM NaCl, 1 mM $MgCl_2$, 10 mM KH_2PO_4) (Oslund *et al.*, 2017) and a glycine-based phosphate buffer (50 mM glycine, 50 mM sodium monophosphate) (Mukai *et al.*, 2013a).

The optimisation of the GAPDH reaction buffer was first investigated in isolation from the TPI reaction to allow for a comparison of GAPDH activity and the activity of the TPI-GAPDH coupled reaction. The TPI-GAPDH reactions were performed with an excess of the initial substrate DHAP (10 mM) compared to the GAP (1 mM) used to initiate the GAPDH catalysed reaction. In previous studies, an excess of DHAP was recommended to overcome the unfavourable equilibrium of the reaction and drive the reaction towards the production of 1,3-biphosphoglycerate (Mukai *et al.*, 2013a). Activities were measured by a change in absorbance at 340 nm due to the reduction of NAD+ to NADH, using a spectrophotometer (Figure 3.6 and Figure 3.7). Activity was only observed in the presence of the initial substrate, either GAP or DHAP.

a)

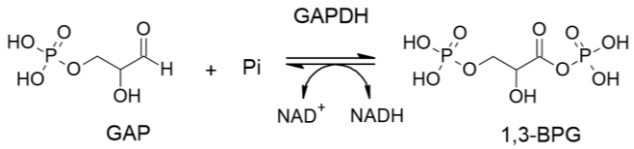

b) c)

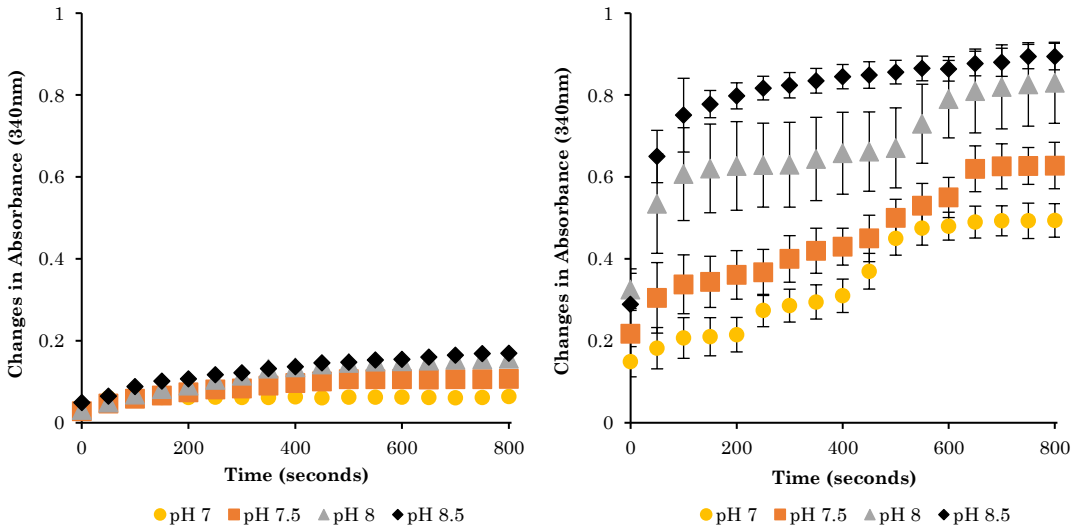

Figure 3.6: Optimisation of the assay buffers for GAPDH forward reaction.
a) Reaction scheme of the forward GAPDH reaction; b) GAPDH batch reaction in 25 mM Tris, 50 mM NaCl, 1 mM $MgCl_2$, 10 mM KH_2PO_4 at different pHs, using GAP as substrate. c) GAPDH batch reaction in 50 mM glycine, 50 mM sodium monophosphate at different pHs. Enzyme concentrations in all reactions were 1 $U.ml^{-1}$. Error bars represent mean ±SD (n=3).

Both reactions showed higher activities when performed in the glycine-based phosphate buffer, independently of the pH. The highest production of NADH was verified at pH 8.5, which is an interesting result since GAP is known to be unstable under alkaline or neutral pH conditions (Gauss, Schoenenberger and Wohlgemuth, 2014).

In the TPI-GAPDH coupled reaction, TPI and GAPDH showed sequential activities, comparable with the activity of GAPDH when alone in solution, suggesting that TPI and GAPDH can work together in solution to produce 1,3-biphosphoglycerate. Since the stoichiometry of the reaction for NAD+ and NADH is at a 1:1 ratio, it can be calculated that the GAPDH catalysed reaction in the glycine-based phosphate buffer at pH 8.5 resulted in a production of 0.16 mM NADH, which corresponds to a NAD+

conversion of 40%. On the other hand, when GAPDH was coupled with TPI at the same buffer conditions, around 0.18 mM of NADH was synthesised, corresponding to a NAD+ 45% conversion.

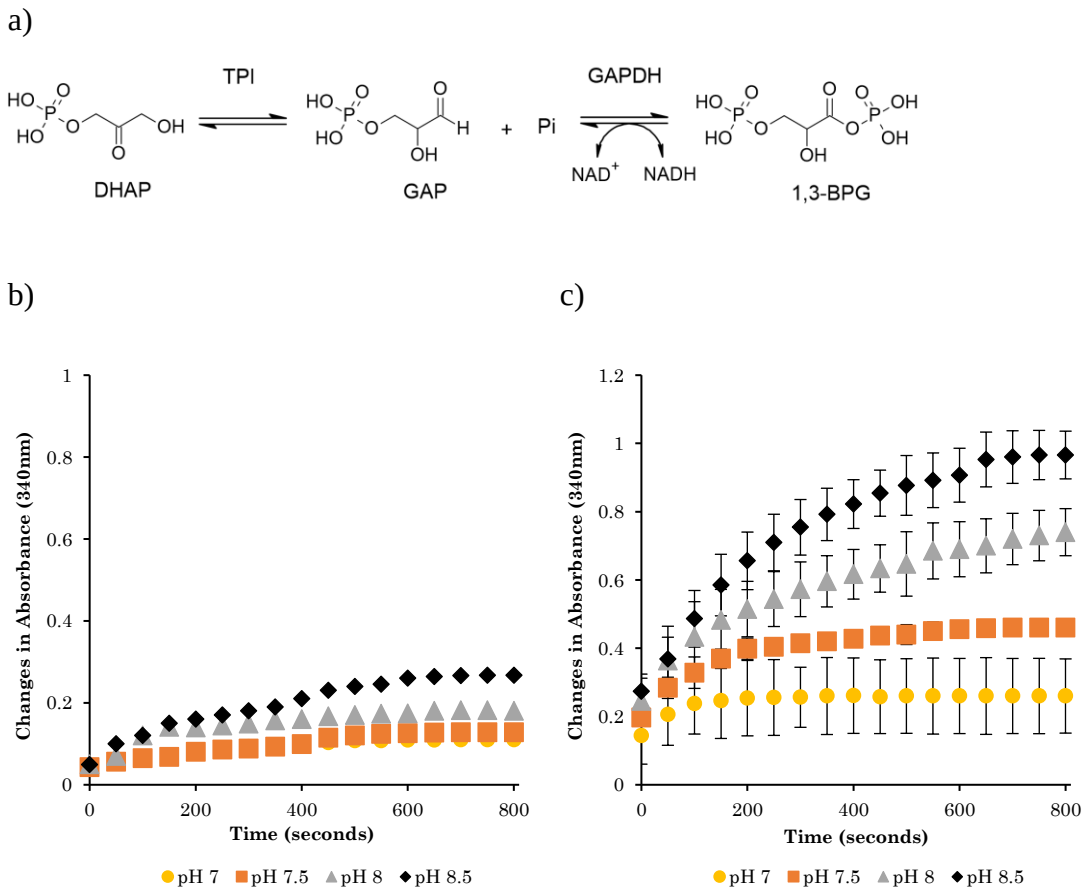

Figure 3.7: Optimisation of the assay buffers for the coupled TPI-GAPDH forward reaction
a) Reaction scheme of the forward TPI-GAPDH coupled reaction; b) TPI-GAPDH batch reaction in 25 mM Tris, 50 mM NaCl, 1 mM $MgCl_2$, 10 mM KH_2PO_4 at different pHs, using DHAP as substrate. c) TPI-GAPDH forward batch reaction in reaction in 50 mM glycine, 50 mM sodium monophosphate at different pHs. Enzyme concentrations in all reactions were 1 $U.ml^{-1}$. Error bars represent mean ±SD (n=3).

3.3.2 Assays of enzymes function in solution

To further investigate the ability of TPI and GAPDH to function sequentially to produce 1,3-biphosphoglycerate, the activity of the TPI-GAPDH forward reaction was compared to that of GAPDH alone in solution, along with associated control experiments. To conduct this kinetic study properly and determine the activity of each enzyme both individually and when coupled in sequence, it would be necessary to detect and quantify the substrates and products involved in the reaction. Since it was

impossible to detect DHAP, GAP, and 1,3-biphosphoglycerate, the rates of these reactions were measured as changes in absorbance at 340 nm using a spectrophotometer, attributed to the reduction of NAD+ to NADH. The results of this experiment are illustrated in Figure 3.8.

The reaction with GAPDH alone in solution was carried out with 0.4 mM of NAD+ and 1 mM GAP. In contrast, the reactions with both enzymes in the solution contained 0.4 mM NAD+ and a higher concentration of DHAP (10 mM) than GAP. As previously determined, all reactions were conducted in the preferred reaction medium, a 50 mM glycine-phosphate buffer at pH 8.5. The reaction profile for GAPDH alone (Figure 3.8a) versus TPI-GAPDH forward reaction (Figure 3.8b) showed no significant difference (p=0.1094), validating the ability of the enzymes to carry out sequential enzymatic reactions leading to the production of 1,3-biphosphoglycerate. Furthermore, the results indicate that in vitro production of this glycolytic metabolite by GAPDH requires the presence of NAD+ and GAP. The same was verified in the TPI-GAPDH catalysed reaction, with the synthesis of NADH occurring only in the presence of the co-factor NAD+ and the substrate DHAP.

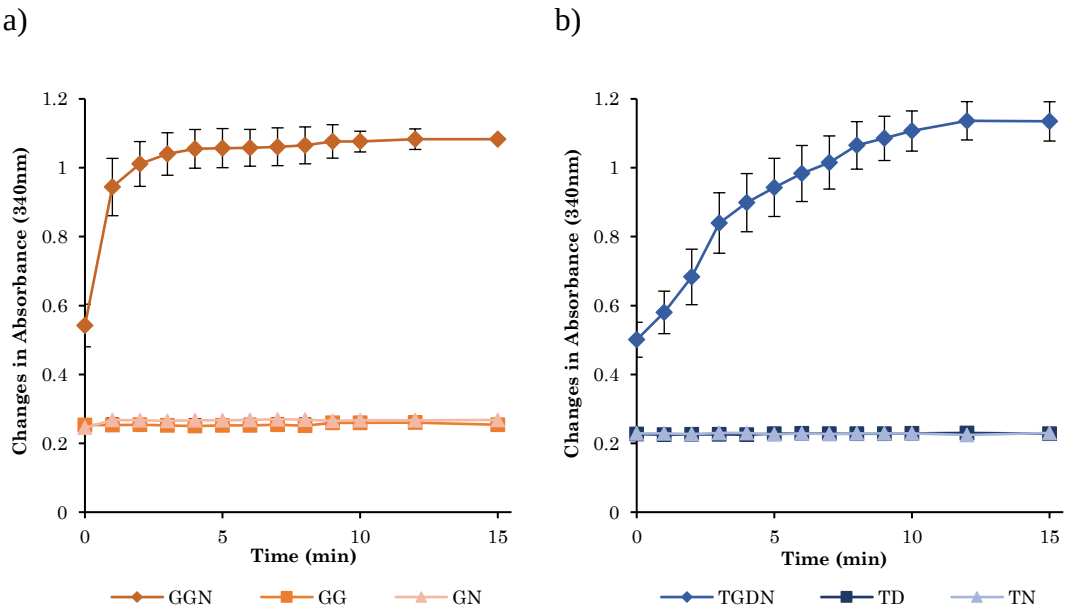

Figure 3.8: Activity of GAPDH and TPI-GAPDH forward reactions in batch.
a) Batch production of 1,3-BPG by GAPDH requires the presence of NAD+ and GAP (GGN condition) as determined by measuring the absorbance of NADH at 340 nm. GGN, GAPDH+GAP+NAD+; GG, GAPDH+GAP; GN, GAPDH+NAD+; b) Batch production of 1,3-BPG by TPI-GAPDH coupled reaction requires the presence of NAD+ and DHAP (TGDN condition) as determined by measuring the absorbance of

NADH at 340 nm. TGDN, TPI+GAPDH+DHAP+NAD+; TD, GAPDH+DHAP; TN, TPI+NAD+; Activity for GAPDHS alone versus TPI-GAPDH forward reaction was not significantly different (p=0.1094). Activity for the GGN condition differed significantly from the GG and GN conditions (p<0.001). Activity for the TGDN condition differed significantly from the TD and TN conditions (p<0.001). Statistics were performed with t-tests. Error bars represent mean ±SD (n=3).

3.3.3 Optimisation of the TPI-GAPDH-LDH cascade reaction

GAPDH exhibits a kinetic mechanism in which NAD+ binds first, and then GAP binds to the active site resulting in the formation of a covalently bound thiohemiacetal intermediate. After oxidation of the thiohemiacetal and subsequent nucleotide exchange, inorganic phosphate and phosphorolysis binding yield the product 1,3-biphosphoglycerate. The binding of NAD+ limits the reaction rate since GAPDH needs this co-factor to accept GAP (Wolfson-Stofko, Hadi and Blanchard, 2013). Therefore, to meet the GAPDH co-factor requirements, a third enzyme was added to the TPI-GAPDH cascade for the *in situ* regeneration of NAD+. The chosen enzyme to do this was lactic dehydrogenase (LDH) which catalyses the reversible conversion of pyruvate to lactate while oxidising NADH to NAD+ (Figure 3.9). Adding LDH to recycle the co-factor also prevents the accumulation of NADH in the reaction media, which could reverse the GAPDH reaction towards GAP production.

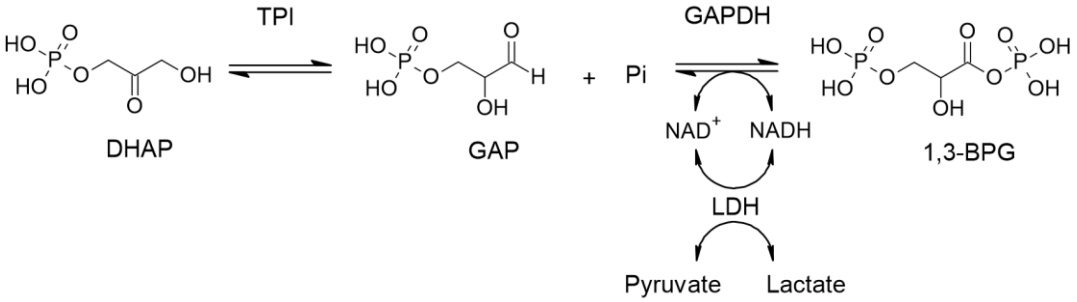

Figure 3.9: TPI-GAPDH-LDH cascade reaction for the synthesis of 1,3-biphosphoglycerate.

Following the protocol used by Oslund *et al.* (Oslund *et al.*, 2017) for the *in vitro* production of 1,3-biphosphoglycerate, LDH was first coupled in solution with GAPDH to examine the capability of LDH to regenerate NAD+ and increase the GAPDH reaction rate towards 1,3-biphosphoglycerate. The reaction mixture contained 1 mM GAP, 0.4 mM NAD+, 3.3 mM pyruvate, 1 $U.ml^{-1}$ GAPDH and 16.7

U.ml^{-1} LDH. Samples were taken in regular intervals and analysed via HPLC for pyruvate and NAD+ concentration profiles, as described in section 3.2.7.1.

The same protocol was followed for coupling TPI, GAPDH and LDH with DHAP as the initial substrate at a 10 mM concentration. Figure 3.10 presents the consumption of pyruvate and the consequent regeneration of NAD+ in both reaction conditions.

The TPI-GAPDH-LDH reaction achieved complete conversion of pyruvate within 30 minutes. In contrast, the coupled GAPDH-LDH reaction only consumed approximately 40% of the pyruvate during the same time frame. However, it's important to note that the GAPDH-LDH reaction was constrained by the limited availability of GAP in the reaction system, which was only present at a concentration of 1 mM. As a result, the consumption of pyruvate was limited to 1 mM. From the perspective of the initial GAP concentration, one could assert that the GAPDH-LDH reaction achieved full substrate conversion within 30 minutes.

In both reaction systems NAD+ concentration remains constant over reaction time, which confirms the ability of LDH to regenerate NAD+.

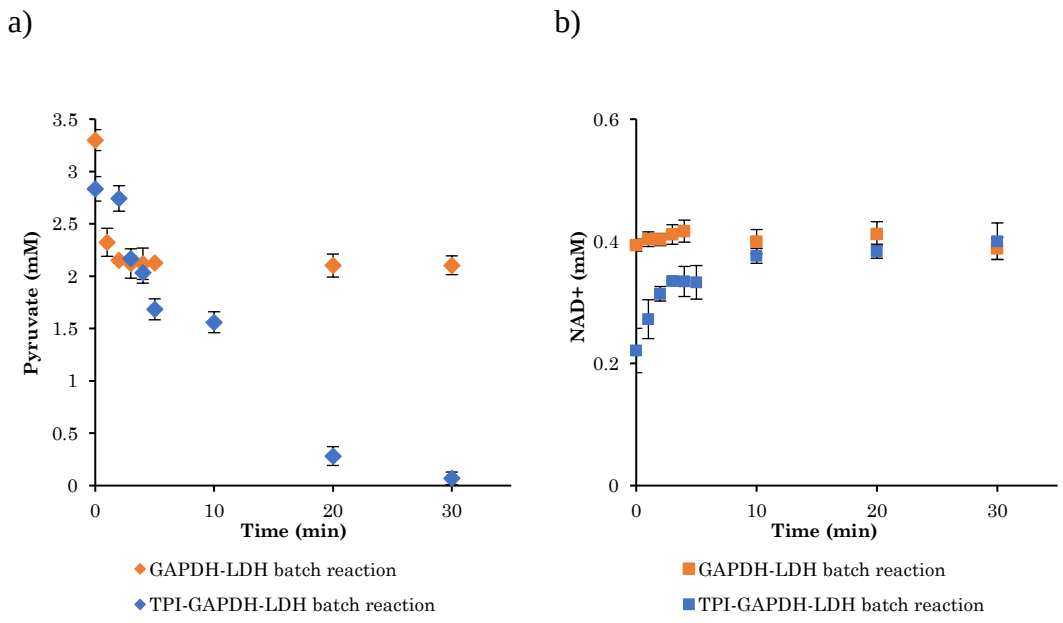

Figure 3.10: GAPDH-LDH and TPI-GAPDH-LDH couple reactions in batch
a) A comparison of the pyruvate profile in a GAPDH-LDH batch reaction starting with 1 mM of GAP, 0.4 mM of NAD+ and 3.3 mM of pyruvate and a TPI-GAPDH-LDH batch reaction starting with 10 mM of DHAP, 0.4 mM of NAD+ and 3.3 mM of pyruvate; b) NAD+ profile in the GAPDH-LDH and in the TPI-GAPDH-LDH batch reactions; Error bars represent mean ±SD (n=3).

3.3.4 Confirmation of the production of 1,3-biphosphoglycerate

Initial attempts at detecting and quantifying 1,3-biphosphoglycerate, GAP and DHAP in the reaction mixture by HPLC were not successful. Since the reaction needs phosphate and all compounds share a phosphate group, separation between compounds was not possible.

In an attempt to detect 1,3-biphosphoglycerate, TPI-GAPDH-LDH reaction samples were analysed by LC-MS as described in section 2.2.7.7. The LC-MS chromatogram from this analysis can be seen in the appendix Figure 6.24 where a signal of m/z 266.9 in negative ion mode is visible, suggesting the presence of 1,3-biphosphoglycerate in the reaction mixture. The presence of 1,3-biphosphoglycerate was further confirmed using a PGK assay (Figure 3.11). Phosphoglycerate kinase catalyses the reversable phosphoryl transfer between 1,3-bisphosphoglycerate and ADP to produce 3-PGA and ATP (R.D.Banks *et al.*, 1978; Palmai *et al.*, 2014).

a)

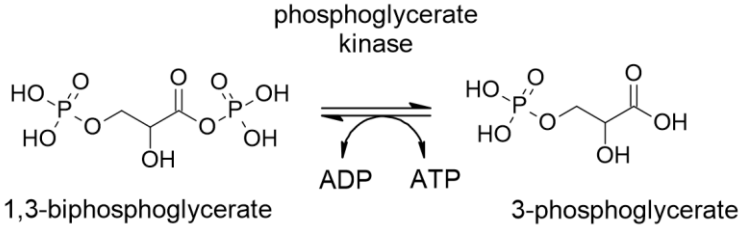

b)

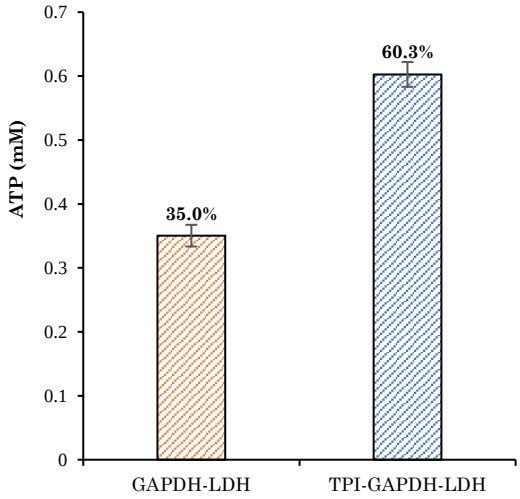

Figure 3.11: PGK assay on GAPDH-LDH and TPI-GAPDH-LDH catalysed batch reactions.
a) Reaction scheme of the PGK assay; b) ATP synthesis by PGK was measured using 1 mM ADP and 50% (v/v) of the reaction supernatant from both the GAPDH-LDH and TPI-GAPDH-LDH batch reactions. The production of ATP is indicated for each residence time, as shown in part a). The higher ATP production observed when using the TPI-GAPDH-LDH reaction supernatant could be attributed to the initial higher concentration of the substrate DHAP, compared to the 1 mM concentration of GAP used in the GAPDH-LDH reaction. Error bars in the graph represent the mean ±SD (n=3).

The supernatants of the GAPDH-LDH and TPI-GAPDH-LDH catalysed reactions were transferred to an Eppendorf containing 1 mM ADP and 3.7 $U.mL^{-1}$ of PGK in 50 mM Tris pH 7.5 supplemented with 5 mM MgCl2, resulting in a 2-fold dilution of the reactants and products as described in section 3.2.6. The reactions were carried out in batch for 30 min, quenched and analysed by HPLC as described in section 3.2.7.1 for ATP production. Figure 3.10c shows the results of this assay.

A 60.3% conversion of ADP into ATP occurred in the batch conducted with the supernatant of the TPI-GAPDH-LDH batch reaction, whereas the supernatant of the

GAPDH-LDH only resulted into a conversion of 35% of the ADP added into ATP. In the absence of PGK or ADP no ATP was detected in all reaction samples. The results suggest that both reactions can produce 1,3-biphosphoglycerate and that the metabolite can serve as an effective substrate to phosphoglycerate kinase.

The preliminary analysis of the pyruvate consumption presented in Figure 3.10 and ATP production shown in Figure 3.11 suggests that the TPI-GAPDH-LDH cascade reaction can synthesise more 1,3-biphosphoglycerate than the GAPDH-LDH coupled reaction. However, further kinetics studies are necessary to validate this assumption.

3.3.5 Investigation of DHAP and LDH concentration requirements

It is assumed that adding LDH to regenerate NAD+ also contributes to shifting the TPI-GAPDH equilibrium towards 1,3-biphosphoglycerate production. Thus, the possibility of conducting the cascade reaction at lower DHAP concentrations was investigated. The results obtained are presented in Figure 3.12.

At lower DHAP concentrations, the need for pyruvate is smaller since GAPDH co-factor requirements are also lower, and therefore so is pyruvate consumption. In concordance, the ATP production from each reaction supernatant was also lower at smaller DHAP concentrations. Therefore, the cascade reaction is more efficient when it starts with 10 mM of DHAP. The data further confirms the viability of the PGK reaction to be used as an assay to confirm the presence of 1,3-biphosphoglycerate (Figure 3.12b).

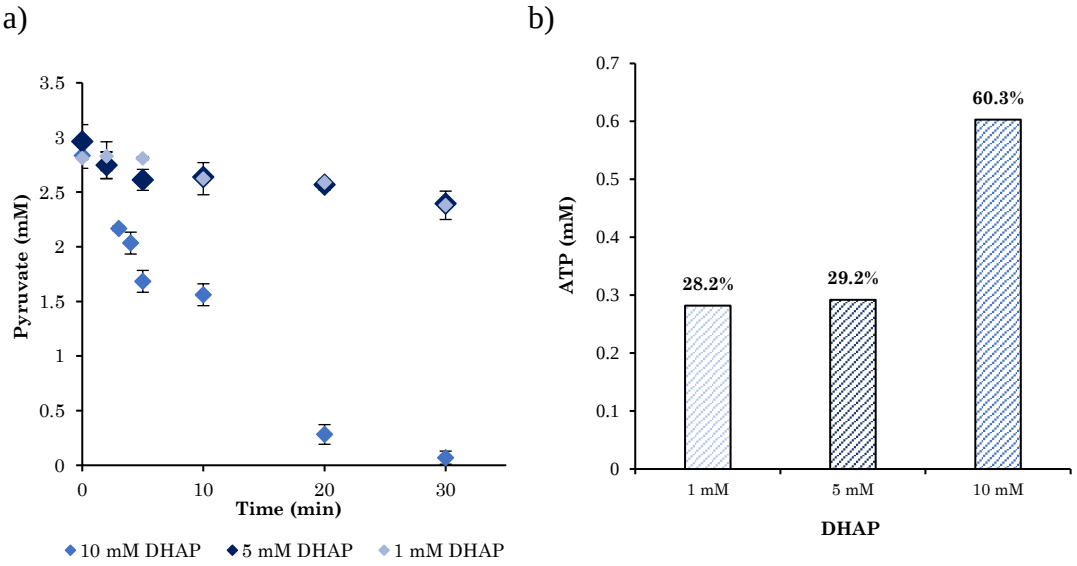

Figure 3.12: TPI-GAPDH-LDH batch reaction at different concentrations of DHAP.
a) Comparison of the pyruvate consumption in TPI-GAPDH-LDH batches starting with different DHAP concentrations (1 mM, 5 mM and 10 mM); b) ATP synthesis by PGK was measured using 1 mM ADP and 50% (v/v) of the TPI-GAPDH-LDH reaction supernatants at different starting concentrations of DHAP. The production of ATP is indicated for each DHAP initial concentration, as shown in a). A higher production of ATP is observed at higher concentrations of the substrate DHAP. Error bars in the graphs represent the mean ±SD (n=3).

ATP synthesis by PGK from 1 mM ADP and 50%(v/v) of the TPI-GAPDH-LDH flow reaction supernatant at different flow rates; conversion of ADP into ATP is indicated in percentage for each residence time of the reactions presented in a);

Next, the minimum amount of LDH necessary to convert 3.3 mM of pyruvate into lactate in 30 minutes in the TPI-GAPDH-LDH cascade was investigated. The results of this experiment are presented in Table 3.4. Enzyme concentrations lower than 16.7 $U.ml^{-1}$ were not enough to convert all the pyruvate under 30 minutes.

Table 3.4: Effect of LDH concentration on pyruvate conversion in a TPI-GAPDH-LDH batch reaction.

LDH concentration ($U.ml^{-1}$)	Residual pyruvate after 30 min (mM)	Pyruvate conversion in 30 min (%)
16.7	0.07	97.9
10	0.98	70.3
5	1.04	68.5
1	1.21	63.3

3.3.6 Continuous flow production of 1,3-biphosphoglycerate

Having optimised the reaction conditions in batch, the performance of a continuous flow system was investigated for the TPI-GAPDH-LDH cascade reaction. For this purpose, a PTFE coil reactor with an internal volume of 135 µL was selected to accommodate the cascade. The set-up included two glass syringes, one with the enzymes and another with substrates. Both solutions were pumped at the same flow rate by a syringe pump into separate inlets of a T-shaped micromixer connected to the coil reactor. A schematic of the flow set-up can be seen in Figure 3.13.

In order to determine the residence time necessary to achieve complete pyruvate conversion, a substrates solution of DHAP, NAD+ and pyruvate was pumped through the coil reactor at the same time and flow rate as an enzymes solution with TPI, GAPDH and LDH at several flow rates (from 3-27 $\mu L.min^{-1}$,

The biocatalysts syringe contained: 2 $U.ml^{-1}$ TPI, 2 $U.ml^{-1}$ GAPDH and 33.4 $U.ml^{-1}$ LDH dissolved in 50 mM glycine-phosphate buffer pH 8.5: while the substrates syringe contained 20 mM DHAP, 0.8 mM NAD+ and 6.6 mM pyruvate in 50 mM glycine-phosphate buffer pH 8.5; the final concentrations in the coil reactor were: 10 mM DHAP, 0.4 mM NAD+, 3.3 mM pyruvate, 1 $U.ml^{-1}$ TPI, 1 $U.ml^{-1}$ GAPDH and 16.7 $U.ml^{-1}$ LDH.

Table 3.5), as described in section 3.2.5. Complete pyruvate conversion was achieved at a flow rate of 3 $\mu L.min^{-1}$ in the coil reactor, which corresponds to a residence time of 45 min (Figure 3.14).

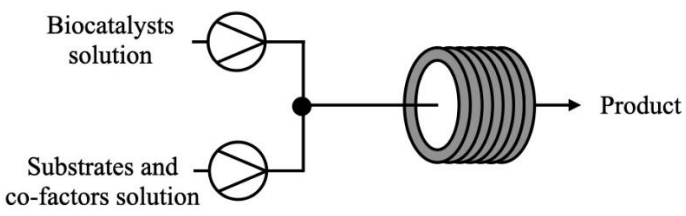

Figure 3.13: Schematic of the continuous flow setup.
The biocatalysts syringe contained: 2 $U.ml^{-1}$ TPI, 2 $U.ml^{-1}$ GAPDH and 33.4 $U.ml^{-1}$ LDH dissolved in 50 mM glycine-phosphate buffer pH 8.5: while the substrates

syringe contained 20 mM DHAP, 0.8 mM NAD+ and 6.6 mM pyruvate in 50 mM glycine-phosphate buffer pH 8.5; the final concentrations in the coil reactor were: 10 mM DHAP, 0.4 mM NAD+, 3.3 mM pyruvate, 1 $U.ml^{-1}$ TPI, 1 $U.ml^{-1}$ GAPDH and 16.7 $U.ml^{-1}$ LDH.

Table 3.5: Flow rates and correspondent residence times inside the coil reactor.

Flow rate inside the coil reactor ($\mu L.min^{-1}$)	Residence time inside the coil reactor (min)
3	45
4.5	30
6.8	20
13.5	10
27	5

A PGK assay was carried out in batches to confirm the synthesis of 1,3-biphosphoglycerate in the coil reactor at each flow rate. The assay was done by collecting samples from the coil reactor's outlet and adding the samples supernatants to batches with PGK (3.7 $U.mL^{-1}$) and ADP (1 mM). The formation of ATP confirmed the presence of 1,3-biphosphoglycerate in the coil reactor at all flow rates, except 27 $\mu L.min^{-1}$, which indicates that 5 minutes is not enough time to achieve an efficient mixing of enzymes and substrates. The supernatant of the flow reaction conducted at 3 $\mu L.min^{-1}$ that led to full conversion of pyruvate also resulted in the highest conversion of ADP into ATP achieved, 62.6%.

a) b)

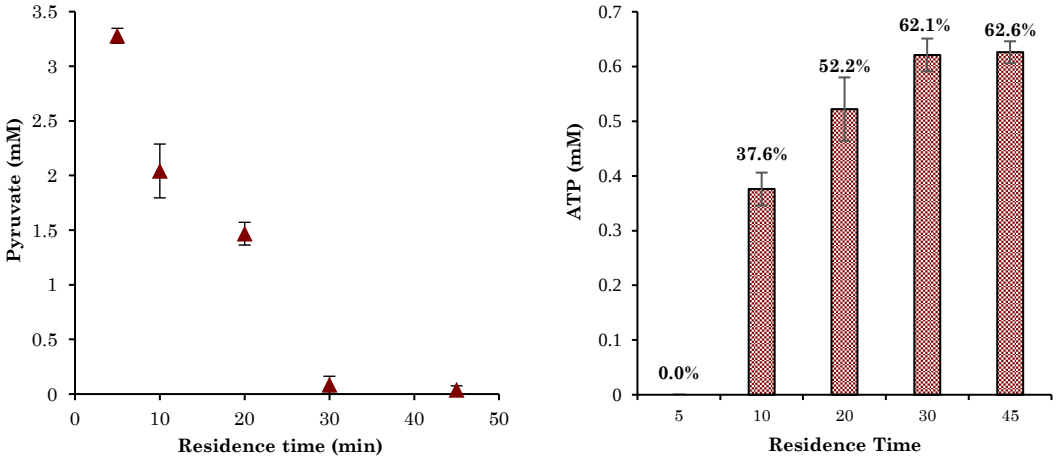

Figure 3.14: TPI-GAPDH-LDH continuous flow reaction
a) Pyruvate consumption profile in a TPI-GAPDH-LDH in a coil reactor with a volume of 135 µL at different flow rates with an initial concentration of 10 mM DHAP, 0.4 mM NAD+ and 3.3 mM pyruvate; b) ATP synthesis by PGK from 1 mM ADP and 50%(v/v) of the TPI-GAPDH-LDH flow reaction supernatant at different flow rates. The production of ATP is indicated for each residence time, as shown in a) A higher ATP production was observed when using supernatants from reactions conducted at higher residence times (slower flow rates). Error bars represent mean ±SD (n=3).

Figure 3.15 shows the results of the PGK assay with reaction supernatants from batch and flow for comparison. Both process modes led to a similar production of ATP indicating that the developed continuous-flow setup can be used to conduct the TPI-GAPDH-LDH cascade reaction for production of 1,3-biphosphoglycerate.

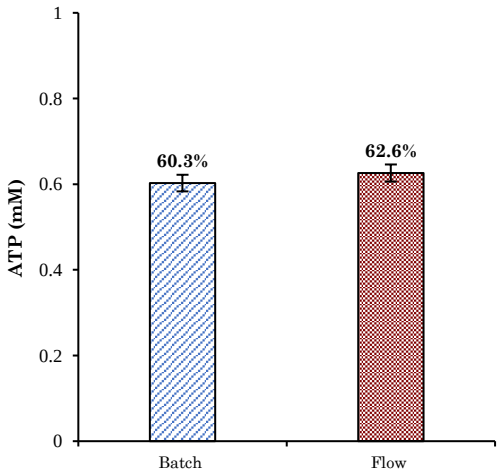

Figure 3.15: Comparison of ATP produced in a PGK catalysed reaction with supernatants from TPI-GAPDH-LDH batch and flow reactions.

ATP synthesis by PGK from 1 mM ADP and 50%(v/v) of the TPI-GAPDH-LDH batch and flow reaction supernatants. Error bars represent mean ±SD (n=3).

3.4 Conclusion

An enzymatic cascade reaction has been designed for the synthesis of 1,3-biphosphoglycerate. The metabolite prepared in the cascade can serve as an effective substrate to phosphoglycerate kinase to produce ATP.

The cascade reaction consists of the coupled TPI-GAPDH forward reaction combined with LDH for *in situ* co-factor regeneration of NAD+. First, TPI catalyses the conversion of DHAP into GAP, which is used as a substrate for GAPDH. In the second step of the cascade, GAPDH converts GAP and NAD+ into 1,3-biphosphoglycerate and NADH, which is then recycled to NAD+ by LDH-catalysed reduction of pyruvate.

During glycolysis, TPI catalyses the conversion of DHAP to GAP. However, several studies have demonstrated TPI preference for the reverse reaction, the catalysis of GAP into DHAP (Harris *et al.*, 1998; Rozovsky and McDermott, 2007; Bennett *et al.*, 2009). Here, the combination of TPI with GAPDH in a one-pot reaction, mimicking what happens in the glycolysis pathway, was crucial to driving the conversion of DHAP to GAP, which led to 1,3-biphosphoglycerate production. This combination was achieved using free enzymes and required improvements towards enzymatic activity, such as optimisation of the reaction media, substrate and co-factor concentrations and pH adjustment. Higher conversion rates were verified at alkaline pHs, specifically at pH 8.5.

The activity of GAPDH alone in solution was measured as a change in absorbance and compared with the activity of the TPI-GAPDH coupled reaction. In the optimal buffer conditions (50 mM glycine phosphate buffer, pH 8.5), the activity for GAPDHS alone was not significantly different from the activity of the TPI-GAPDH coupled reaction, validating the ability of the enzymes to carry out sequential reactions towards the production of 1,3-biphosphoglycerate. Furthermore, compared with associated controls, it was possible to verify that the synthesis of NADH only occurs in the presence of the co-factor NAD+ and the substrate DHAP or GAP. Considering these results, the following assumptions can be made concerning the TPI-GAPDH coupled reaction: 1) the number of 1,3-biphosphoglycerate molecules generated is equal to the number of GAP consumed; 2) the number of GAP molecules consumed is equal to the number of DHAP consumed, 3) the number of DHAP consumed is equal to the

number of NADH molecules generated; and therefore, NADH generation rate is equal to the conversion rate of GAP into 1,3-biphosphoglycerate catalysed by GAPDH in a coupled reaction with TPI. Hence, the conversion rate of DHAP to GAP by TPI versus the rate at which GAPDH catalyses GAP determines the overall conversion. More specifically, the concentration of GAP in the reaction is the rate-limiting factor for the two-step enzymatic cascade. GAP accumulation in the reaction medium in the presence of TPI could drive the equilibrium towards DHAP production and, therefore, away from 1,3-biphosphoglycerate synthesis. Furthermore, GAPDH activity depends on the co-factor NAD+. Thus, the TPI-GAPDH cascade is limited by lower GAP conversion rates and low NAD+ concentrations.

In an attempt to solve this issue and drive the TPI-GAPDH cascade towards the production of 1,3-biphosphoglycerate, a third enzyme was added to the cascade to regenerate NAD+. The efficiency of the LDH to recycle the GAPDH co-factor was investigated in batches with LDH coupled with GAPDH and with the TPI-GAPDH reaction. Complete conversion of pyruvate was achieved in the TPI-GAPDH-LDH reaction. In contrast, in the GAPDH-LDH coupled reaction, only around 40% of the pyruvate was consumed, indicating that the TPI-GAPDH-LDH cascade is a more promising route to 1,3-biphosphoglycerate than GAPDH-LDH. However, kinetics studies on NADH binding to GAPDH and LDH and on the displacement of enzyme-bound NADH by LDH or GPDH are required to support the results obtained. Further kinetics studies on the mechanism of substrate transference between TPI and GAPDH are also necessary. The development of analytic methods to detect and quantify all the metabolites in the cascade are crucial to enable these studies.

Initial attempts at detecting DHAP and GAP in the same reaction sample were unsuccessful. DHAP and GAP are isomers and therefore share the same molecular mass, which makes their separation and detection difficult. An HPLC method on an Aminex HPX-87H column using a refractive index detector was developed that allowed the detection and quantification of DHAP and GAP in Tris buffer (appendix Figure 6.12). However, the presence of phosphate in the reaction media made it impossible to detect the metabolites with this method. As for 1,3-biphosphoglycerate, given that the metabolite is not commercially available, it is challenging to develop methods to allow its quantification. Reaction samples were analysed by LC-MS as

described in section **Error! Reference source not found.** in an attempt to detect 1,3-biphosphoglycerate. The LC-MS chromatogram from this analysis can be seen in the appendix Figure 6.24 where a signal of m/z 266.9 in negative ion mode is visible, suggesting the presence of 1,3-biphosphoglycerate in the reaction mixture.

Given the analytical challenge of detecting the cascade substrates and product, the successful preparation of the desired glycolytic metabolite was confirmed by using the cascade supernatant as a substrate for a PGK-catalysed ATP synthesis. In this PGK-catalysed reaction, each mole of 1,3-bisphosphoglycerate generates 1 mole of ATP from ADP. Production of 0.6 mM of ATP was possible from the supernatant of the TPI-GAPDH-LDH cascade after a reaction time of 30 min. The production of ATP validated the assumption that the three glycolytic enzymes can work together to prepare 1,3-biphsophoglycerate.

Following the optimisation, in batch, the TPI-GAPDH-LDH cascade was tested in a continuous flow coil reactor. Here, at the same reaction conditions as in batch, complete conversion of pyruvate was achieved at a flow rate of 3 $\mu L.min^{-1}$, corresponding to a residence time of 45. The supernatant of this flow reaction led to a 62.6% conversion of ADP into ATP, which is similar to the conversion obtained with the supernatant of the batch reaction. Although the results suggest no benefit in conducting the reaction in a continuous flow, the automation of flow systems and their ability to integrate analytics and downstream operation units could be essential to carry out posterior isolation of 1,3-biphosphoglycerate.

The developed cascade reaction could further benefit from an *in situ* pyruvate feeding strategy to increase the synthesis of 1,3-biphosphoglycerate. The following chapter will explore feeding-strategies in a fed-batch and in a continuous flow system.

4 Process Intensification Strategies in Continuous Flow Biocatalysis

4.1 Introduction

The use of microreactors in Chapter 2 allowed for coupling a chemical and enzymatic reaction with incompatible reaction conditions in yields that would not be feasible in a batch process. In Chapter 3, a multi-enzymatic cascade was developed and applied to a continuous flow system to facilitate continuous product removal and isolation. Although both cascades benefitted from being conducted in continuous flow systems, the products' concentrations were relatively low, and the resulting product streams still require offline downstream processing. Therefore, this chapter aims to investigate the feasibility of applying upstream and downstream process intensification strategies to the biocatalytic flow cascades presented in Chapters 2 and 3.

To increase the productivity of the Diels-Alder-transketolase (DA-TK) cascade developed in Chapter 2 a numbering-up approach was employed by doubling the productivity of the DA packed-bed reactor and by using two TK coil reactors instead of one. The flexibility and modular configuration of continuous flow systems allow for increased volumetric productivity simply by increasing the number of microchannels or by connecting several microreactors in series and/or in parallel. This numbering-up strategy enabled the reactions to be performed under identical conditions, maintaining the same mass transfer and mixing efficiencies of the single TK coil reactor optimised in Chapter 2 (Dong *et al.*, 2021).

Another strategy for upstream process intensification in flow biocatalysis is enzyme immobilisation. Although solubilised enzymes are used in microreactors, immobilisation of the biocatalysts onto solid supports may contribute to enzyme stability and lifetime. In a microreactor with immobilised enzymes, the reaction conditions, such as temperature and operational flow rate, can be easily adjusted to compensate for the enzyme deactivation and sustain the quality of product output. Additionally, enzyme immobilisation simplifies downstream processing by efficiently separating enzymes from products (Tamborini *et al.*, 2018; De Santis, Meyer and Kara, 2020). Therefore, since the chemoenzymatic cascade was conducted with TK lysate, an immobilisation strategy using poly(vinyl alcohol)-based hydrogel particles

was explored. This immobilisation method was based on the work of Fernandes *et al*. (Fernandes *et al*., 2008) and assayed for the continuous production of 1-(3,4-dimethyl-3-cyclohexen-1-yl)-1,3-dihydroxypropan-2-one (DCDHP) in a packed-bed reactor. While using immobilised biocatalysts can lead to longer stabilities, free enzymes can result in higher activities per area within the microchannel. Thus, a further product purification approach through enzyme retention was explored by integrating the DA-TK flow cascade with a micro-scale tangential flow filtration (TFF) downstream unit.

The modular nature of microreactors also facilitates the implementation of in situ feeding strategies to overcome substrate or end-product inhibition, shorten the reaction times and increase the overall yield of the process (Marques *et al.*, 2012; Lawrence *et al.*, 2013; Gruber *et al.*, 2017). Therefore, a feeding strategy was investigated to intensify the production of 1,3-biphosphoglycerate in the enzymatic cascade reaction developed in Chapter 3. Here, a feeding strategy mimicking a fed-batch reactor was explored in a continuous-flow system to meet the substrate requirements of lactate dehydrogenase (LDH) and drive the cascade towards the production of 1,3-biphosphoglycerate.

4.2 Materials and methods

All continuous flow reactions were conducted using glass syringes (Hamilton Bonaduz, Switzerland) and a Nemesys syringe pump (290N Nemesys, Cetoni GmbH, De).

4.2.1 Reagents and analysis

Unless otherwise stated, all commercially available chemicals were purchased from Sigma-Aldrich (Gillingham, UK), and used without further purification.

The D469T transketolase (TK) mutant used in this chapter was produced as described in section 2.2.3. The specifications of the commercial enzymes used in this chapter can be found in Table 3.1. Protein concentrations were measured by SDS–PAGE electrophoresis as described in section 2.2.4.1.

HPLC analysis of substrates used in the transketolase-catalysed reactions were performed on an Aminex HPX-87H column (Bio Rad, UK) as described in section 2.2.7.2. The product of the transketolase-catalysed reaction was quantified *via* a colorimetric assay as described in section 2.2.7.6 and its production was validated by a Thin layer chromatography (TLC) assay as described in section 2.2.7.5.

The product of the Diels-Alder reaction was quantified using ThermoScientific Trace 1300 flame ionization detector gas chromatograph (GC-FID) with a Rxi® 5 Sil MS column (Sigma Aldrich, Gillingham, UK) as described in section 2.2.7.3.

All substrates, co-factors and products catalysed by TPI, GAPDH, LDH and PGK were analysed by HPLC on a Synergy Hydro-RP column (Phenomenex, UK) as described in section 3.2.7.1.

4.2.2 DA-TK continuous flow reaction

A substrate solution of 200 mM of acrolein and 200 mM of 2,3-dimethylbutadiene in acetonitrile was pumped through the packed-bed reactor packed with aluminium chloride immobilised on silica gel (particle size 40-63 μm) at a flow rate of 4 $\mu L.min^{-1}$, which corresponds to a residence time of 2 hours. Samples were collected once the reaction reached completion and analysed by GC-FID for CCA production. The resulting flow was then diluted with 100 mM HPA in 25 mM Tris-HCl buffer pH 7 at

4 μL.min^{-1} and a transketolase (TK) solution of 1.43 U.mL^{-1}, previously incubated for 30 minutes with co-factors (ThDP 2.4 mM, and $MgCl_2$ 9.6 mM), at a flow rate of 32 μL.min^{-1} using a four-way connector before entering a coil reactor (PTFE, ID 0.75 mm, VWR International Ltd, Lutterworth, UK). Total flow rate entering the coil reactor was 40 μL.min^{-1} which corresponded to a residence time of 75 min. Samples from the coil reactor outlet were quenched via a 1:10 dilution with 0.1% trifluoroacetic acid, analysed by HPLC for HPA depletion and by colorimetric assay for DCDHP formation. The production of DCDHP was further confirmed through TLC analysis.

4.2.3 Chemoenzymatic continuous flow setup with 2 coil reactors

To increase the productivity of the continuous flow setup, the Diels-Alder packed-bed reactor was connected to two coil reactors instead of one. The chemoenzymatic cascade reaction was initiated by pumping an equimolar solution of 200 Mm of 2,3-dimethyl 1,3-butadiene and acrolein in acetonitrile at a flow rate of 4 μL.min^{-1} through the packed bed reactor. After 3 residence times the stream outlet of the packed bed was diluted with a 50 mM Tris-HCl buffer solution at pH 7 entering the system at a flow rate of 4 μL.min^{-1} and split into two flow streams. Each flow stream was then mixed with a 50 mM HPA (4 μL.min^{-1}) and a transketolase solution of 1.43 U.mL^{-1} (32 μL.min^{-1}) in a four-way connector, before entering the coil reactor. Samples were collected from the outlets of both coil reactors, quenched via a 1:10 dilution with 0.1% trifluoroacetic acid, and analysed by HPLC for HPA depletion and by colorimetric assay for DCDHP formation. The production of DCDHP was further confirmed by TLC analysis of the product stream.

4.2.4 TK immobilisation in PVA-based hydrogel particles

A simple approach for biocatalyst immobilization using PVA-based hydrogel particles was followed based on the work developed by Fernandes *et al.* (Fernandes *et al.*, 2008). To entrap transketolase in PVA, a LentiKat®Liquid (GeniaLab, Germany) solution was heated at 95°C and then cooled to 50°C. 0.5 ml of D469T transketolase mutant lysate was added to 4.5 ml of LentiKat®Liquid and mixed under magnetic stirring. This enzyme solution was then extruded through a needle into 150 mL of PEG 600 under mild magnetic stirring to form the enzymatic capsules. After a 2 h period of beads gelation, the hemispheric capsules were harvested and washed with acetate buffer, weighed after removal of excess buffer with qualitative filter paper. The

capsules were resuspended in the acetate buffer and either immediately used or stored at 4°C.

4.2.5 Determination of immobilisation yield and activity

Immobilisation yield was determined as the ratio between the specific activities of immobilised transketolase and the transketolase lysate. The activity of the transketolase mutant immobilised in PVA-based hydrogel particles was assayed in batch reactions with 0.329 g of the encapsulated enzyme, pre-incubated with co-factor solution (ThDP 2.4 mM, and $MgCl_2$ 9.6 mM) for 30 min in a 1.5 mL Eppendorf, with a 1 mL solution of 50 mM HPA and 3-FBA in 25 mM Tris-HCl pH 7. Samples were taken every minute for 3 minutes, quenched with 0.1% Trifluoroacetic acid (TFA) and analysed by HPLC for HPA and 3-FBA depletion.

4.2.6 Effect of solvent on the activity of immobilised enzyme

The effect of acetonitrile on the initial activity of immobilised TK was assessed in batch reactions with and without 10% (v/v) acetonitrile. Immobilised TK was incubated for 30 min with a co-factors solution (2.4 mM ThDP and 9.6 mM MgCl2) in 25 mM Tris-HCl at pH 7. The reactions conducted with 5 mM HPA and 10 mM racemic CCA. The CCA added was either commercially bought or produced by the Diels-Alder reaction conducted in the packed bed reactor in acetonitrile. Samples were taken in regular intervals of time for 2 hours, quenched via a 1:10 dilution with 0.1% trifluoroacetic acid, analysed by HPLC for HPA depletion and by colorimetric assay for DCDHP formation. Production of DCDHP was further confirmed by TLC analysis.

4.2.7 Packed bed reactor with immobilised TK setup

A 3 mL plastic syringe (Norm-Ject®, Germany) was used as a packed bed reactor (Figure 4.1). The reactor was packed to the limited with 1.835 g of immobilised TK and the volume of the packed bed reactor was determined to be 1 mL, by measuring the residence time of a 25 mM Tris buffer solution pumped through the reactor at a flow rate of 50 $\mu L.min^{-1}$.

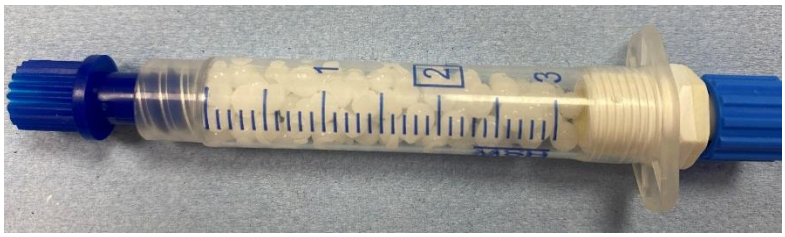

Figure 4.1: Packed bed reactor with immobilised TK

4.2.8 Integration of the DA packed bed reactor with the TK packed bed reactor

To integrate the Diels-Alder (DA) packed bed reactor with the packed bed reactor with immobilised TK a solution of 100 mM of 2,3-dimethyl 1,3-butadiene and acrolein in acetonitrile was pumped through the DA packed bed reactor at a flow rate of 4 $\mu L.min^{-1}$. After 3 residence times the output of the DA packed bed reactor was connected to the packed bed with immobilised TK using a T-shaped connector for the addition of HPA at 36 $\mu L.min^{-1}$. Total flow rate entering the TK packed bed reactor was 40 $\mu L.min^{-1}$ and contained 5 mM of HPA and 10 mM of racemic CCA in in 25 mM Tris-HCl buffer pH 7 with 10% (v/v) acetonitrile. Samples were collected from the outlet of the packed bed reactor, after 3 residence times and analysed by HPLC for HPA depletion and by colorimetric assay for DCDHP production, which was also confirmed by TLC analysis. SDS-PAGE gels were also run to determine the entrapment efficiency of the reactor.

4.2.9 Fabrication of the tangential flow filtration device

The tangential flow filtration (TFF) device was designed and fabricated previously to this research by the author of this thesis as described in Santos, 2016 (Santos, 2016).

All components of the continuous flow microfluidic reactor and filtration unit were designed using SolidWorks (Dassault Systèmes, Vélizy-Villacoublay, France) computer-aided design (CAD) software and machined from 4mm thick PMMA with a laser making head c25wc02 (Kyocera, Kyoto, Japan).

Both the retentate and permeate sides had a 1 x 1 x 45 mm channel milled into the centre and a 1 mm diameter hole at bond ends of the channel for fluid connection. The recess for the gasket was offset from this channel wall by 1 mm and was 0.75 mm

deep. The gaskets of poly(dimethylsiloxane) (PMDS) were made accordingly with the manufacturer's instructions (PDMS, Sylgard 184, Dow Corning, Midland, USA) from moulds of PMMA made with the laser cutting machine described previously. The membranes used for the filtration were cut to size from commercially available regenerated cellulose sheets of 10kDa (Ultracel R, Merck Millipore, UK) using a CO2 laser marking head (Synrad Inc., Mukilteo, WA, USA). The retentate and permeate side plates were clamped together by means of M3 screws placed along the filtration device, creating a reversible seal around the membrane.

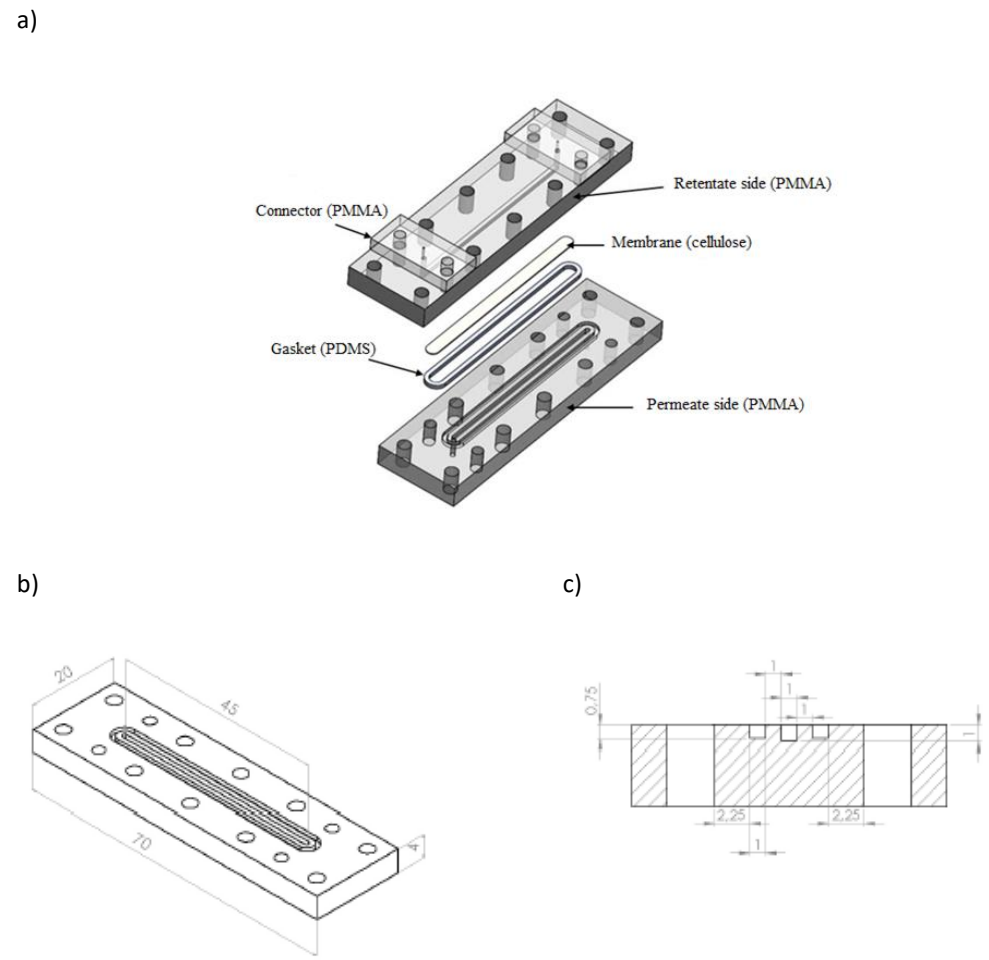

Figure 4.2: Tangential flow filtration device
a) Exploded view of tangential flow filtration device – the membrane fits inside the space created by the gasket and is sealed in place when permeate and retentate plates are clamped together by M3 screws; b) Isometric view of the permeate plate of the filtration device with dimensions in mm; c) Cross-sectional view of the retentate plate of the filtration device with dimensions of the microchannels in mm.

4.2.10 Burst pressure characterization

The seal achieved in the TFF device was dependent upon the pressure applied with the screws. A torque driver was used to apply different torques on the main assembly screws (10 – 40 Ncm) while the screws on the port attachments were screwed as tight as possible. The effect of the clamping pressure on the seal quality was evaluated by pumping air through the filtration device's retentate side while the membrane's permeate side was sealed. Pressure profiles were obtained through a pressure sensor connected with LabVIEW, showing a steady increase of pressure in the system with the volume of air pumped in and a sudden pressure drop indicating the bursting point of the device.

4.2.11 Back pressure measurements and proof of concept

The ability of the tangential flow filter to purify a solution of TK and DCDHP was investigated using the reaction media from a TK batch conducted containing 1.14 $U.mL^{-1}$ of TK and 5 mM of DCDHP. The reaction media was pumped through the retentate of the filtration device at flow rate of 40 $\mu L.min^{-1}$. To force the fluid flux across the membrane back pressure regulators of 20 and 40 psi (Upchurch Scientific R BPR, Oak Harbor, WA, USA) were attached to the retentate outlet. Samples were collected at the retentate and permeate outlets for analysis by colorimetric assay for DCDHP quantification and SDS–PAGE.

4.2.12 Integration of the DA-TK continuous flow cascade with the filtration device

An equimolar mixture of 100 mM of 2,3-dimethyl 1,3-butadiene and acrolein in acetonitrile was pumped through the Diels-Alder packed bed reactor packed with aluminum chloride at a flow rate of 4 $\mu L.min^{-1}$. After 3 residence times the packed bed reactor was connected to a coil reactor (PTFE, ID 0.75 mm, VWR International Ltd, Lutterworth, UK) for the TK reaction using a four-way connector. The outlet of the packed-bed reactor was diluted with 50 mM HPA in 25 mM Tris-HCl buffer pH 7 at 4 $\mu L.min^{-1}$ and a transketolase solution of 1.43 $U.mL^{-1}$, previously incubated for 30 minutes with co-factors, at a flow rate of 32 $\mu L.min^{-1}$. Total flow rate entering the coil reactor was 40 $\mu L.min^{-1}$. After 3 residence times the outlet of the coil reactor was connected to the inlet of the retentate side of the filtration device. The enzymatic

solution entered the filtration device at a flow rate of 40 μL.min^{-1} with a TK concentration of 1.14 U.mL^{-1} and a DCDHP concentration of 5 mM confirmed by colorimetric assay. A back pressure regulator of 40 psi (Upchurch Scientific R BPR, Oak Harbor, WA, USA) was attached to the retentate outlet. Samples taken from the retentate and permeate outlets were analysed by colorimetric assay and SDS-PAGE.

4.2.13 TPI-GAPDH-LDH batch reaction at different pyruvate concentrations

Reactions were carried out in 1.5 mL Eppendorfs containing 0.4 mM NAD+, 10 mM DHAP and with pyruvate concentrations between 3.3 and 10 mM in 50 mM glycine-phosphate buffer pH 8.5. The reactions were initiated by adding 1 U.ml^{-1} TPI, 1 U.ml^{-1} GAPDH and 16.7 U.ml^{-1} LDH. After 30 min, samples were collected and analysed by HPLC for pyruvate consumption.

4.2.14 TPI-GAPDH-LDH fed-batch reactions

Fed-batch reactions were conducted in 1.5 mL Eppendorfs. Each Eppendorf contained 1 mL reaction volume with 0.4 mM NAD+, 10 mM DHAP, 3.3 mM pyruvate, 1 U.ml^{-1} TPI, 1 U.ml^{-1} GAPDH and 16.7 U.ml^{-1} LDH in 50 mM glycine-phosphate buffer pH 8.5. Further solutions of pyruvate were added every 30 min for 90 min, for a final concentration of 3.3 mM. Endpoint samples before each addition of pyruvate were collected and analysed by HPLC.

4.2.15 *In situ* substrate supply

The setup comprised three coil reactors (PTFE, ID 0.75 mm, VWR International Ltd, Lutterworth, UK), connected by T-shape connectors (Upchurch Scientific, through VWR, Pennsylvania, USA), carrying out the TPI-GAPDH-LDH enzymatic reaction. Syringe pumps were connected to the reactors at different points in the fluidic path for the addition of pyruvate, as explained in the schematic Figure 4.3.

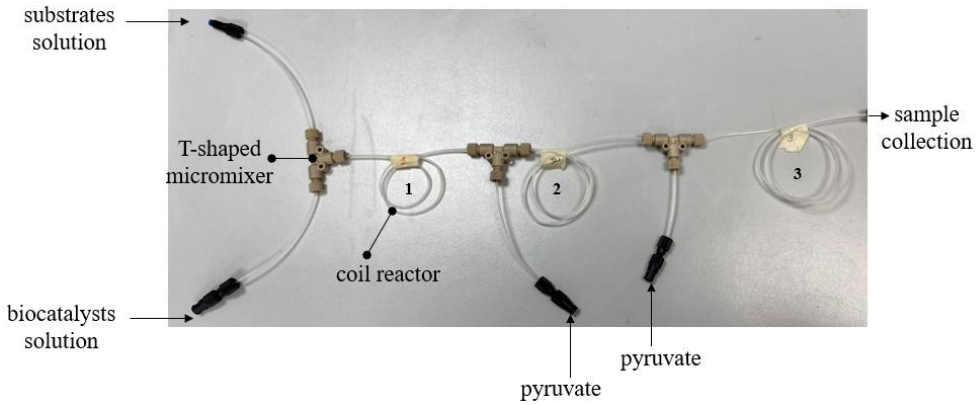

Figure 4.3: Schematic of the TPI-GAPDH-LDH cascade flow setup compromising four coil reactors.

The substrates solution contained 20 mM DHAP, 0.8 mM NAD+ and 6.6 mM pyruvate in 50 mM glycine-phosphate buffer pH 8.5; while the biocatalyst solution contained: 2 $U.ml^{-1}$ TPI, 2 $U.ml^{-1}$ GAPDH and 33.4 $U.ml^{-1}$ LDH dissolved in 50 mM glycine-phosphate buffer pH 8.5. Solutions were pumped at a flow rate of 3 $\mu L.min^{-1}$, into a T-shape micromixer connected to the 1st coil reactor. The final concentrations in the 1st coil reactor were: 10 mM DHAP, 0.4 mM NAD+, 3.3 mM pyruvate, 1 $U.ml^{-1}$ TPI and GAPDH, and 16.7 $U.ml^{-1}$ LDH. After three residence times, a 2nd coil was added. A 13.2 mM pyruvate solution was pumped through the 2nd coil at a flow rate of 1 $\mu L.min^{-1}$ for a total flow rate inside the coil of 4 $\mu L.min^{-1}$. After three residence times samples were collected from the outlet of the 2nd coil reactor, and a 3rd coil was added. A 16.5 mM pyruvate solution was pumped through the 3rd coil at a flow rate of 1 $\mu L.min^{-1}$ for a total flow rate inside the coil of 5 $\mu L.min^{-1}$. All coil reactors were cut to accommodate a residence time of 45 min, depending on the flow rate. Samples were collected from the outlet of each coil and analysed by HPLC.

4.3 Results and discussion

4.3.1 DA-TK continuous flow system performance with 200 mM of butadiene and acrolein

In previous experiments (Chapter 2), the DA packed bed reactor was run with a 100 mM 2,3-dimethyl-1,3-butadiene and acrolein solution in acetonitrile at a flow rate of 4 µL.min^{-1}. At these conditions, complete conversion of substrates to 100 mM CCA was achieved after a residence time of 2 h. The DA packed-bed reactor outlet was then connected with a TK coil reactor, where the complete conversion of HPA into 5 mM of DCDHP occurred in 75 min. In the work conducted by Pia Gruber (Gruber, 2019) the DA packed-bed reactor was run with substrate concentrations of 200 mM leading to complete conversion in 2 h. However, at these initial substrate concentrations, the DA-TK continuous flow setup only produced 3.5 mM of DCDHP. The low product yield was attributed to the low solubility of DCDHP. To verify this assumption, the DA-TK cascade was rerun starting with a 200 mM of 2,3-dimethyl-1,3-butadiene and acrolein solution. A schematic of this continuous flow setup can be seen in Figure 4.4.

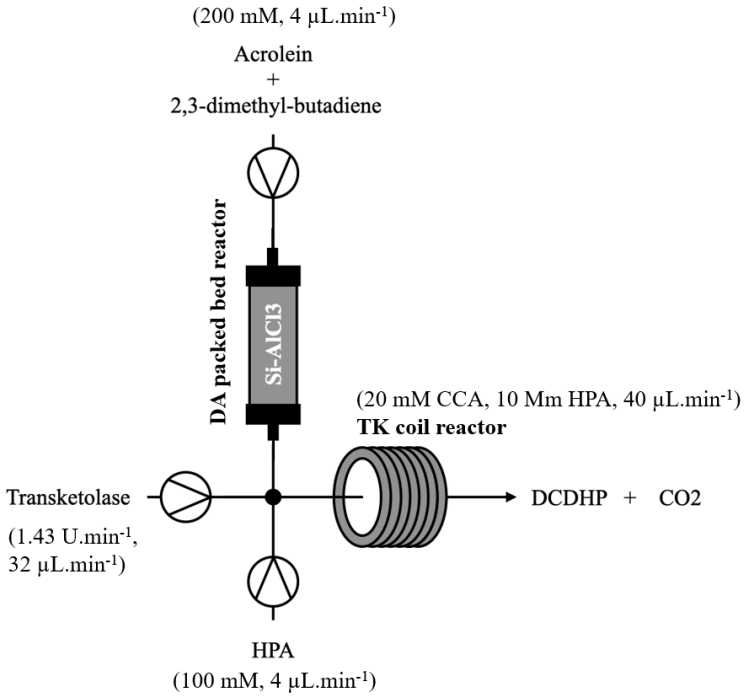

Figure 4.4: Schematic of the continuous flow setup of the chemoenzymatic reaction starting with 200 mM of acrolein and butadiene.

Operating the DA packed-bed reactor at a flow rate of 4 µL.min^{-1} and at double the concentration of substrates resulted in the double production of CCA (200 mM) in the same amount of time (2 h) as in Chapter 2. Samples taken from the outlet of the TK coil reaction revealed the production of DCDHP of 5.56 mM, which corresponds to only 56% of HPA conversion (Figure 4.5). However, no HPA was detected in the collected samples, which indicates that a complete conversion of HPA was achieved. Therefore, despite the 1.6-fold increase in DCDHP production versus the results reported by Pia Gruber the assumption that DCDHP has a solubility limit was confirmed.

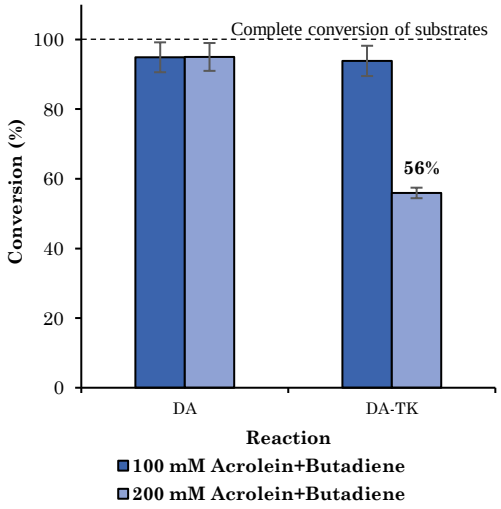

Figure 4.5: Comparison of conversions achieved in the DA and in the DA-TK reaction at starting concentration of 100 mM and 200 mM of acrolein and butadiene.
The data presented for each concentration is from 3 individual runs in each microreactor. Error bars represent mean ±SD (n=3).

4.3.2 Investigation of a numbering-up strategy to scale-up the DA-TK continuous flow system

Doubling the concentration of acrolein and butadiene fed to the DA-TK system proved ineffective in its attempt to increase the system's productivity. Although complete conversion at the double of substrates was achieved in the DA back-bed reactor, the product recovery from the TK reaction seems limited by the product solubility limit. To overcome this solubility issue, a numbering-up approach was investigated to scale-up the production of DCDHP without compromising its solubility by doubling the TK coil reactors connected to the DA packed-bed. A schematic of the setup compromising

1 packed-bed reactor, 1 T-shaped connector, 2 four-way connectors and 2 coil reactors can be seen in Figure 4.6. The outlet stream of the DA packed-bed suffered a 2-fold dilution with a feeding solution of Tris buffer at a flow rate of 4 µL.min^{-1} before being bifurcated and diluted again by an HPA and a TK solution in each of the four-way connectors before entering the coil reactors. These dilutions are needed to dilute the CCA concentration and keep the acetonitrile percentage in the TK reaction medium at 10%(v/v). Thus, the reaction conditions in each coil reactor are the same as the ones optimised in Chapter 2. To ensure uniform and precise flow in each coil reactor, samples were collected from the coil reactors' outlets for a certain amount of time to calculate the operating flow rate at each coil. As expected, each coil reactor worked at a flow rate of 40 µL.min^{-1}. A summary of the reaction conditions in each step of the continuous flow system is presented in Table 4.1.

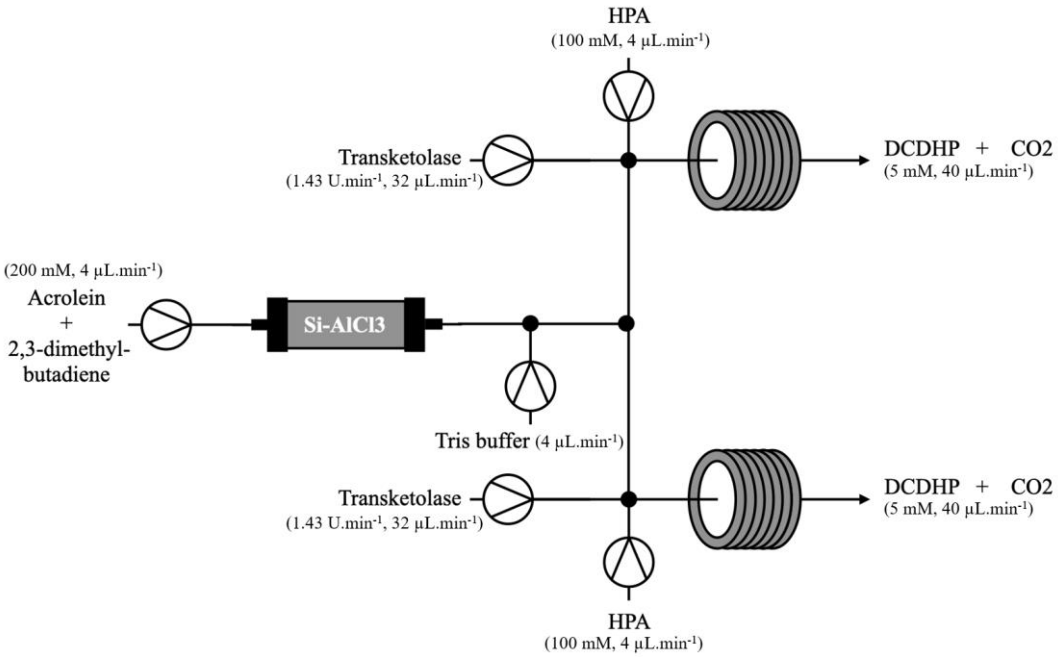

Figure 4.6: Chemoenzymatic continuous flow setup with 2 coil reactors.

Table 4.1: Experimental conditions in the DA-TK continuous flow system with 2 coil reactors.

	Diels-Alder packed-bed reactor	TK coil reactors (2)
Residence time	120 min	75 min
Flow rate	4 µL.min^{-1}	40 µL.min^{-1}
Substrates input	200 mM Acrolein and butadiene	5 mM HPA, 10 mM racemic CCA
Reaction medium	Acetonitrile	Tris-HCl buffer pH 7 with 10% (v/v) acetonitrile
Product output	200 mM CCA	5 mM DCDHP
Conversion	95 ± 4 %	94 ± 4 % (conversion of HPA)

Samples taken of the outlets of the coil reactors were analysed by HPLC for HPA depletion and by thin-layer chromatography (TLC) to confirm the presence of DCDHP. Figure 4.7 shows the product stream's TLC analysis from both coil reactors, showing a clear spot at the same Rf value as the DCDHP standard. A colorimetric assay further determined DCDHP concentration in the samples at 485 nm, to be 5 mM. The continuous flow system was run for ~200 min (excluding the equilibration time) and led to the production of 2 flow streams with 5 mM of DCDHP each in the same amount of time as the system operated in Chapter 2 that led to the production of 1 flow stream with 5 mM DCDHP. This means that the productivity was successfully increased by numbering-up the coil reactors.

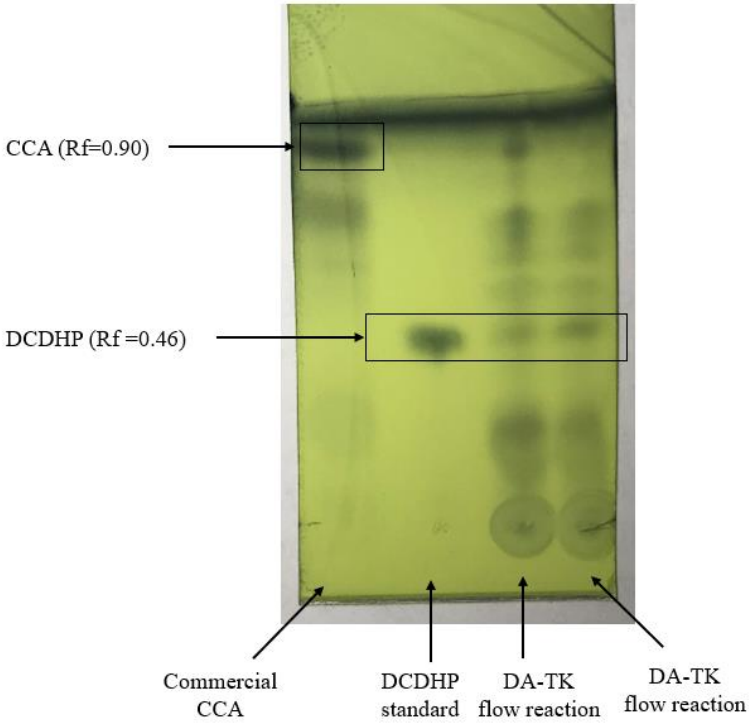

Figure 4.7: DCDHP production in each coil reactor.
The TLC plate shows commercial CCA in the first lane, a sample of DCDHP in the second lane, and the third and fourth lane were stained with supernatants from the TK flow reactions from each coil when coupled with a DA packed-bed reactor. There is a clear DCDHP spot in the third and fourth lane, confirming the presence of the product in both coil reactors.

4.3.3 TK immobilization in batch

Many techniques are used to immobilise enzymes in microreactors (Table 1.2) to help achieve better productivity and enhanced yields. Here, an immobilisation technique was attempted to entrap TK in PVA-based hydrogel capsules and facilitate the downstream purification processing of DCDHP.

The TK lysate produced as described in section 2.2.3 was immobilised in PVA particles following a similar protocol to the one developed by Fernandes *et al.* (Fernandes *et al.*, 2008). The efficiency of the immobilisation method was determined by the following equation:

$$\text{Immobilisation yield (\%)} = \frac{A_{imm}}{A_{free}} \times 100 \quad (4.1)$$

Where A_{imm} is the specific activity of immobilised TK and A_{free} is the specific activity of the TK lysate (Rahim *et al.*, 2013). The activity of the immobilised TK was determined in batch reactions with a 50 mM solution of HPA and 3-FBA in 25 mM Tris-HCL pH 7, with 0.329 g of the encapsulated enzyme, pre-incubated with co-factor solution (ThDP 2.4 mM, and $MgCl_2$ 9.6 mM) for 30 min. No traces of protein were observed in the supernatants resulting from the batch with immobilised TK, and the immobilisation yield was determined to be 27±5 %.

Since the aim was to use the immobilised TK to convert the CCA produced in the DA packed-bed reactor into DCDHP, the effect of acetonitrile on the immobilised TK was assessed. Figure 4.8 presents the results from this assay, showcasing the obtained time-course reaction profiles for batches with 10 mM of commercial CCA and 5 mM of HPA with and without 10 % (v/v) of acetonitrile. The HPA conversions obtained after 120 minutes in batches with and without acetonitrile were 45% and 48%, respectively.

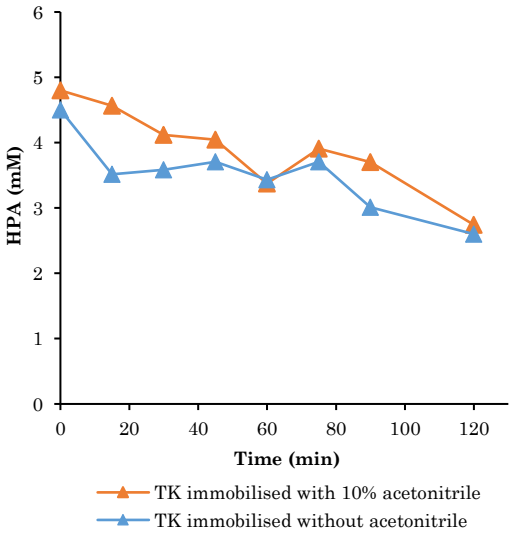

Figure 4.8: Activity profile for immobilised TK in batch with and without acetonitrile.
The HPA depletion profiles suggest that the activity of the immobilised TK is not affected by the presence of the organic solvent up to 10 % (v/v); Error bars represent mean ±SD (n=3).

4.3.4 DA-TK continuous flow cascade with immobilised catalysts

A plastic syringe of 3 mL was used as a packed-bed reactor and filled to the limit with 1.835g of hemispheric particles of immobilised TK. The void fraction (ε) was determined experimentally by pumping a 25 mM Tris buffer solution through the

packed-bed reactor at a flow rate of 50 µL.min^{-1} and measuring the residence time. The following equation calculated the void fraction:

$$\varepsilon = \frac{\text{Volume of void}}{\text{Reactor volume}} \tag{4.2}$$

The volume of the pack back reactor was determined to be 1 mL, and therefore the packed-bed void fraction was determined to be 0.33.

In order to investigate the continuous synthesis of DCDHP in a DA-TK continuous flow setup with both catalysts immobilised, the outlet of the DA packed-bed was connected via a T-shaped connector to the inlet of the immobilised TK packed-bed reactor. A schematic of the continuous flow setup is presented in Figure 4.9. A solution of 100 mM of 2,3-dimethyl 1,3-butadiene and acrolein in acetonitrile was pumped through the DA packed-bed reactor at a flow rate of 4 µL.min^{-1}. After 3 residence times, the output of the DA packed-bed reactor was diluted with an HPA solution at 36 µL.min^{-1} before entering the immobilised TK packed-bed reactor. The total flow rate entering the TK packed-bed reactor was 40 µL.min^{-1} and contained 5 mM of HPA and 10 mM of racemic CCA in 25 mM Tris-HCl buffer pH 7 with 10% (v/v) acetonitrile. Samples were collected from the outlet of the packed bed reactor after 3 residence times and analysed by HPLC and colorimetric assay, confirming the production of 1.8 ±0.35 mM DCDHP.

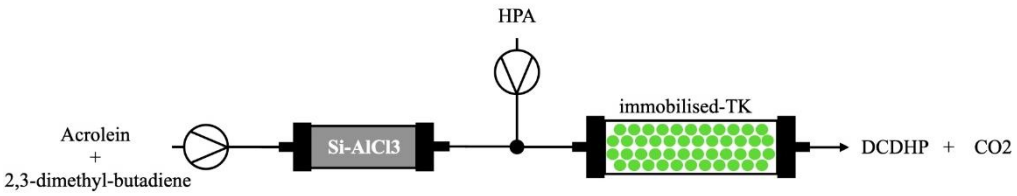

Figure 4.9: Schematic of the DA-TK continuous flow setup with both catalysts immobilised in packed-bed reactors.

Table 4.2: Operational condition and HPA conversion in the DA-TK continuous flow setup with immobilised catalysts.

Flow rate (µL.min^{-1})	Residence time (min)	Conversion (%)
40	25	40±7

The operational efficiency of the packed-bed reactor during 75 min at a flow rate of 40 µL.min^{-1}, was determined to be 100% since no enzyme leakage was detected in the samples collected from the outlet of the packed-bed reactor at these operational conditions. The entrapment efficiency of the enzyme was calculated using the following equation:

$$\text{Entrapment Efficiency (\%)} = \frac{C_{en} - C_{un}}{C_{en}} \times 100 \quad (4.3)$$

Where C_{en} is the enzyme initial amount and C_{un} is the enzyme amount in the outlet of packed-bed reactor.

4.3.5 Tangential flow filtration device characterisation

A TFF device previously designed and fabricated by the author of this thesis (Santos, 2016) was integrated in-line with the DA-TK continuous flow system developed in Chapter 2, in order to separate the TK lysate from the synthesised DCDHP. A TFF is a process approach used to separate biomolecules based on their size. It differs from dead-end or standard filtration because the material passes across the membrane rather than through it. In this case, the goal is to selectively recover the DA-TK reaction's supernatant in the filtration's permeate and retain the transketolase lysate.

The tangential flow filtration was fabricated in PMMA, as described in section 4.2.9. The design was adapted from that of O'Sullivan and co-workers (O'Sullivan *et al.*, 2012) to allow for the sealing of the membrane by clamping and facilitating the use of any membrane type. The device was composed of two parts, the permeate and the retentate side, each with a straight channel in the middle and machined from 4 mm thick PMMA. The retentate part contained a recess around the channel to hold a PDMS gasket around a filter membrane. The plates were clamped together through M3

screws along the edges, creating a reversible seal around the membrane. A schematic of the device can be seen in Figure 4.10.

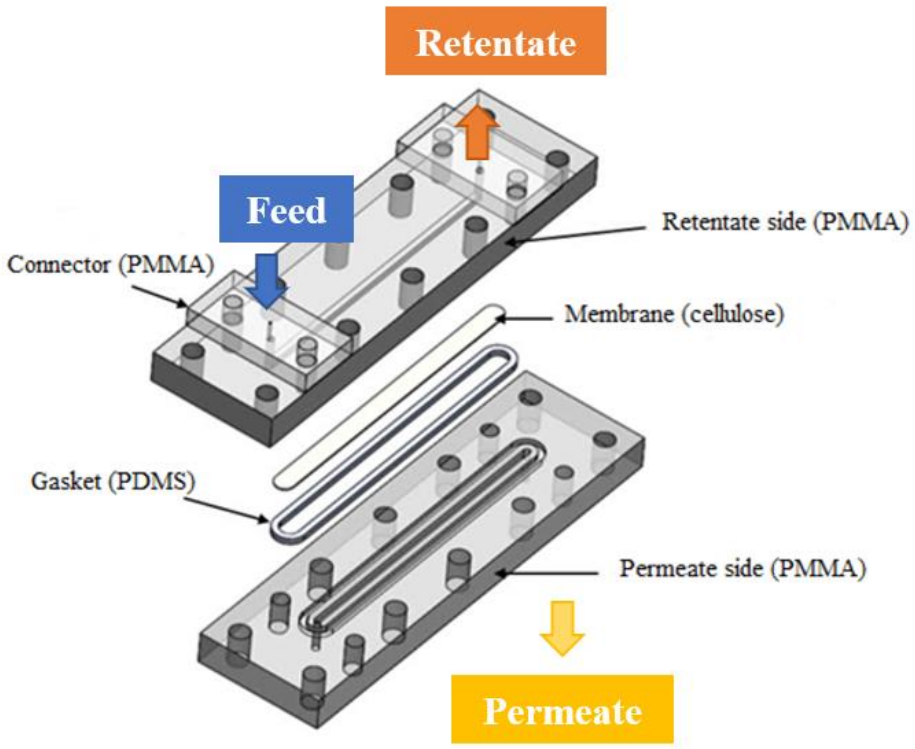

Figure 4.10: Schematic of the design of the tangential flow filtration device.

In order to verify the complete sealing of the membrane and determine the maximum pressure handled by the device, a pressure sensor was attached to the outlet of the retentate, and air flowed into the inlet of the retentate side with a syringe pump while the permeate side was capped off. Since the device's seal depended on the clamping pressure applied by the screws, different torques were applied to the screws (10 – 40 Ncm). Figure 4.11 shows the pressure profiles obtained through a pressure sensor connected with LabVIEW, showing a steady increase of pressure in the system with the volume of air pumped in and a sudden pressure drop indicating the bursting point of the device. Using a 20 Ncm torsion creates a more effective seal than the other torques applied, sealing the device up to a pressure of 100 psi.

a)

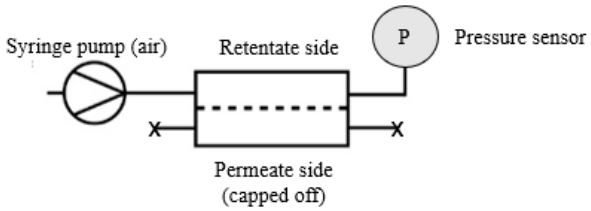

b)

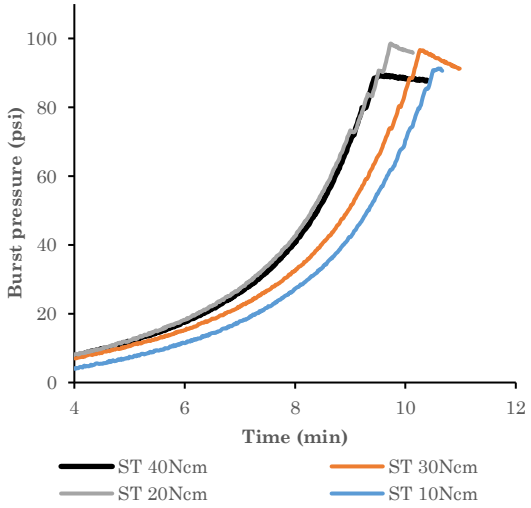

Figure 4.11: Tangential flow filtration device burst pressure characterisation. a) Schematic of the setup used to measure the burst pressure of the tangential flow filtration device; b) Pressurisation profiles recorded after device was sealed with various assembly screw torques; ST refers to the screw torque on device and torque units are Ncm; these profiles were obtained by the author of this thesis before this research in Santos, 2016 (Santos, 2016).

4.3.6 Tangential flow filtration device proof of concept

The ability of the filtration device to remove the transketolase lysate from the outlet of the TK coil reactor of the DA-TK continuous flow system developed in Chapter 2 was tested using a solution from a TK batch containing 1.14 $U.mL^{-1}$ of TK and 5 mM DCDHP. This solution was fed to the retentate side of the filtration at a flow rate of 40 $\mu L.min^{-1}$ with different back pressure regulators, one of 20 psi and another of 40 psi, attached to the retentate outlet. The use of back pressure regulators on the retentate side was necessary in order to apply resistance and force the fluid across the membrane. The permeate and retentate volume outputs were measured and used to

calculate the flow rate of each outlet stream at different points in time. Figure 4.12 shows the results of this experiment. As the filtration progresses, the membrane gets fouled, and fluid emerges from the retentate side. The appearance of retentate later in the filtration process indicates a higher fluid flux across the membrane and, therefore, a higher amount of DCDHP in the permeate. Thus, of the two back pressure regulators tested, a back pressure of 40 psi led to a higher permeate volumetric output.

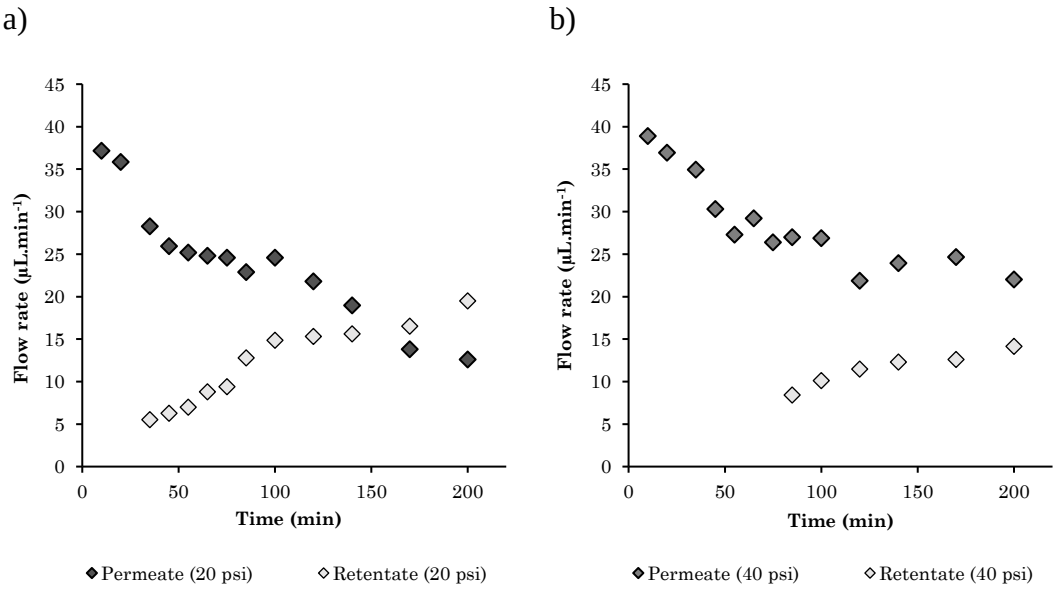

Figure 4.12: Back-pressure effect on permeate and retentate flow rates over filtration time.
a) Permeate and retentate profiles with a back pressure regulator of 20 psi; b) Permeate and retentate profiles with a back pressure regulator of 40 psi;

The samples obtained from both the permeate and retentate outlets of the filtration device were analysed using by colorimetric assay. The results showed that similar concentrations of DCDHP were present in both the permeate and retentate outputs as those initially fed into the filtration device. This observation indicates that the compound has the capability to traverse the membrane and become separated from the TK lysate.

The collected samples were also subjected to analysis using SDS-PAGE. The results, as depicted in Figure 4.13, indicate the absence of any proteins at the outlet of the device. This finding confirms the membrane's capacity to completely retain the proteins, irrespective of the back pressure regulator employed. Additionally, the

presence of other proteins in the samples, besides TK, is evident. These proteins could potentially contribute to the membrane's susceptibility to clogging.

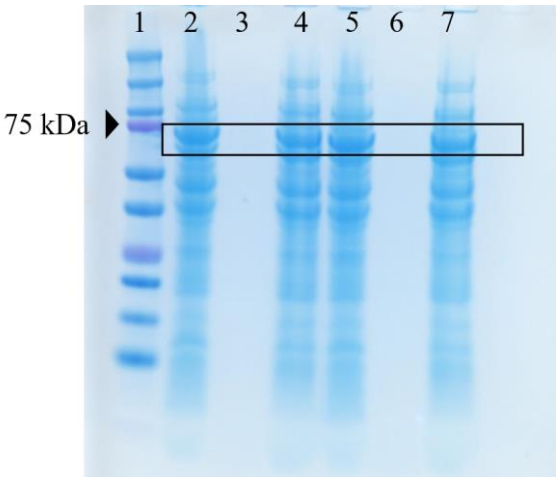

Figure 4.13: SDS-PAGE gel showing protein in the retentate outlet after filtration with back pressure regulators of 20 and 40 psi.
Lane 1: protein ladder; lane 2: feeding solution; lane 3: permeate solution with a back pressure regulator of 20 psi; lane 4: retentate solution with a back pressure regulator of 20 psi; lane 5: feeding solution; lane 6: permeate solution with a back pressure regulator of 40 psi; lane 7: retentate solution with a back pressure regulator of 40 psi; lane 3 and 6 do not contain any proteins, indicating that the TK is completely retained by the membrane.

4.3.7 DA-TK continuous flow cascade integrated with a tangential flow filtration device

The ability of the TFF to be integrated in-line with the DA-TK continuous flow system developed in Chapter 2 was investigated. To do this, the outlet of the TK coil reactor was connected in series with the inlet of the retentate side of the filtration device as exemplified in Figure 4.14. The DA-TK continuous flow system was run at the optimised conditions determined previously in Chapter 2. Confirmation of complete conversion of 5 mM HAP into DCDHP in the TK coil reactor was verified by a colorimetric assay before connecting the coil with the filtration device. The reaction stream contained 5 mM DCDHP and 1.14 $U.mL^{-1}$ of TK and entered the filtration device at a flow rate of 40 $\mu L.min^{-1}$. A back pressure regulator of 40 psi was fitted to the retentate outlet to drive the flux across the membrane and maximise the permeate volumetric yield and, therefore, the amount of DCDHP recovered.

The filtration was operated for 200 min, during which the permeate output declined by half due to the fouling of the membrane. Figure 4.15 presents the permeate volumetric output as a percentage of the total output volume of the TFF unit when connected with the DA-TK continuous flow system. An average permeate yield of 70% was achieved during the operational time of 200 min. Complete separation of the TK lysate from the reaction stream was achieved, and 5 mM of DCDHP were detected on the permeate and retentate outputs.

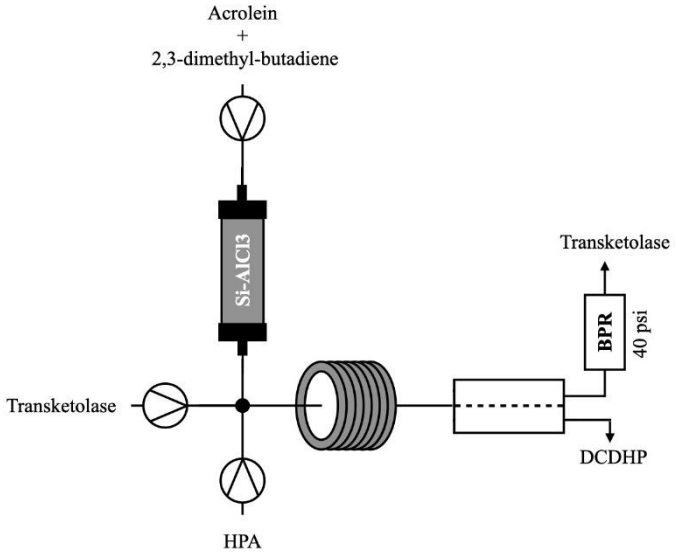

Figure 4.14: Schematic of the DA-TK continuous flow system integrated with a tangential flow filtration device.

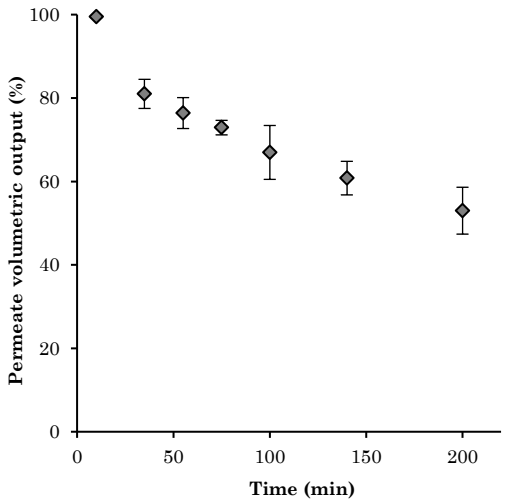

Figure 4.15: Permeate output as a percentage of the total volume output from a tangential flow filtration device connected to the DA-TK flow cascade to produce DCDHP.
Amount of fluid recovered in the permeate as a percentage of the output from the permeate and the retentate outlets during a filtration time of 200 min; Error bars represent mean ±SD (n=3).

4.3.8 Fed-batch strategy for enzymatic production of 1,3-biphosphoglycerate

In previous experiments (see Chapter 3), the TPI-GAPDH-LDH cascade reaction showed promise in synthesising 1,3-biphosphoglycerate. Complete conversion of 3.3 mM of pyruvate was achieved from a starting concentration of 10 mM DHAP in the TPI-GAPDH-LDH cascade reaction, both in batch and in a continuous flow microreactor (Figure 4.16). The results suggested that adding an LDH reaction to the TPI-GAPDH coupled reaction to regenerate NAD+ pushes the reaction equilibrium towards 1,3-biphosphoglycerate production.

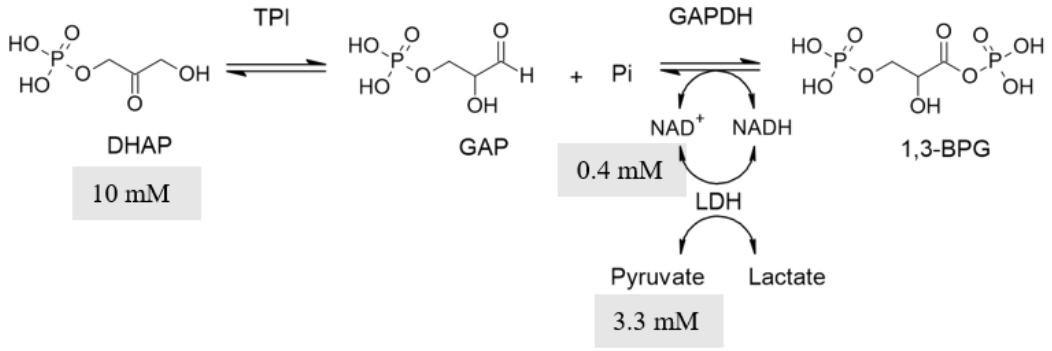

Figure 4.16: Schematic of the TPI-GAPDH-LDH cascade reaction with the concentrations on the substrates used.

To investigate the effect of pyruvate concentration on the TPI-GAPDH-LDH cascade, batch reactions were run with 3.3, 5 and 10 mM of pyruvate, starting with 10 mM of DHAP and 0.4 mM of NAD+. Figure 4.17 presents the results of this experiment. By increasing the input of pyruvate from 3.3 mM to 5 mM, complete conversion was achieved in 50 minutes, and a further increase to 10 mM led to a ~70% conversion after 120 minutes.

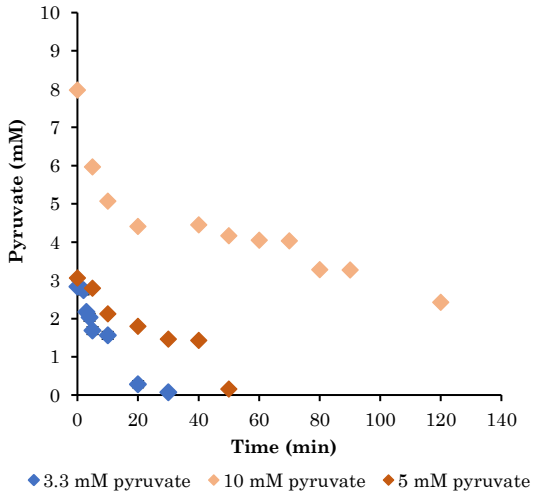

Figure 4.17: TPI-GAPDH-LDH batch reaction at different pyruvate concentrations.

The conversion of pyruvate by LDH depends on the conversion rate of GAP to 1,3-biphosphoglycerate by GAPDH, which is dependent on the conversion rate of DHAP

to GAP by TPI. Given the complex kinetics of the reaction system, a fed-batch strategy for the stepwise addition of pyruvate could be an effective strategy to increase the overall reaction rate. To investigate this, a constant concentration of pyruvate of 3.3 mM was fed every 30 minutes into a batch reaction with TPI-GAPDH-LDH starting with 10 mM DHAP and 0.4 mM NAD+. Figure 4.18 shows the results of this investigation. The 1st addition of pyruvate occurred at t=0, and as expected, complete conversion was achieved in 30 min. The 2nd addition of pyruvate led to approximately 66% conversion and the 3rd addition to 34% (Table 4.3). In total 9.9 mM of pyruvate were added, resulting in a 70.7% conversion in 90 min (Table 4.4). Compared with the results shown above for the TPI-GAPDH-LDH batch reaction, the use of a fed-batch strategy resulted in a faster conversion of pyruvate.

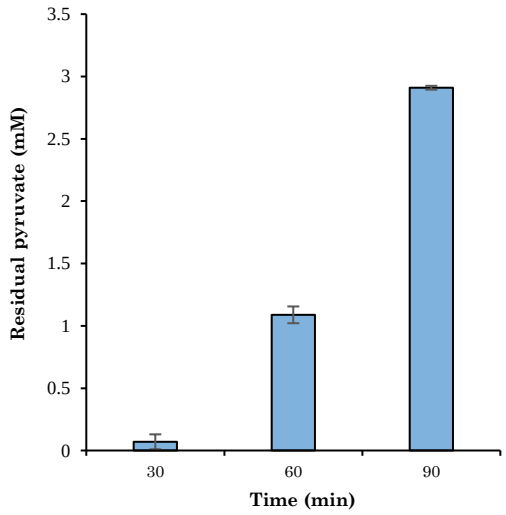

Figure 4.18: Endpoint concentrations of pyruvate from fed-batch synthesis of 1,3-biphosphoglycerate.
Stepwise addition of pyruvate to the reaction mixture every 30 minutes for 90 min; pyruvate concentration in reaction mixture was kept at 3.3Mm; Error bars represent mean ±SD (n=3).

Table 4.3: Pyruvate input and consumption in the TPI-GAPDH-LDH fed-batch reaction.

	1st addition of pyruvate	2nd addition of pyruvate	3rd addition of pyruvate
Reaction volume (mL)	1	1.05	1.100

Pyruvate concentration after addition (mM)	3.3	3.3	3.3
Pyruvate consumed (mM)	3.3	2.2	1.5
Residual pyruvate (mM)	0	1.1	2.9

Table 4.4: Pyruvate conversion in 90 min in the TPI-GAPDH-LDH fed-batch reaction.

Total amount of pyruvate added (mM)	9.9
Total amount of pyruvate consumed (mM)	7
Conversion in 90 min	70.7 %

To validate the assumption that the conversion of pyruvate is linked to production of 1,3-biphosphoglycerate, a PGK assay was performed with the supernatants of the TPI-GAPDH-LDH fed-batch reaction after each pyruvate addition as described in section 3.2.6. Figure 4.19 shows the results of this assay. The production of ATP validates the presence of 1,3-biphosphoglycerate in the reaction mixture. Complete conversion of ADP (1 mM) to ATP occurred with the supernatants from the fed-batch reactions with 2 and 3 additions of pyruvate versus a 60.3% conversion from the supernatant with only one addition of pyruvate. The higher production of ATP achieved at higher pyruvate concentrations indicates an increase in 1,3-biphosphoglycerate synthesis.

a)

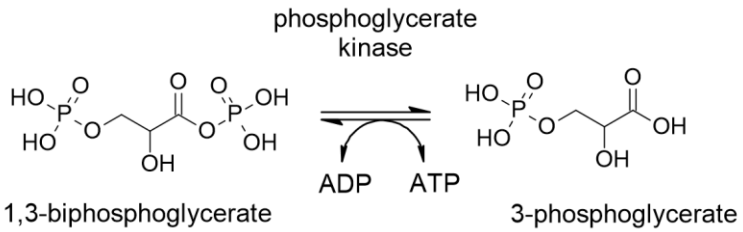

b)

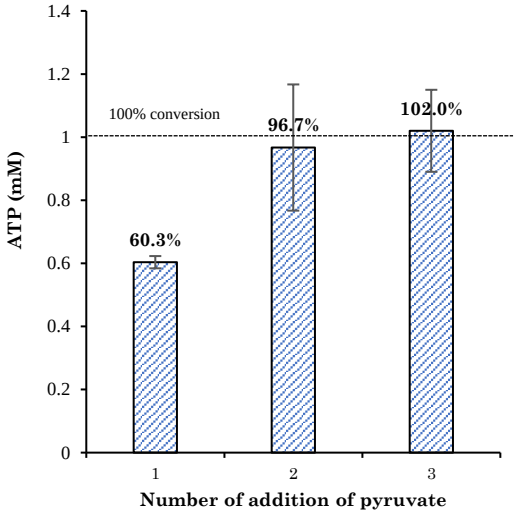

Figure 4.19:PGK assay in batch using the supernatant of the TPI-GAPDH-LDH fed-batch reaction.
a) Reaction scheme of the PGK assay; b) ATP synthesis by PGK from 1 mM ADP and 50%(v/v) of the TPI-GAPDH-LDH fed-batch reactions supernatants after each addition. Error bars represent mean ±SD (n=3).

4.3.9 *In situ* substrate supply strategy for flow production of 1,3-biphosphoglycerate

A continuous flow system with multiple inputs of pyruvate was designed to mimic the fed-batch process. The setup comprised three coil reactors connected by T-shape connectors through which the pyruvate was fed to the reaction mixture, as explained in Figure 4.20. The reaction was initiated by pumping a substrates solution (20 mM DHAP, 0.8 mM NAD+ and 6.6 mM pyruvate) and a biocatalysts solution (2 U.ml-1 TPI, 2 $U.ml^{-1}$ GAPDH and 33.4 U.ml-1 LDH) at a combined flow rate of 3 $\mu L.min^{-1}$

through the first coil reactor for 45 min. To minimise the dilution of the enzymes and product in the mixture, the pyruvate was fed into the system at a flow rate of 1 µL.min^{-1}. The feeding concentration of pyruvate (i.e. the concentration in the reaction mixture after the input of pyruvate) was set at 3.3 mM. The coil reactors used varied in length to accommodate for the increase in flow rate (

Table 4.5).

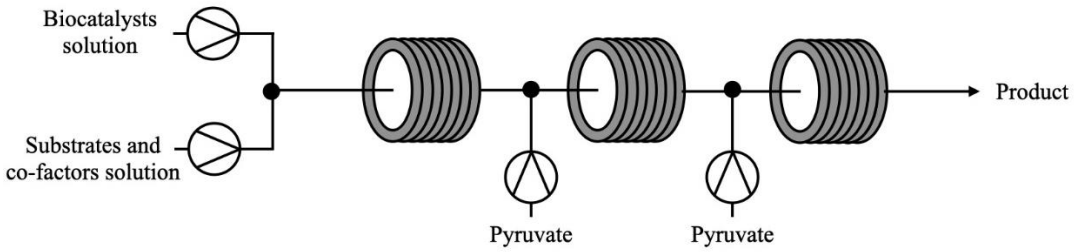

Figure 4.20: Schematic of the flow set up with *in situ* substrate supply of pyruvate.

Table 4.5: Volume and flow rate of each coil reaction considering the input of pyruvate.

	1st coil reactor	2nd coil reactor	3rd coil reactor
Volume (µL)	135	180	225
Flow rate	3	4	5
Input of pyruvate (mM)	6.6	13.2	16.5
Residence time	45	45	45

Figure 4.21a) shows the endpoint concentrations of pyruvate in each coil reactor. In the 1st coil reactor, complete conversion of the pyruvate occurred. In the 2nd and 3rd coil reactor, pyruvate conversion was 67% and 21%, respectively. A total of 9.9 mM of pyruvate were fed to the continuous flow system, resulting in a 64% conversion in 135 min. A PGK assay was conducted with the supernatant of the outputs of each coil reactor to confirm the presence of 1,3-biphosphoglycerate. The results suggest no improvement in the conversion of pyruvate or in the ATP production in the flow

system compared with the fed-batch approach. Both systems can synthesise amounts of 1,3-biphosphoglycerate capable of converting 1 mM ADP into 1 mM ATP in a PGK-catalysed reaction. Considering that the PGK assay was conducted with only 50%(v/v) of the TPI-GAPDH-LDH reaction supernatants, it possible that the enzymatic cascade can synthesise more than 1 mM of 1,3-biphosphoglycerate, either in fed-batch or in the continuous flow system. However, to properly access the production of 1,3-biphosphoglycerate in the developed enzymatic cascade, further kinetic studies through the development of analytics for substrate and product quantification are necessary.

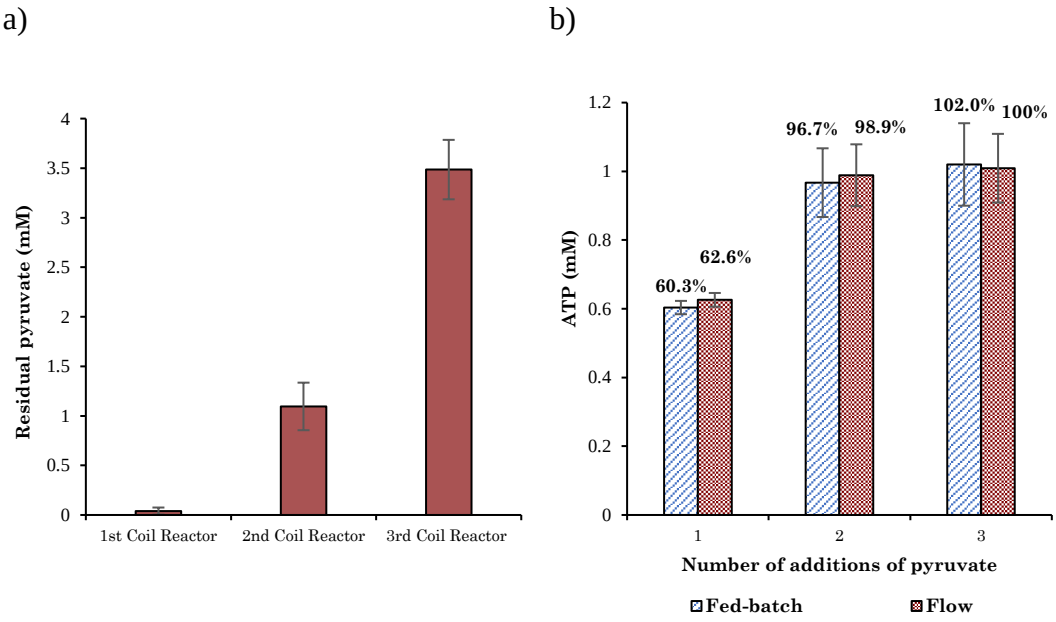

Figure 4.21: TPI-GAPDH-LDH cascade reaction with *in situ* supply of pyruvate in continuous flow.
a) Endpoint concentration of pyruvate in each coil reactor; b) Comparison of ATP synthesis in batch by PGK from 1 mM ADP and supernatants from TPI-GAPDH-LDH fed-batch and flow reactions; ATP synthesis by PGK from 1 mM ADP and 50%(v/v) of the TPI-GAPDH-LDH flow reaction supernatant at different flow rates; conversion of ADP into ATP is indicated in percentage for each residence time of the reactions presented in a); Error bars represent mean ±SD (n=3).

4.4 Conclusion

In this chapter, process intensification strategies for continuous flow biocatalysis have been shown. The first part of this chapter focused on increasing the productivity of the chemoenzymatic cascade developed in Chapter 2. Initial attempts at doubling the DA-TK cascade's production were unsuccessful due to the solubility limit of DCDHP. To overcome this issue, a numbering-up approach was developed based on the ability of the DA packed-bed reactor to produce double the amount of CCA and the facile parallel arrangement of two identical TK coil reactors. This approach doubled the capacity of the DA-TK continuous flow system to synthesise DCDHP. The numbering-up approach, also known as the parallel arrangement of a number of identical reactors, is a standard method in the scale-up of microreactors. This approach allowed for upscaling the synthesis of DCDHP without the need to re-optimise the TK reaction conditions. The operation of 2 TK coil reactors simultaneously for 75 min led to the production of 5 mM in the stream of each TK coil reactor. This means that the parallelisation of 2 coil reactors successfully increased the system's productivity. Despite the increase in DCDHP production, the presented strategy is far from meeting industrial needs. However, the developed method indicates that the use of multiple flow microreactors in parallel is effective for the scaling-up of flow synthesis.

Strategies for *in situ* product purification *via* enzyme immobilisation and integration with a downstream filtration unit were also demonstrated. TK was immobilised in PVA-based hydrogel particles, retaining the activity of 27±5 %. A conversion of 45% and 48% of 5 mM HPA was achieved in 120 min in batch reactions with and without 10% (v/v) acetonitrile, respectively. As a proof of concept, a plastic syringe of 3 mL was used as a tubular reactor and packed with 1.835g of immobilised TK in PVA. This packed-bed reactor's void fraction (ε) was determined to be 0.33. In order to investigate the continuous synthesis of DCDHP in a DA-TK continuous flow setup with both catalysts immobilised, the outlet of the DA packed-bed developed and optimised in Chapter 2 was connected using a T-shaped connector to the inlet of the immobilised TK packed-bed reactor. The continuous flow system led to a 40% conversion of HPA, producing 1.8 ±0.35 mM of DCDHP. Although activity and diffusion limitations were observed, the immobilised TK packed-bed reactor

displayed high operational stability when operated for in three consecutive flow runs at 40 µL.min^{-1} with no significant loss of activity and no enzyme leakage detected.

To effectively separate the TK from the product stream without compromising the enzyme activity and stability, a tangential flow filtration device was fabricated in PMMA and used in-line with the DA-TK continuous flow setup presented in Chapter 2. The filtration device was designed to seal the membrane between the retentate and permeate parts by screwing the parts together, thereby facilitating the change of the membrane as needed. A strong seal was achieved using a torsion of 20 cN-m on all assembly screws, giving a burst pressure of 100 psi. When connected in-line with the DA-TK continuous flow setup, the filtration device was operated with a back pressure regulator of 40 psi fitted to the retentate outlet to drive the flux across the membrane and maximise the permeate volumetric yield. Complete separation of the TK lysate from the product stream was achieved, affording an average permeate yield of 70% during the operational time of 200 min. The yield of DCDHP recovery was, therefore, dependent on the division of fluid between the permeate and retentate. The operability time of the membrane could be extended by utilizing purified TK protein in the reaction. The presence of other proteins in the lysate contributes to membrane clogging, thereby affecting the yield of recovered DCDHP.

Nevertheless, the coupling of a DA packed-bed reactor with a TK coil reactor with an in-line filtration unit for the continuous synthesis of DCDHP showcases the flexibility of continuous flow systems to cascade reactions and integrate separation units. Thus, the developed system paves the way towards realising complete biocatalytic processes from upstream to downstream in continuous flow.

The second part of this chapter dealt with the optimisation of the TPI-GAPDH-LDH cascade designed in Chapter 3 to synthesise 1,3-biphosphoglycerate. In this cascade, it is assumed that pyruvate consumption is directly related to the production of 1,3-biphosphoglycerate. Therefore, the pyruvate requirements of the cascade were optimised in different operation modes. First, the conversion of pyruvate was investigated in batch, where a 70 % conversion of 10 mM of pyruvate was achieved in 120 min. Next, a stepwise addition of pyruvate in a fed-batch was investigated, where 3.3 mM of pyruvate were added to the cascade every 30 min for 90 min. In total, 9.9 mM of pyruvate were added to the cascade leading to a 70% conversion in

90 min. The results indicated that adding the pyruvate stepwise shortens the reaction time. Thus, a feeding strategy mimicking the fed-batch reactor was explored in a continuous-flow system to meet the pyruvate requirements and drive the cascade towards the production of 1,3-biphosphoglycerate. The continuous flow setup was easily fabricated from commercially available PTFE tubing. The easy fabrication of coil devices allowed for the possibility of increasing the length of the reactors to extend to the residence time and allow for the addition of pyruvate at specific times. A total of 9.9 mM of pyruvate were fed to the continuous flow system, resulting in a 64% conversion in 135 min. The production of 1,3-biphosphoglycerate was confirmed by PGK assays conducted with the supernatants of fed-batch and continuous flow reactions. Complete conversion of 1 mM of ADP into ATP was achieved with the supernatants from both operation modes, indicating that the stepwise addition of pyruvate in batch and flow led to at least a 40 % increase in 1,3-biphosphoglycerate production versus the cascade conditions presented in Chapter 3. The results further validated the assumption that the amount of pyruvate converted in the cascade is responsible for the amount of 1,3-biphosphoglycerate generated. However, to properly the exact amount of 1,3-biphosphoglycerate produced in the developed enzymatic cascade, further kinetic studies through the development of analytics for substrate and product quantification are necessary.

This chapter's findings showcase the advantages of continuous flow approaches for biocatalytic process intensification through the integration of microreactors connected in-line with various enzymatic and chemical transformations and with *in situ* product purification and addition of substrates.

5 General Conclusions and Future Work

5.1 General conclusions

This work aimed to investigate the advantages of using continuous flow microreactors over batch reactors to establish chemoenzymatic and multi-enzymatic cascades. For this purpose, two biocatalytic cascades were developed.

In Chapter 2, a successful synthesis of DCDHP, a valuable pharmaceutical precursor, was achieved through the combination of a DA reaction with a TK-catalyzed reaction using microreactors. The DA reaction was carried out in a packed-bed reactor using aluminium chloride as the chemical catalyst. The outlet of the packed-bed reactor was connected to a coil reactor where the TK reaction took place. Before entering the coil reactor, the product stream of the DA reaction was diluted to a 10% (v/v) concentration of organic solvent in order to avoid TK deactivation. The compartmentalisation of both reaction steps in different microreactors allowed each catalyst to be operated at its own ideal conditions, which was key in establishing this chemoenzymatic cascade. Furthermore, complete substrate conversion was achieved by performing the DA reaction in continuous flow in the packed-bed reactor, while previous conversions reported in batch were only around 37.5%. The continuous flow system also allowed for quick adjustments to flow rates, which helped minimise the amount of organic solvent in the enzymatic step. The DA-TK continuous flow setup produced 5 mM DCDHP in 195 minutes, which was a 1.4-fold increase in productivity compared to previous preliminary experiments using the same setup, which had produced 3.5 mM of DCDHP in 200 minutes (Gruber, 2019). The TK mutant demonstrated stereospecificity for the R-enantiomer of the DA reaction product, CCA. A method for synthesising the CCA enantiomers in batch was also developed to facilitate these selectivity studies.

In Chapter 3 a *de novo* enzymatic cascade was developed to synthesise 1,3-biphosphoglycerate, a non-commercially available glycolytic metabolite. The most promising cascade for synthesising the metabolite involved coupling TPI and GAPDH with LDH for in situ co-factor regeneration. The cascade was optimised in batch before being transferred to a continuous flow system. A PGK assay was used to

confirm the cascade's ability to synthesise 1,3-biphosphoglycerate, with the amount of ATP produced corresponding to at least half of the 1,3-biphosphoglycerate synthesised. The supernatants from the cascade run in batch, and in the continuous flow microreactor produced around 0.6 mM of ATP. While the yields were similar in both operation modes, using a continuous flow microreactor has the potential to offer additional benefits, such as integration with downstream operations and analytics, which are crucial for the isolation and quantification of 1,3-biphosphoglycerate.

In Chapter 4, strategies were implemented to intensify the upstream and downstream processes of the cascades developed in previous chapters in order to increase their overall productivity. One approach involved scaling up the production of DCDHP in the DA-TK chemoenzymatic cascade by doubling the substrate input in the DA packed-bed reactor, resulting in double the production of CCA. This allowed for the use of two TK coil reactors instead of one, increasing the synthesis of the final product. The parallel arrangement of two identical microreactors, known as numbering-up, enabled the performance of the TK reaction under the same optimised conditions as in a single coil reactor. The resulting continuous flow system consisted of one packed-bed reactor connected to two coil reactors, producing flow streams of 5 mM of DCDHP each. This demonstrated the potential of continuous flow systems to scale out reactions rather than scaling up, preserving the benefits of micro-scale environments in terms of hydrodynamic and mass transfer. However, using hundreds of microreactors, which may be necessary to meet industrial needs, could pose challenges in maintaining uniform fluid and equal mixing conditions (Dong *et al*., 2021). Therefore, further investigation is needed to evaluate the potential of numbering-up strategies fully.

Next, a method was developed to immobilise TK in PVA-based hydrogel particles, which were then used to pack a tubular reactor. A proof-of-concept for a continuous flow cascade of the DA-TK reaction with both catalysts immobilised was demonstrated. The immobilisation yield was determined to be 27±5%, and the entrapment efficiency of the enzyme in the packed-bed reactor was 100% at a flow rate of 40 $\mu L.min^{-1}$, as no enzyme leakage was detected. The continuous flow setup led to a 40% conversion of HPA, producing 1.8 ±0.35 mM of DCDHP in a residence time of 25 min. Although further optimisations are required, the results suggest that

TK can be successfully immobilised in PVA-based hydrogel particles. The immobilised TK packed-bed reactor also displayed high operational stability, with no significant activity loss between reaction runs and no enzyme leakage. Further studies are needed to fully understand the efficiency of the packed-bed reactor using immobilised TK. These studies should focus on factors such as diffusion, optimal residence time, and enzyme and substrate concentrations.

In an effort to separate the TK lysate from the product stream, the DA-TK continuous flow setup developed in Chapter 2 was integrated with a tangential flow filtration device made of PMMA. This device, which can be sterilized by autoclaving and reused multiple times with different membranes, was able to retain the TK lysate using a 10 kDa membrane when integrated into the continuous flow setup for the production of DCDHP. By adjusting the back pressure at the retentate outlet, an average permeate yield of 70% was achieved over 200 minutes. While this yield can be improved by purifying the TK lysate used in the reaction (which would reduce the amount of protein and the risk of membrane fouling), the results are similar to those obtained by O'Sullivan *et al*. using a similar device, which afforded permeate yields of approximately 65% over 420 minutes (O'Sullivan *et al*., 2012). The successful integration of downstream processing device with a biocatalytic flow setup demonstrated in this study sets the stage for the development of complete biocatalytic processes in continuous flow from start to finish. Additionally, the ability to separate the biocatalyst from the product stream allows for the incorporation of additional chemical and enzymatic steps without the risk of inhibition or cross-reactions.

Finally, an upstream process intensification approach involving *in situ* substrate supply was applied to the multi-enzymatic cascade developed in Chapter 3. The high cost of NAD+ prompted the implementation of a recycling method using LDH to oxidize NADH from pyruvate, a cheap substrate. This linked the production of 1,3-biphosphoglycerate to the conversion of pyruvate within the cascade. To assess the cascade's ability to convert higher concentrations of pyruvate batch and fed-batch processes were evaluated. The fed-batch process with stepwise addition of pyruvate had the highest conversion rate and shortest reaction time, converting 70% from a total of 9.9 mM pyruvate added in 90 minutes. Therefore, a continuous flow system mimicking the fed-batch process was developed using three coil reactors operated in

single-flow mode with *in situ* additions of pyruvate at fixed intervals. A total of 9.9 mM of pyruvate were fed to the continuous flow system, resulting in a 64% conversion in 135 min. A PGK assay of the supernatants from the fed-batch and continuous flow processes produced 1 mM ATP, corresponding to an approximately 40% increase in 1,3-biphosphoglycerate production compared to the conditions presented earlier in Chapter 3. While the obtained results suggest that the cascade benefits from a stepwise addition of pyruvate to increase the production of 1,3-biphosphoglycerate and shorten the reaction times, further kinetic studies are needed to fully understand the reaction rates in each operating mode. To develop these kinetic studies, analytical methods capable of detecting and quantifying DHAP, GAP, and 1,3-biphosphoglycerate in the reaction mixture will need to be applied. Nevertheless, the results showcase the ability of microreactors to perform rapid, high-throughput experiments, which are ideal for developing and optimising new biocatalytic routes, such as this one. Microreactors can also provide a more controlled and consistent reaction environment, which can help improve the reproducibility of experiments and reduce the impact of external factors on the reaction.

5.2 Future work

Whilst a chemoenzymatic cascade in continuous flow has been successfully demonstrated in this project, further studies are required to increase overall productivity, facilitate the purification of the product, and enable better control over reaction conditions through the development and integration of analytics.

Although complete conversion of HPA was achieved in the TK coil reactor at room temperature, operating at higher temperatures between 30 and 50 °C could lead to a faster conversion and therefore decrease the overall reaction time. The TK reaction rate could further be optimised by using a different TK mutant with an affinity towards cyclic substrates like CCA and with a higher tolerance for organic solvents. The use of an efficient enzyme immobilisation method, such as an His-tag Ni-NTA interaction could also improve the stability of TK. While other methods of immobilisation would also be possible, using the strong affinity interaction between His-tagged proteins and Ni-NTA supports results in a fast and easy method of immobilisation (Moser, White and Kovacs, 2014) that has previously been demonstrated in TK mutants and applied for continuous flow synthesis (Abdul Halim, Szita and Baganz, 2013b; Binti and Halim, 2013; Kulsharova *et al.*, 2018b, 2018a). Enzyme immobilisation would also facilitate downstream product purification.

A histidine-tagged TK could also be useful for protein purification by applying the clarified enzyme lysate to a Ni-NTA column with a binding buffer followed by an elution buffer to clean the lysate from other proteins. Using a TK lysate with less protein content would improve the permeate yields obtained in the tangential flow filtration developed in Chapter 4, increasing the yield of DCDHP recovered. Further investigation of the activity of the TK removed in the filtration unit is required to establish a recycling loop to feed the TK retained in the membrane back to the system. Furthermore, conducting experiments to assess the transmembrane pressure by utilizing various back pressure regulators and altering flow rates becomes imperative to determine the ideal filtration conditions and enhance the permeate yield of the process. The incorporation of pressure sensors within the tangential flow filtration device is pivotal for overseeing and fine-tuning transmembrane pressure, back pressure, and flow dynamics. Another optimisation could be increasing the filtration area of the device, either by increasing the channel length or by widening it. This could

increase the efficiency of the filtration process, allowing more material to be filtered in a given amount of time. Another advantage of increasing the filtration area is that it can reduce the pressure drop across the filter, which decreases the resistance to flow, thereby increasing the filtration rate and, therefore, the amount of permeate produced. However, there are also some disadvantages to consider. One disadvantage is that increasing the filtration area may also increase the size and cost of the device, which could be a drawback in some applications. Another disadvantage is that the increased filtration area may also increase the risk of fouling or clogging due to the increased surface area available for material to deposit on. The choice to expand the filtration area of a tangential filtration device will ultimately depend on the trade-offs between potential advantages and disadvantages.

Further optimisations to the Diels-Alder reaction could also be explored, such as the performance of the chemical reaction in aqueous media. This would facilitate the integration with the TK-catalysed reaction and increase the system production, as the product of the DA reaction would no longer need to be diluted. Operating the entire cascade in aqueous media would also increase the stability and activity of the TK mutant used, as enzymes often have higher activity in aqueous environments. However, there are challenges to consider such as the low solubility of the cascade product DCDHP in aqueous media.

Another optimisation of the DA reaction would be the use of organocalatysts in flow for an asymmetric synthesis of CCA. Currently the developed cascade is producing a racemic mixture of CCA from which only the R-enantiomer is being converted. Further experiments with organocatalysts are necessary in order to decrease the reaction time from 3 days to a couple of hours in order for the reaction to be viable in continuous flow.

Detection of DCDHP was successfully achieved through a colorimetric assay adapted from Smith *et al* and used as a complementary assay to the HPLC analysis (Kaulmann, *et al*., 2006). This colorimetric assay is based on the oxidation of the hydroxyl groups of DCDHP to a ketone by tetrazolium red forming a dye of pink colour. However, this assay has a limitation in that tetrazolium red can also oxidize HPA, so it must be used in conjunction with HPLC analysis to accurately detect DCDHP. Initial attempts with an MP-carbonate resin to remove HPA from reaction

samples were unreliable, as the amount of HPA absorbed by the resin varied from samples within samples with the same HPA concentration. Therefore, further optimisation is needed to improve the accuracy and reliability of the colorimetric assay for detecting DCDHP.

Considering that the cascade produces CO_2 as a side product, the reaction could be controlled by monitoring the changes in pH since CO_2 can react with water to form carbonic acid, a weak acid. At low concentrations of CO_2, the concentration of carbonic acid will also be low, and the pH of the solution will be relatively high. As the concentration of CO_2 increases, the concentration of carbonic acid will also increase, leading to a decrease in the pH of the solution. Therefore, monitoring the pH of the solution during the cascade reaction makes it possible to indirectly measure the concentration of CO_2 being produced as a side product. Thus, implementing pH sensors into microreactors to monitor the increase in pH due to CO_2 formation in the cascade could be an interesting optimisation strategy to explore (Gruber *et al.*, 2017).

The development of a multi-enzymatic cascade for the synthesis of 1,3-biphosphoglycerate has also been demonstrated in this project. However, further experiments are still required to isolate and quantify all the metabolites present in the cascade. The main bottleneck in this multi-enzymatic cascade was the need for more analytical methods to determine the reaction kinetics. As discussed before, the acyl phosphate group of 1,3-biphosphoglycerate makes the metabolite extremely unstable and particularly sensitive to spontaneous hydrolysis or isomerization to 3-PGA and 2,3-bisphosphoglycerate, respectively. Thus, it is a challenge to isolate and quantify this metabolite. A possible future experiment could be the application of the chemical trap developed by Chang *et al*. to isolate 1,3-biphosphoglycerate with hydroxylamine in order to enable its analysis by targeted LC−MS/MS (Chang *et al*., 2016). This chemical trap could be done in flow simply by adding a fourth coil reactor to mix the metabolite with hydroxylamine and yield a stable hydroxamic acid (3PGha) with a mass of 199.98 Da. A possible continuous flow setup for this experiment is presented in Figure 5.1.

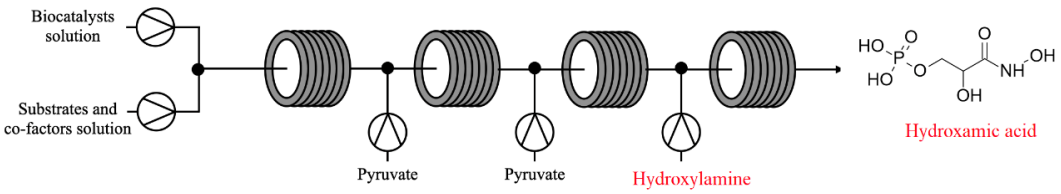

Figure 5.1: Possible continuous flow system with downstream unit operation for hydroxylamine.

Oslund and co-workers developed an LC-MS method to detect 1,3-biphosphoglycerate that could be used in the future to quantify 1,3-biphosphoglycerate in the developed cascade. Here, the metabolite was enzymatically made using a GAPDH and LDH coupled reaction. In this work, the purification of 1,3-biphosphoglycerate was performed by LC–MS analysis with a Synergi Hydro-RP column (150 mm × 2 mm; 4 µm particle size; Phenomenex) using a gradient of solvent A (97%:3% H_2O:MeOH with 10 mM tributylamine and 15 mM acetic acid), and solvent B (100% MeOH). The retention time of the compounds in the mixture were: 1,3-biphosphoglycerate 31.5 min, 2,3-biphosphoglycerate 33.3 min, 3-PGA 25.9 min, GAP 13.3 min and pyruvate 16.7 min. The fractions containing 1,3-biphosphoglycerate from multiple injections were then combined and used as a substrate in a PGK assay to validate the presence of 1,3-biphosphoglycerate (Oslund *et al*., 2017).

Enzyme immobilisation could also facilitate the detection of the metabolites in the cascade. Although no method has been reported for this exact cascade, neither in batch nor in continuous flow, some studies using histidine-tagged glycolytic enzymes have been successful demonstrated (Mukai *et al*., 2013a, 2017). Mukai and workers have shown a reaction of 11 histidine-tagged glycolytic enzymes tethered to Ni-NTA functionalized silica nanoparticles for the conversion of glucose to lactate. In comparison with enzymes free in solution the tethered enzymes showed a significantly higher efficiency of lactate produced from each nmol of glucose consumed (Mukai *et al*., 2017). An immobilisation strategy could also facilitate the study of the cascade kinetics through site-specific immobilisation of enzymes to evaluate the mechanism of substrate transference in the cascade.

The integration of analytics and control sensors into the continuous flow biocatalytic systems developed in this thesis is crucial for enhancing their efficiency, productivity, and reliability. This integration would enable the monitoring and controlling of data related to reaction conditions, ultimately leading to reduced process development times. A wide range of analytical tools is available for integration with continuous flow microreactors. These tools include optical, spectroscopic, optofluidic, and electrochemical detection methods. They facilitate real-time measurements of essential reaction variables like pH, carbon dioxide production, and specific reactants and products. Integrating inline spectroscopic sensors, such as UV-Vis, IR, NMR, and MS, would further enable the exploration of reaction kinetics and the optimization of reaction conditions (McMullen and Jensen, 2010). One can continuously monitor their impact on reaction kinetics and product formation by adjusting parameters such as temperature, pH, and substrate concentrations within the flow system. Moreover, the integration with analytics would ensure high control over reaction conditions and product quality, thereby upholding rigorous standards of safety and product integrity.

In addition, integrating the developed continuous-flow systems with HPLC columns could prove advantageous for in-line purification and the separation of reaction products (Duan *et al.*, 2006; Miložič *et al.*, 2017). This approach offers the advantage of rapid, high-throughput reactions and purifications, which is essential when working with unstable compounds such as 1,3-biphosphoglycerate. However, several challenges remain to be addressed when integrating microreactors with analytical methods. These include considerations related to sample preparation, compatibility of microreactor materials, and reaction conditions such as reactant and product concentrations, pH, temperature, pressure, and flow rates.

Given the challenges faced with analytics in both reaction systems a mathematical model could be of use to optimize reaction conditions and model reaction kinetics (Rios-Solis *et al.*, 2015). *In silico* modelling has revolutionized the field of pharmacology, expanding its scope from drug discovery to gaining insights into the intricate workings of complex enzymatic reactions. Specifically, when dealing with multi-step enzymatic reactions, computational techniques have proven to be extremely valuable. These models allow to test hypothesis and create novel reaction pathways. Moreover, the integration of extensive biological and medical data sources becomes

achievable through machine learning, data mining algorithms, and network analysis tools, enhancing our comprehensive understanding of enzymatic processes (Helmy *et al.*, 2020). In essence, in silico modelling simplifies the traditionally intricate and time-consuming process of deciphering multi-step enzymatic reactions, making it more efficient and streamlined. Furthermore, mathematical models can also be instrumental in evaluating and comparing the optimal process modes for the presented reactions, including batch, fed-batch, and continuous flow methods (Shaeri *et al.*, 2006).

References

Abbott, A. P., Capper, G., Gray, S. (2002). Quaternary ammonium zinc- or tin-containing ionic liquids: water insensitive, recyclable catalysts for Diels–Alder reactions. *Green Chemistry*, 4(1), 24-26.

Abdelraheem, E. M. M., Sattler, J., Wu, S., Hollmann, F., Wang, M., Kragl, U., Schwaneberg, U., Holtmann, D., Bornscheuer, U. T., Zhang, W., and Berkessel, A. (2019). Biocatalysis explained: from pharmaceutical to bulk chemical production. *Reaction Chemistry & Engineering*, 4(11), 1878-1894.

Abdul Halim, A., Szita, N., & Baganz, F. (2013a). Characterization and multi-step transketolase-ω-transaminase bioconversions in an immobilised enzyme microreactor (IEMR) with packed tube. *Journal of Biotechnology*, 168(4), 567–575.

AB Halim, A. (2014). In vitro metabolic pathway construction in an immobilised enzyme microreactor (IEMR). Doctoral thesis (PhD), UCL (University College London).

Ahmed, S. T., de los Santos, E. L. C., Wagner, N., Schwaneberg, U., & Bocola, M. (2015). Chemoenzymatic Synthesis of Optically Pure l- and d-Biarylalanines through Biocatalytic Asymmetric Amination and Palladium-Catalyzed Arylation. *ACS Catalysis*, 5(9), 5410–5413.

Alcántara, A. R., Taylor, N. M. I., & Minteer, S. D. (2022). Biocatalysis as Key to Sustainable Industrial Chemistry. *ChemSusChem*, 15(9), e202102709.

Ardao, I., Hwang, E. T., and Zeng, A. P. (2013). In vitro multienzymatic reaction systems for biosynthesis. *Advances in biochemical engineering/biotechnology*, 137, 153–184.

Benítez-Mateos, A. I., Roura Padrosa, D., and Paradisi, F. (2022). Multistep enzyme cascades as a route towards green and sustainable pharmaceutical syntheses. *Nature Chemistry*. 14(5), 489-499.

Bennett, B. D., Rabinowitz, J. D., and Escherichia coli (2009). Absolute metabolite concentrations and implied enzyme active site occupancy in *Escherichia coli*. *Nature*

Chemical Biology, 5(8), 593–599.

Bi, Y., Chen, J., soybean oil, et al. (2017). A flow-through enzymatic microreactor immobilizing lipase based on layer-by-layer method for biosynthetic process: Catalyzing the transesterification of soybean oil for fatty acid methyl ester production. *Process Biochemistry*, 54, 73–80.

Biggelaar, L. van den, Soumillion, P., and Debecker, D. P. (2017). Enantioselective Transamination in Continuous Flow Mode with Transaminase Immobilised in a Macrocellular Silica Monolith. *Catalysts*, 7(2), 54.

Bong, Y. K., Park, S. M., Esomeprazole, et al. (2018). Baeyer-Villiger Monooxygenase-Mediated Synthesis of Esomeprazole As an Alternative for Kagan Sulfoxidation. *Journal of Organic Chemistry*, 83(14), 7453-7458.

Bras, E. J. S., Barbosa, M. O., biocatalysis, et al. (2021). Recent developments in microreactor technology for biocatalysis applications. *Reaction Chemistry and Engineering*, 6(5), 815-827.

Britton, J., Majumdar, S., and Weiss, G. A. (2018). Continuous flow biocatalysis. *Chemical Society Reviews*. 47(15), 5891-5918.

Bunik, V. I. (2013) Thiamin-dependent enzymes: New perspectives from the interface between chemistry and biology, *The FEBS Journal*, 280(24), 6373.

Cao, K., Linhardt, R. J., Saxagliptin (BMS-477118), et al. (2007). Carbon-14 labeling of Saxagliptin (BMS-477118). *Journal of Labelled Compounds and Radiopharmaceuticals*, 50(13), 1224–1229.

Cavill, J. L., Peters, J., and Tomkinson, N. C. O. (2003). Iminium ion catalysis : Use of the α-effect in the acceleration of the Diels – Alder reaction. *Chemical communications*, (6), 728-729.

Chang, J. W., Lee, H. H., Huang, M. T., Tsai, P. J., Pan, S. H., and Analytical Chemistry (2016). Profiling reactive metabolites via chemical trapping and targeted mass spectrometry. *Analytical Chemistry*, 88(13), 6658–6661.

Chen, I. H., Young, J. N., and Yu, S. J. (2004). Recyclable organotungsten Lewis acid

and microwave-assisted Diels-Alder reactions in water and in ionic liquids. *Tetrahedron*, 60(51), 11903–11909.

Claassens, N. J., Mendez-Sanchez, D., Rahimi, M., and Current Opinion in Biotechnology (2019). A critical comparison of cellular and cell-free bioproduction systems. *Current Opinion in Biotechnology*, 60, 221–229.

Contente, M. L., and Paradisi, F. (2018). Self-sustaining closed-loop multienzyme-mediated conversion of amines into alcohols in continuous reactions. Nature Catalysis, 1(6), 452–459. doi: 10.1038/s41929-018-0082-9.

Coward, L. G. (2012). Chemoenzymatic synthesis of novel, structurally diverse compounds. Doctoral thesis (PhD), UCL (University College London).

Cutlan, R., (2020). Using enzyme cascades in biocatalysis: Highlight on transaminases and carboxylic acid reductases. *Biochimica et Biophysica Acta (BBA) - Proteins and Proteomics*, 1868(2), p. 140322.

Davenport, R. C., Bash, P. A., Seaton, B. A., Karplus, P. A., and Biochemistry (1991). Structure of the triosephosphate isomerase-phosphoglycolohydroxamate complex: An analogue of the intermediate on the reaction pathway. *Biochemistry*, 30(24), 5821–5826.

Delville, Mariëlle M.E., Organic and Biomolecular Chemistry (2015). Chemoenzymatic flow cascade for the synthesis of protected mandelonitrile derivatives. *Organic and Biomolecular Chemistry*, 13(6), 1634–1638.

Cutlan, R., Brodhagen, M., Jensen, R. A., & Jez, J. M. (2020). Using enzyme cascades in biocatalysis: Highlight on transaminases and carboxylic acid reductases. Biochimica et Biophysica Acta (BBA) - *Proteins and Proteomics*, 1868(2), 140322.

Davenport, R. C., Bash, P. A., Seaton, B. A., & Karplus, P. A. (1991). Structure of the triosephosphate isomerase-phosphoglycolohydroxamate complex: An analogue of the intermediate on the reaction pathway. *Biochemistry*, 30(24), 5821–5826.

Delville, Mariëlle M. E., Verdoes, J. C., Scholten, J. D., & Feringa, B. L. (2015a). Chemoenzymatic flow cascade for the synthesis of protected mandelonitrile

derivatives. *Organic and Biomolecular Chemistry*, 13(6), 1634–1638.

Dong, Z., Zheng, M., Panke, S., & Chemical Engineering Science: X (2021). Scale-up of micro- and milli-reactors: An overview of strategies, design principles and applications. *Chemical Engineering Science*: X, 10.

Dräger, G., Hilterhaus, L., Kissau, L., & Seyfang, G. (2007). Enzyme-purification and catalytic transformations in a microstructured PASS flow reactor using a new tyrosine -based Ni-NTA linker system attached to a polyvinylpyrrolidinone-based matrix. *Organic & Biomolecular Chemistry*, 5(22), 3657–3664.

Duan, J., Liang, Z., Li, L., Zou, H. (2006). Rapid protein identification using monolithic enzymatic microreactor and LC-ESI-MS/MS. *PROTEOMICS*, 6(2), 412–419.

Fernandes, P., & de Carvalho, C. C. (2021). Multi-Enzyme Systems in Flow Chemistry. *Processes*, 9(2), 225.

Fernandes, P., Marques, M. P., Carvalho, F., & Cabral, J. M. (2009). A simple method for biocatalyst immobilization using PVA-based hydrogel particles. *Journal of Chemical Technology & Biotechnology: International Research in Process, Environmental & Clean Technology*, 84(4), 561-564

France, S. P., Hussain, S., Hill, A. M., Hepworth, L. J., Howard, R. M., & ACS Catalysis (2017). Constructing Biocatalytic Cascades: In Vitro and in Vivo Approaches to de Novo Multi-Enzyme Pathways. *ACS Catalysis*, *7*(1), 710-724.

Fuchs, M., Farnberger, J. E., & Kroutil, W. (2015). The Industrial Age of Biocatalytic Transamination. *European Journal of Organic Chemistry*, 2015(32), 6965–6982.

Gauss, D., Schoenenberger, B., & Wohlgemuth, R. (2014). Chemical and enzymatic methodologies for the synthesis of enantiomerically pure glyceraldehyde 3-phosphates. *Carbohydrate Research*, 389(1), 18–24.

Ghislieri, D., & Turner, N. J. (2014). Biocatalytic approaches to the synthesis of enantiomerically pure chiral amines. *Topics in Catalysis*, 57, 284-300.

Green, A. P., Turner, N. J., & O'Reilly, E. (2014). Chiral amine synthesis using ω-

transaminases: An amine donor that displaces equilibria and enables high-throughput screening. *Angewandte Chemie - International Edition*, 53(40), 10714–10717.

Gruber, P., Rocaboy-Faquet, E., Biotechnology Journal (2017). Real-time pH monitoring of industrially relevant enzymatic reactions in a microfluidic side-entry reactor (μSER) shows potential for pH control. *Biotechnology Journal*, 12(6).

Gruber, P., Rocaboy-Faquet, E., Holtmann, D., Biotechnology and Bioengineering (2018). Enzymatic synthesis of chiral amino-alcohols by coupling transketolase and transaminase-catalyzed reactions in a cascading continuous-flow microreactor system. *Biotechnology and Bioengineering*, 115(3), 586–596.

Gruber, P. (2019). Challenges of Chemoenzymatic and Biocatalytic Reaction Cascades and Online Monitoring at a Microscale. Doctoral thesis (PhD), UCL (University College London).

Grunwald, P. (Ed.). (2019). *Pharmaceutical biocatalysis: chemoenzymatic synthesis of active pharmaceutical ingredients*. CRC Press.

Hailes, H. C., Dalby, P. A. and Woodley, J. M. (2007) 'Integration of biocatalytic conversions into chemical syntheses', *Journal of Chemical Technology and Biotechnology: International Research in Process, Environmental & Clean Technology,* 82(12), 1063-1066.

Hanson, R. (1981) 'Glycolysis and gluconeogenesis', *Biochemical Education*, 9(3), 89–91.

Harris, T. K., Abeygunawardana, C. and Mildvan, A. S. (1997) 'NMR studies of the role of hydrogen bonding in the mechanism of triosephosphate isomerase', *Biochemistry*, 36(48), 14661–14675.

Hartley, C. J., French, N. G., Scoble, J. A., Williams, C. C., Churches, Q. I., Frazer, A. R., & Scott, C. (2017). Sugar analog synthesis by in vitro biocatalytic cascade: A comparison of alternative enzyme complements for dihydroxyacetone phosphate production as a precursor to rare chiral sugar synthesis. *Plos one*, 12(11), e0184183.

Hartley, C. J., Williams, C. C., Scoble, J. A., Churches, Q. I., North, A., French, N.

G., & Scott, C. (2019). Engineered enzymes that retain and regenerate their cofactors enable continuous-flow biocatalysis. *Nature Catalysis*, 2(11), 1006-1015.

Heinrich, P. C., Steffen, H., Janser, P., & Wiss, O. (1972). Studies on the reconstitution of apotransketolase with thiamine pyrophosphate and analogs of the coenzyme. *European Journal of Biochemistry*, 30(3), 533-541.

Helmy, M., Smith, D., & Selvarajoo, K. (2020). Systems biology approaches integrated with artificial intelligence for optimized metabolic engineering. *Metabolic Engineering Communications*, 11, e00149.

Higashio, K., Katsuragi, S., Kundu, D., Adebar, N., Plass, C., Kühn, F., ... & Akai, S. (2020). Continuous-Flow Dynamic Kinetic Resolution of Racemic Alcohols by Lipase–Oxovanadium Cocatalysis. *European Journal of Organic Chemistry*, 2020(13), 1961-1967.

Honda, K., Kimura, K., Ninh, P. H., Taniguchi, H., Okano, K., & Ohtake, H. (2017). In vitro bioconversion of chitin to pyruvate with thermophilic enzymes. *Journal of bioscience and bioengineering*, 124(3), 296-301.

Hoyos, P., Pace, V. and Alcántara, A. R. (2019) 'Biocatalyzed synthesis of statins: A sustainable strategy for the preparation of valuable drugs', *Catalysts*, 9(3), 260.

Hughes, G. and Lewis, J. C. (2018) 'Introduction: Biocatalysis in Industry', *Chemical Reviews*, 118(1), 1-3.

Jahromi, R. R., Morris, P., Martinez-Torres, R. J., & Dalby, P. A. (2011). Structural stability of E. coli transketolase to temperature and pH denaturation. *Journal of biotechnology*, 155(2), 209-216.

J.P. Richard (1984) 'Acid-base catalysis of the elimination and isomerization reactions of triose phosphates', *Journal of the American Chemical Society* , 106(17), 4926-4936.

Kanno, K., Hiraiwa, M., Takamura, A., Okada, Y., (2002) 'Rapid enzymatic transglycosylation and oligosaccharide synthesis in a microchip reactor.', *Lab on a Chip*, 2(1), 15–8.

Kazan, A., Grünberger, A., Aksu, S., (2017) 'Formulation of organic and inorganic

hydrogel matrices for immobilization of β-glucosidase in microfluidic platform', *Engineering in Life Sciences*. Wiley-VCH Verlag, 17(7), 714–722.

Koh, J. H., Park, C. S., Hong, S. S., & Tetrahedron Letters (1999) 'Enzymatic resolution of secondary alcohols coupled with ruthenium-catalyzed racemization without hydrogen mediator', *Tetrahedron Letters*. Pergamon, 40(34), 6281–6284.

Kourist, R., Brundiek, H. and Bornscheuer, U. T. (2010) 'Protein engineering and discovery of lipases', *European Journal of Lipid Science and Technology*, 112(1), 64–74.

Kr, H., And, C. and Wsttestdes, G. M. (1989) Lactate dehydrogenase-catalyzed regeneration of NAD from NADH for use in enzyme-catalyzed synthesis. *Bioorganic Chemistry*, 17(4), 400-409.

Krimsky, I. (1958) 'Enzymatic Formation of High Levels of 1,3-Diphosphoglycerate from 3-Phosphoglycerate : Isolation and Futher Metabolism', *J. Biol. Chem.*, 234(2), 228–231.

Kroutil, W., & Rueping, M. (2014). Introduction to ACS catalysis virtual special issue on cascade catalysis. *ACS Catalysis*, 4(6), 2086-2087

Kulsharova, G., Dimov, N., Marques, M. P., Szita, N., & Baganz, F. (2018). Simplified immobilisation method for histidine-tagged enzymes in poly (methyl methacrylate) microfluidic devices. *New biotechnology*, 47, 31-38.

LAMBEIR, A. M., OPPERDOES, F. R., & WIERENGA, R. K. (1987). Kinetic properties of triose-phosphate isomerase from Trypanosoma brucei brucei: A comparison with the rabbit muscle and yeast enzymes. *European journal of biochemistry*, 168(1), 69-74.

Laurenti, E., & dos Santos Vianna Jr, A. (2016). Enzymatic microreactors in biocatalysis: history, features, and future perspectives. *Biocatalysis*, 1(1), 148-165.

Lawrence, J., O'Sullivan, B., Lye, G. J., Wohlgemuth, R., & Szita, N. (2013). Microfluidic multi-input reactor for biocatalytic synthesis using transketolase. *Journal of Molecular Catalysis B: Enzymatic*, 95, 111-117.

Liang, J., Lalonde, J., Borup, B., Mitchell, V., Mundorff, E., Trinh, N., ... & Pai, G. G. (2010). Development of a biocatalytic process as an alternative to the (−)-DIP-Cl-mediated asymmetric reduction of a key intermediate of montelukast. *Organic Process Research & Development*, 14(1), 193-198.

Liu, X., Meng, X. Y., Xu, Y., Dong, T., Zhang, D. Y., Guan, H. X., ... & Wang, J. (2019). Enzymatic synthesis of 1-caffeoylglycerol with deep eutectic solvent under continuous microflow conditions. *Biochemical Engineering Journal*, 142, 41-49.

Luckarift, H. R., Ku, B. S., Dordick, J. S., & Spain, J. C. (2007). Silica-immobilized enzymes for multi-step synthesis in microfluidic devices. *Biotechnology and bioengineering*, 98(3), 701-705.

Ma, S. K., Gruber, J., Davis, C., Newman, L., Gray, D., Wang, A., ... & Sheldon, R. A. (2010). A green-by-design biocatalytic process for atorvastatin intermediate. *Green Chemistry*, 12(1), 81-86.

Marques, M. P., Fernandes, P., Cabral, J. M., Žnidaršič-Plazl, P., & Plazl, I. (2012). Continuous steroid biotransformations in microchannel reactors. *New biotechnology*, 29(2), 227-234.

Maruyama, T., Uchida, J. I., Ohkawa, T., Futami, T., Katayama, K., Nishizawa, K. I., ... & Goto, M. (2003). Enzymatic degradation of p-chlorophenol in a two-phase flow microchannel system. *Lab on a Chip*, 3(4), 308-312.

Mattey, A. P., Ford, G. J., Citoler, J., Baldwin, C., Marshall, J. R., Palmer, R. B., ... & Flitsch, S. L. (2021). Development of continuous flow systems to access secondary amines through previously incompatible biocatalytic cascades. *Angewandte Chemie International Edition*, 60(34), 18660-18665.

McMullen, J. P. and Jensen, K. F. (2010) 'Integrated Microreactors for Reaction Automation: New Approaches to Reaction Development', *Annual Review of Analytical Chemistry*, 3(1), pp. 19–42.

Miložič, N., Lubej, M., Lakner, M., Žnidaršič-Plazl, P., & Plazl, I. (2017). Theoretical and experimental study of enzyme kinetics in a microreactor system with surface-immobilized biocatalyst. *Chemical Engineering Journal*, 313, 374-381.

de Miranda, A. S., Silva, M. V. D. M., Dias, F. C., de Souza, S. P., Leão, R. A., & de Souza, R. O. (2017). Continuous flow dynamic kinetic resolution of rac-1-phenylethanol using a single packed-bed containing immobilized CAL-B lipase and VOSO 4 as racemization catalysts. *Reaction Chemistry & Engineering*, 2(3), 375-381.

Moellering, R. E., & Cravatt, B. F. (2013). Functional lysine modification by an intrinsically reactive primary glycolytic metabolite. *Science*, 341(6145), 549-553.

Molla, G. S., Wohlgemuth, R. and Liese, A. (2016) 'One-pot enzymatic reaction sequence for the syntheses of d-glyceraldehyde 3-phosphate and l-glycerol 3-phosphate', *Journal of Molecular Catalysis B: Enzymatic*. Elsevier B.V., 124, 77–82.

Moser, A. C., White, B. and Kovacs, F. A. (2014) 'Measuring binding constants of his-tagged proteins using affinity chromatography and Ni-NTA-immobilised enzymes', *Methods in Molecular Biology*. Humana Press Inc., 1129, 423–434.

Mukai, C., Gao, L., Bergkvist, M., Nelson, J. L., Hinchman, M. M., & Travis, A. J. (2013). Biomimicry enhances sequential reactions of tethered glycolytic enzymes, TPI and GAPDHS. *PloS one*, 8(4), e61434.

Nagy, F., Szabó, K., Bugovics, P., & Hornyánszky, G. (2019). Bisepoxide-activated hollow silica microspheres for covalent immobilization of lipase from Burkholderia cepacia. *Periodica Polytechnica Chemical Engineering*, 63(3), 414-424.

Nakashima, D., & Yamamoto, H. (2005). Reversal of Chemoselectivity in Diels− Alder Reaction with α, β-Unsaturated Aldehydes and Ketones Catalyzed by Brønsted Acid or Lewis Acid. *Organic letters*, 7(7), 1251-1253.

Negelein, E. (1965) 'd-1,3-Diphosphoglycerate', in *Methods of Enzymatic Analysis*, pp. 234–237.

Nicolaou, K. C., Edmonds, D. J., & Bulger, P. G. (2006). Cascade reactions in total synthesis. *Angewandte Chemie International Edition*, *45*(43), 7134-7186.

Nilsson, U., Meshalkina, L., Lindqvist, Y., & Schneider, G. (1997) Examination of Substrate Binding in Thiamin Diphosphate- dependent Transketolase by Protein Crystallography and Site-directed Mutagenesis, *The Journal of Biological Chemistry*,

272(3), 1864–1869.

O'Sullivan, B., Al-Bahrani, H., Lawrence, J., Campos, M., Cázares, A., Baganz, F., ... & Szita, N. (2012). Modular microfluidic reactor and inline filtration system for the biocatalytic synthesis of chiral metabolites. *Journal of Molecular Catalysis B: Enzymatic*, *77*, 1-8.

Oslund, R. C., Su, X., Haugbro, M., Kee, J. M., Esposito, M., David, Y., ... & Rabinowitz, J. D. (2017). Bisphosphoglycerate mutase controls serine pathway flux via 3-phosphoglycerate. *Nature chemical biology*, *13*(10), 1081-1087.

Pais, D. A. M. (2013). Towards a Microfluidic Chemoenzymatic Reactor.

Palmai, Z., Seifert, C., Gräter, F., & Balog, E. (2014). An allosteric signaling pathway of human 3-phosphoglycerate kinase from force distribution analysis. *PLoS computational biology*, *10*(1), e1003444.

Patel, R. N. (2006). Biocatalysis: synthesis of chiral intermediates for pharmaceuticals. *Current Organic Chemistry*, *10*(11), 1289-1321.

Payongsri, P., Steadman, D., Strafford, J., MacMurray, A., Hailes, H. C., & Dalby, P. A. (2012). Rational substrate and enzyme engineering of transketolase for aromatics. *Organic & biomolecular chemistry*, *10*(45), 9021-9029.

Planchestainer, M., Contente, M. L., Cassidy, J., Molinari, F., Tamborini, L., & Paradisi, F. (2017). Continuous flow biocatalysis: production and in-line purification of amines by immobilised transaminase from Halomonas elongata. *Green Chemistry*, *19*(2), 372-375.

Pohar, A., Plazl, I., & Žnidaršič–Plazl, P. (2009). Lipase-catalyzed synthesis of isoamyl acetate in an ionic liquid/n–heptane two-phase system at the microreactor scale. *Lab on a Chip*, *9*(23), 3385-3390.

Poznansky, B., Thompson, L. A., Warren, S. A., Reeve, H. A., & Vincent, K. A. (2020). Carbon as a simple support for redox biocatalysis in continuous flow. *Organic process research & development*, *24*(10), 2281-2287.

Banks, R. D., Blake, C. C. F., Evans, P. R., Haser, R., Rice, D. W., Hardy, G. W., ...

& Phillips, A. W. (1979). Sequence, structure and activity of phosphoglycerate kinase: a possible hinge-bending enzyme. *Nature*, *279*(5716), 773-777.

Rahim, S. N., Sulaiman, A., Hamzah, F., Hamid, K. H. K., Rodhi, M. N. M., Musa, M., & Edama, N. A. (2013). Enzymes encapsulation within calcium alginate-clay beads: Characterization and application for cassava slurry saccharification. *Procedia Engineering*, *68*, 411-417.

Ríos-Lombardía, N., Vidal, C., Cocina, M., Morís, F., García-Álvarez, J., & González-Sabín, J. (2015). Chemoenzymatic one-pot synthesis in an aqueous medium: combination of metal-catalysed allylic alcohol isomerisation–asymmetric bioamination. *Chemical Communications*, *51*(54), 10937-10940.

Rios-Solis, L., Morris, P., Grant, C., Odeleye, A. O. O., Hailes, H. C., Ward, J. M., & Lye, G. J. (2015). Modelling and optimisation of the one-pot, multi-enzymatic synthesis of chiral amino-alcohols based on microscale kinetic parameter determination. *Chemical Engineering Science*, 122, 360-372.

Rozovsky, S., & McDermott, A. E. (2007). Substrate product equilibrium on a reversible enzyme, triosephosphate isomerase. *Proceedings of the National Academy of Sciences*, *104*(7), 2080-2085.

De Santis, P., Meyer, L. E., & Kara, S. (2020). The rise of continuous flow biocatalysis–fundamentals, very recent developments and future perspectives. *Reaction Chemistry & Engineering*, *5*(12), 2155-2184.

Santos, M. (2016) *Biocatalytic Production of Pharmaceutical Intermediates in Flow: a Process Integration Approach*

Sasaki, R., & Chiba, H. (1983). Role and induction of 2, 3-bisphosphoglycerate synthase. *Molecular and Cellular Biochemistry*, *53*, 247-256.

Savile, C. K., Janey, J. M., Mundorff, E. C., Moore, J. C., Tam, S., Jarvis, W. R., ... & Hughes, G. J. (2010). Biocatalytic asymmetric synthesis of chiral amines from ketones applied to sitagliptin manufacture. *Science*, *329*(5989), 305-309.

Schmidt-Dannert, C., & Lopez-Gallego, F. (2016). A roadmap for biocatalysis–

functional and spatial orchestration of enzyme cascades. *Microbial biotechnology*, *9*(5), 601-609.

Schrittwieser, J. H., Velikogne, S., Hall, M., & Kroutil, W. (2018). Artificial biocatalytic linear cascades for preparation of organic molecules. *Chemical reviews*, 118(1), 270-348.

Sehl, T., Hailes, H. C., Ward, J. M., Wardenga, R., von Lieres, E., Offermann, H., & Rother, D. (2013). Two steps in one pot: enzyme cascade for the synthesis of nor (pseudo) ephedrine from inexpensive starting materials. *Angewandte Chemie International Edition*, *52*(26), 6772-6775.

Sen, P., Deb, S., Bhattacharjee, C., & Chowdhury, R. (2012). Feasibility studies on enzymatic production of galacto-oligosaccharides from lactose and recovery of enzyme through ultrafiltration. *Procedia Engineering*, *44*, 1056-1059.

Shaeri, J., Wohlgemuth, R., & Woodley, J. M. (2006). Semiquantitative process screening for the biocatalytic synthesis of D-xylulose-5-phosphate. *Organic process research & development*, 10(3), 605-610.

Shaeri, J., Wright, I., Rathbone, E. B., Wohlgemuth, R., & Woodley, J. M. (2008). Characterization of enzymatic D-xylulose 5-phosphate synthesis. *Biotechnology and bioengineering*, *101*(4), 761-767.

Siedentop, R., Claaßen, C., Rother, D., Lütz, S., & Rosenthal, K. (2021). Getting the most out of enzyme cascades: Strategies to optimize in vitro multi-enzymatic reactions. *Catalysts*, *11*(10), 1183.

Singh, R. K., Tiwari, M. K., Singh, R., & Lee, J. K. (2013). From protein engineering to immobilization: promising strategies for the upgrade of industrial enzymes. *International journal of molecular sciences*, *14*(1), 1232-1277.

Sirover, M. A. (2014). Structural analysis of glyceraldehyde-3-phosphate dehydrogenase functional diversity. *The international journal of biochemistry & cell biology*, *57*, 20-26.

Smith, M. E., Kaulmann, U., Ward, J. M., & Hailes, H. C. (2006). A colorimetric assay

for screening transketolase activity. *Bioorganic & medicinal chemistry*, *14*(20), 7062-7065.

Smith, M. E., Smithies, K., Senussi, T., Dalby, P. A., & Hailes, H. C. (2006). The first mimetic of the transketolase reaction. *European Journal of Organic Chemistry*, (5), pp. 1121–1123.

Smithies, K., Smith, M. E., Kaulmann, U., Galman, J. L., Ward, J. M., & Hailes, H. C. (2009). Stereoselectivity of an ω-transaminase-mediated amination of 1, 3-dihydroxy-1-phenylpropane-2-one. *Tetrahedron: Asymmetry*, *20*(5), 570-574.

Sperl, J. M., & Sieber, V. (2018). Multienzyme Cascade Reactions Status and Recent Advances. *Acs Catalysis*, *8*(3), 2385-2396.

Sprenger, G. A., Schörken, U., Sprenger, G., & Sahm, H. (1995). Transketolase A of Escherichia coli K12: purification and properties of the enzyme from recombinant strains. *European Journal of Biochemistry*, *230*(2), 525-532.

Stevens, A. C., & Pagenkopf, B. L. (2010). Diels− Alder Chemistry of Siloles and Their Transformation into Cyclohex-2-ene-1, 4-cis-diols. *Organic letters*, *12*(16), 3658-3661.

Sukumaran, J., & Hanefeld, U. (2005). Enantioselective C–C bond synthesis catalysed by enzymes. *Chemical Society Reviews*, *34*(6), 530-542.

Sun, H., Zhang, H., Ang, E. L., & Zhao, H. (2018). Biocatalysis for the synthesis of pharmaceuticals and pharmaceutical intermediates. *Bioorganic & medicinal chemistry*, *26*(7), 1275-1284.

Suveges, N. S., Rodriguez, A. A., Diederichs, C. C., de Souza, S. P., Leão, R. A., Miranda, L. S., ... & de Souza, R. O. (2018). Continuous-Flow Synthesis of (R)-Propylene Carbonate: An Important Intermediate in the Synthesis of Tenofovir. *European Journal of Organic Chemistry*, *2018*(23), 2931-2938.

Szymańska, K., Pudło, W., Mrowiec-Białoń, J., Czardybon, A., Kocurek, J., & Jarzębski, A. B. (2013). Immobilization of invertase on silica monoliths with hierarchical pore structure to obtain continuous flow enzymatic microreactors of high

performance. *Microporous and mesoporous materials*, *170*, 75-82.

Taarning, E., & Madsen, R. (2008). Unsaturated aldehydes as alkene equivalents in the Diels–Alder reaction. *Chemistry–A European Journal*, *14*(18), 5638-5644.

Tamborini, L., Fernandes, P., Paradisi, F., & Molinari, F. (2018). Flow bioreactors as complementary tools for biocatalytic process intensification. *Trends in biotechnology*, *36*(1), 73-88.

Tušek, A. J., Tišma, M., Bregović, V., Ptičar, A., Kurtanjek, Ž., & Zelić, B. (2013). Enhancement of phenolic compounds oxidation using laccase from Trametes versicolor in a microreactor. *Biotechnology and bioprocess engineering*, *18*, 686-696.

Valikhani, D., Bolivar, J. M., & Nidetzky, B. (2020). Enzyme Immobilization in Wall-Coated Flow Microreactors. *Immobilization of Enzymes and Cells: Methods and Protocols*, 243-257.

Venkatesan, R., Alahuhta, M., Pihko, P. M., & Wierenga, R. K. (2011). High resolution crystal structures of triosephosphate isomerase complexed with its suicide inhibitors: The conformational flexibility of the catalytic glutamate in its closed, liganded active site. *Protein Science*, *20*(8), 1387-1397.

Vobecká, L., Tichá, L., Atanasova, A., Slouka, Z., Hasal, P., & Přibyl, M. (2020). Enzyme synthesis of cephalexin in continuous-flow microfluidic device in ATPS environment. *Chemical Engineering Journal*, *396*, 125236.

Warburg, O. and Christian, W. (1942) Isolation and Crystallization of Enolase. Biochemische Zeitschrift, 310, 384-421.

Wei, C., Zhou, Y., Zhuang, W., Li, G., Jiang, M., & Zhang, H. (2018). Improving the performance of immobilized β-glucosidase using a microreactor. *Journal of bioscience and bioengineering*, *125*(4), 377-384.

Wilding, K. M., Schinn, S. M., Long, E. A., & Bundy, B. C. (2018). The emerging impact of cell-free chemical biosynthesis. *Current opinion in biotechnology*, *53*, 115-121.

Winkler, C. K., Schrittwieser, J. H., & Kroutil, W. (2021). Power of biocatalysis for

organic synthesis. *ACS central science*, *7*(1), 55-71.

Wohlgemuth, R., & Littlechild, J. (2022). Complexity reduction and opportunities in the design, integration and intensification of biocatalytic processes for metabolite synthesis. *Frontiers in Bioengineering and Biotechnology*, *10*, 958606.

Wolfson-Stofko, B., Hadi, T., & Blanchard, J. S. (2013). Kinetic and mechanistic characterization of the glyceraldehyde 3-phosphate dehydrogenase from Mycobacterium tuberculosis. *Archives of biochemistry and biophysics*, *540*(1-2), 53-61.

Woodley, J. M. (2008). New opportunities for biocatalysis: making pharmaceutical processes greener. *Trends in biotechnology*, *26*(6), 321-327.

Wu, N., Wang, S., Yang, Y., Song, J., Su, P., & Yang, Y. (2018). DNA-directed trypsin immobilization on a polyamidoamine dendrimer-modified capillary to form a renewable immobilized enzyme microreactor. *International journal of biological macromolecules*, *113*, 38-44.

Wu, Z. Q., Li, Z. Q., Li, J. Y., Gu, J., & Xia, X. H. (2016). Contribution of convection and diffusion to the cascade reaction kinetics of β-galactosidase/glucose oxidase confined in a microchannel. *Physical Chemistry Chemical Physics*, *18*(21), 14460-14465.

Xu, M. *et al.* (2021) 'Recent advance of chemoenzymatic catalysis for the synthesis of chemicals: Scope and challenge', *Chinese Journal of Chemical Engineering*. doi: 10.1016/j.cjche.2020.12.016.

Ye, X., Honda, K., Sakai, T., Okano, K., Omasa, T., Hirota, R., ... & Ohtake, H. (2012). Synthetic metabolic engineering-a novel, simple technology for designing a chimeric metabolic pathway. *Microbial cell factories*, *11*, 1-12.

Yue, J., Schouten, J. C., & Nijhuis, T. A. (2012). Integration of microreactors with spectroscopic detection for online reaction monitoring and catalyst characterization. *Industrial & engineering chemistry research*, *51*(45), 14583-14609.

Zhao, B., Zhou, L., Ma, L., He, Y., Gao, J., Li, D., & Jiang, Y. (2018). Co-

immobilization of glucose oxidase and catalase in silica inverse opals for glucose removal from commercial isomaltooligosaccharide. *International journal of biological macromolecules*, *107*, 2034-2043.

Žnidaršič-Plazl, P. (2021). Biocatalytic process intensification via efficient biocatalyst immobilization, miniaturization, and process integration. *Current Opinion in Green and Sustainable Chemistry*, *32*, 100546.

Žnidaršič-Plazl, P., & Plazl, I. (2009). Modelling and experimental studies on lipase-catalyzed isoamyl acetate synthesis in a microreactor. *Process Biochemistry*, *44*(10), 1115-1121.

6 Appendix

6.1 Calibration curves

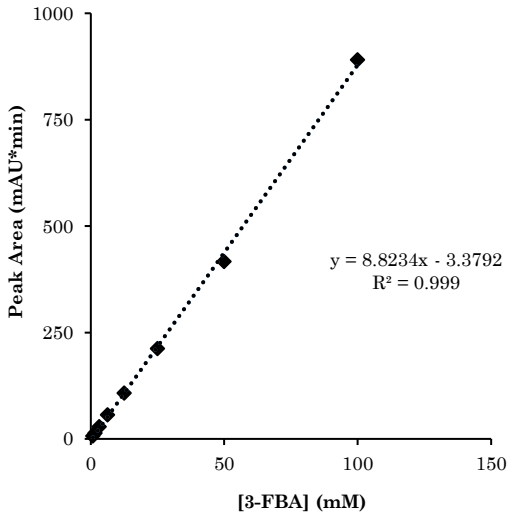

Figure 6.1: Calibration curve of 3-formylbenzoic acid by HPLC analysis using an ACE 5 C18 RP column and detection at 254 nm.

a) b)

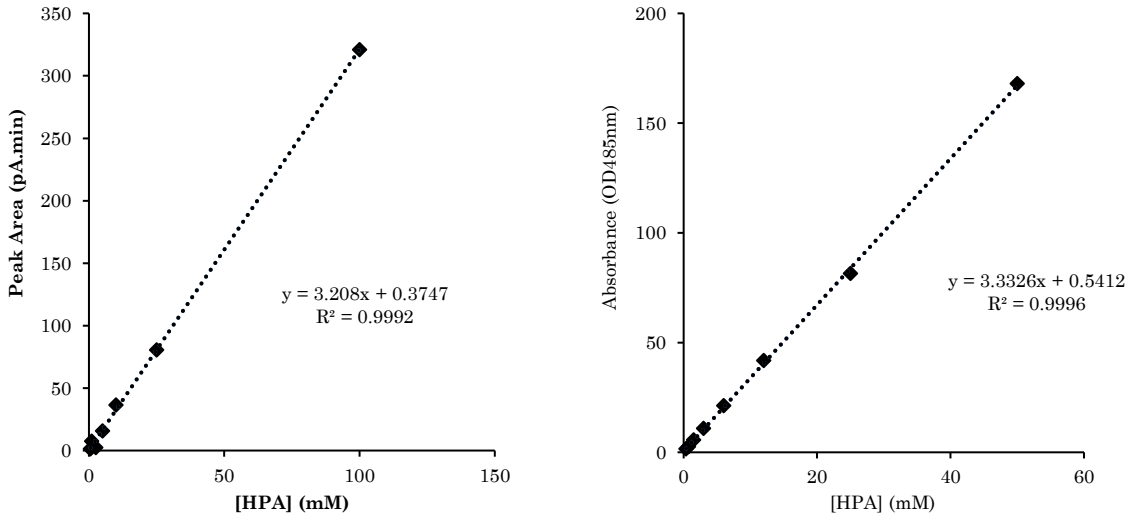

Figure 6.2: HPA calibration curves by HPLC and by colorimetric assay.
a) Calibration curve of hydroxypyruvate in 25 mM Tris-HCL pH 7, by HPLC analysis using an Aminex HPX-87H column at 60 ºC and detection at 210 nm. b) Calibration curve of HPA achieved through a colorimetric assay on a FLUOstar Optima plate reader at OD485nm.

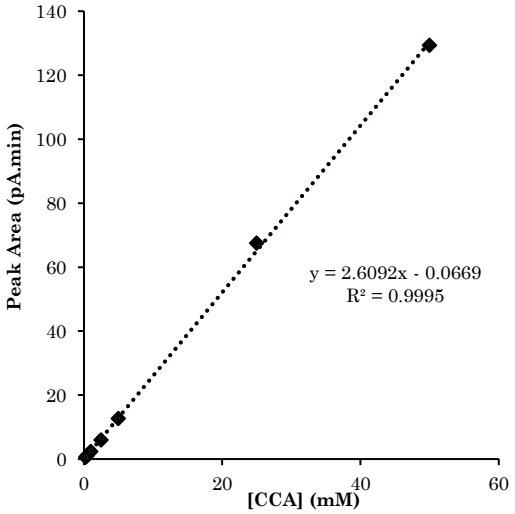

Figure 6.3: Calibration of 3,4-dimethyl-3-cyclo-hexene-1-carboxaldehyde by GC-FID.

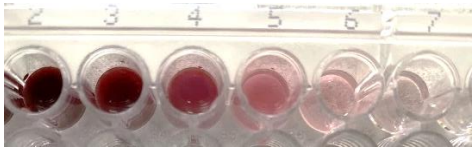

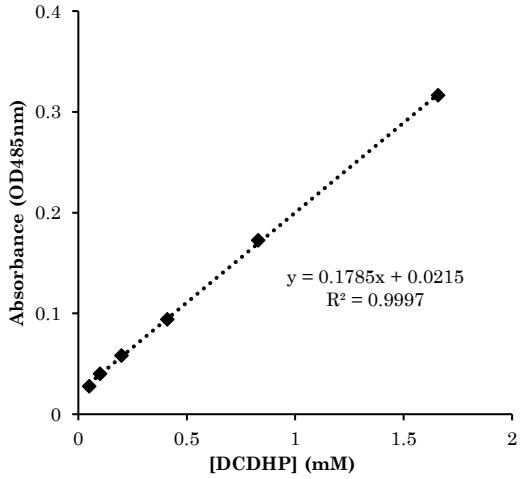

Figure 6.4: Calibration curve of DCDHP achieved through a colorimetric assay on a FLUOstar Optima plate reader at OD485nm.

a) b)

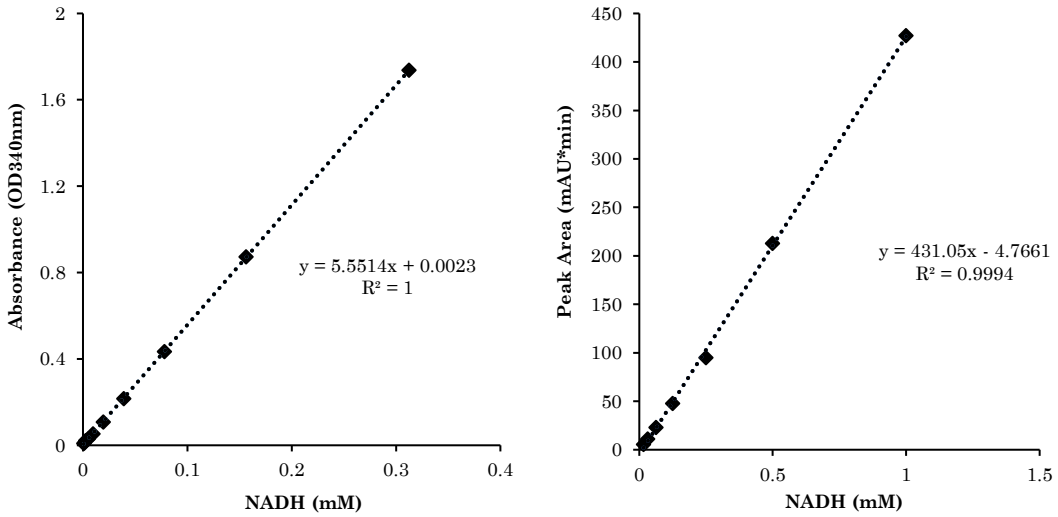

Figure 6.5: Calibration curves of NADH.
a) Calibration in FLUOstar Optima plate reader at 340 nm; b) Calibration curve by HPLC analysis using an Synergy Hydro-RP column and detection at 254 nm.

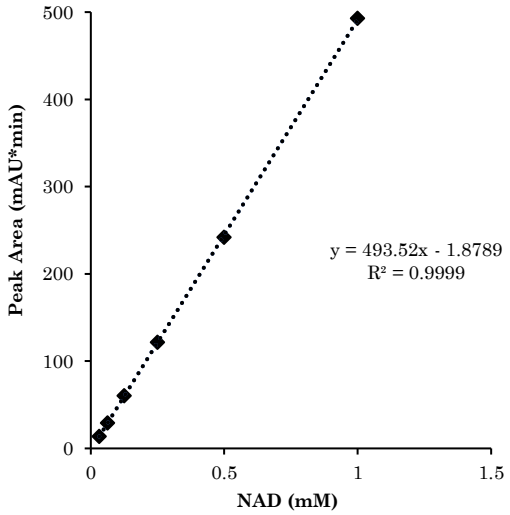

Figure 6.6: Calibration curve of NAD+ by HPLC analysis using an Synergy Hydro-RP column and detection at 254 nm.

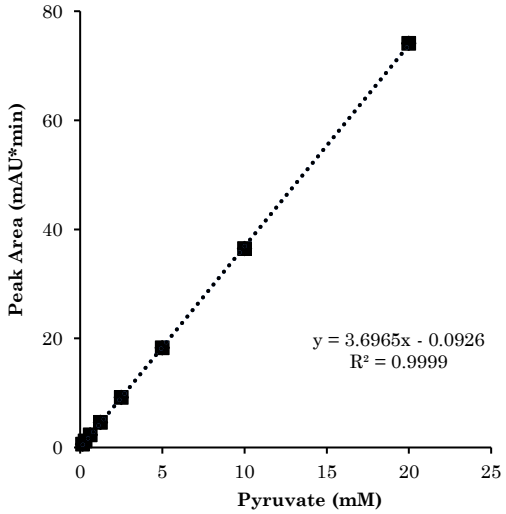

Figure 6.7: Calibration curve of pyruvate by HPLC analysis using an Synergy Hydro-RP column and detection at 254 nm.

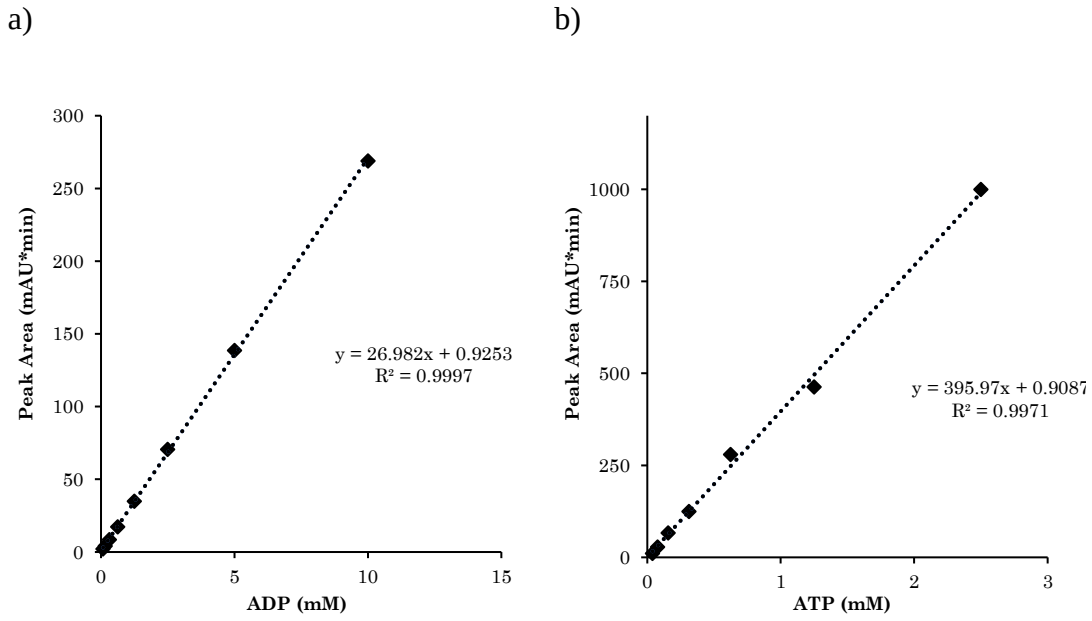

Figure 6.8: Calibration curve of ADP and ATP by HPLC analysis using an Synergy Hydro-RP column and detection at 254 nm.
a) Calibration curve of ADP; b) calibration curve of ATP.

a) b)

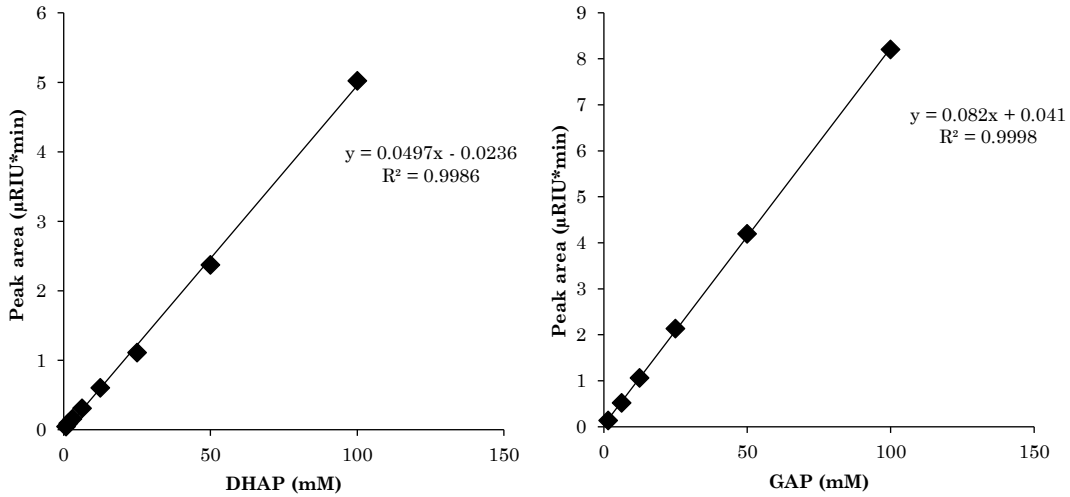

Figure 6.9: Calibration curve of DHAP and GAP by HPLC analysis using an Aminex HPX-87H column and detection at 254 nm

a) Calibration of DHAP; b) calibration of GAP; substrates solutions were prepared in 15 mM Tris buffer pH 7.6.

6.2 Chromatograms

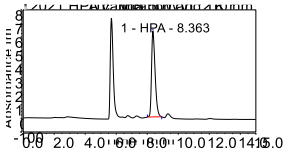

Figure 6.10: Chromatogram for HPA.

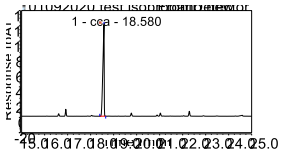

Figure 6.11: Chromatogram for CCA.

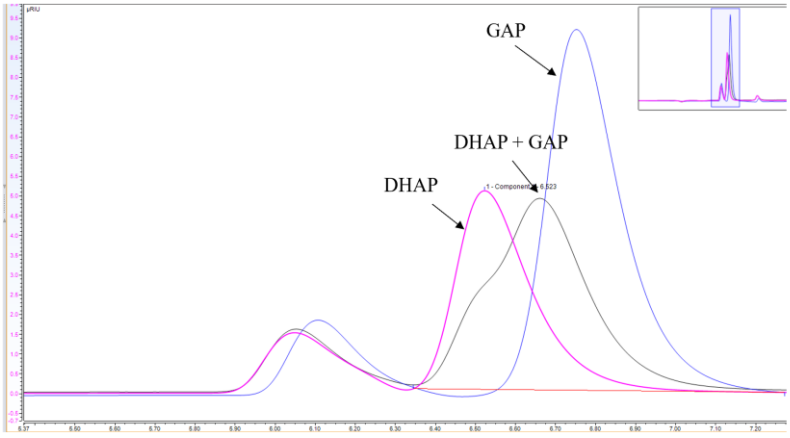

Figure 6.12: Chromatogram for DHAP, GAP and both substrates in 15 mM Tris buffer pH 7.6.

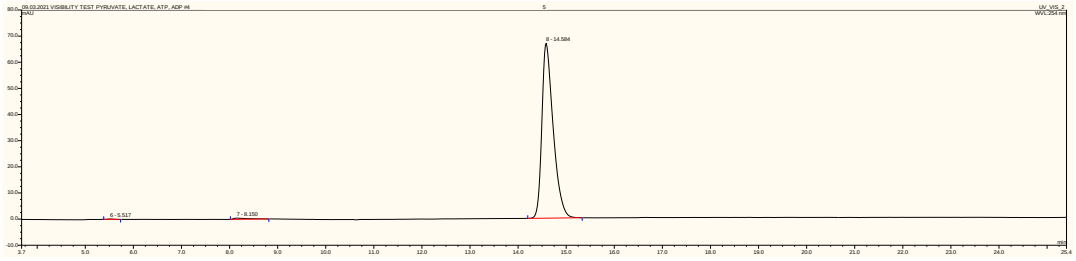

Figure 6.13: Chromatogram for pyruvate.

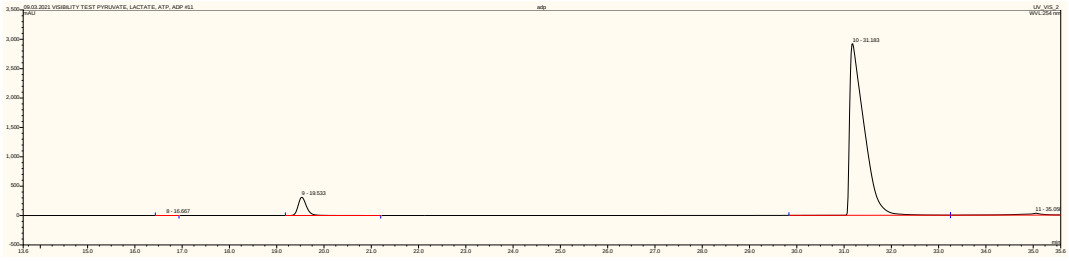

Figure 6.14: Chromatogram for ADP.

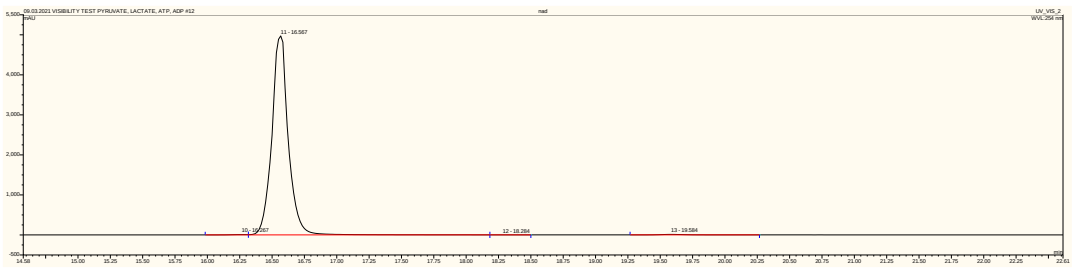

Figure 6.15: Chromatogram for NAD+.

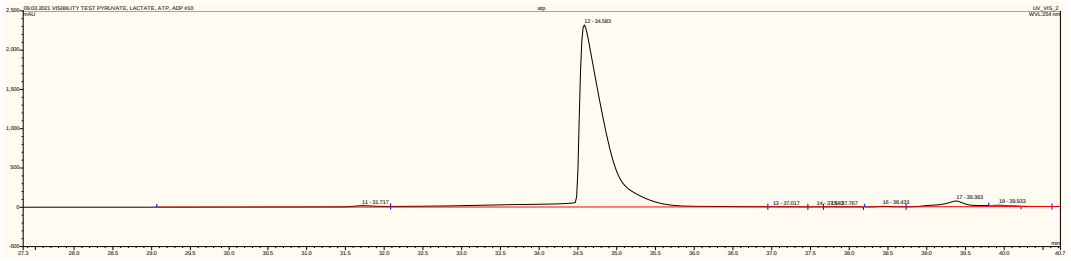

Figure 6.16: Chromatogram for ATP.

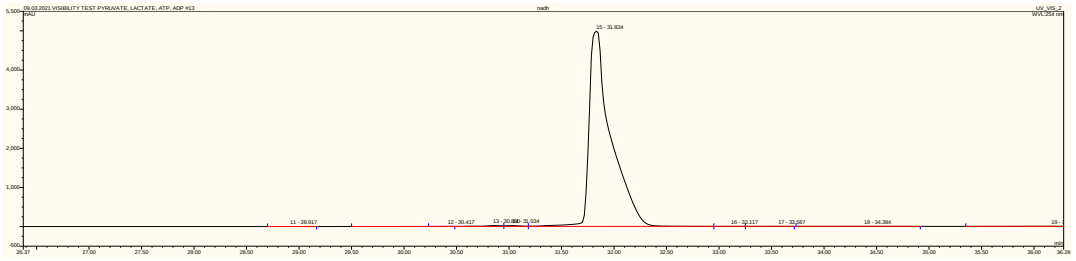

Figure 6.17: Chromatogram for NADH.

6.3 Supplementary results

Table 6.1:Diels-Alder reaction with 200 mM acrolein and butadiene catalysed by different catalyst and solvents.
The data presented in this table was obtained prior to this thesis by Dr Pia Gruber (Gruber, 2019). Conversions presented were achieved after 2 hours at room temperature and determine by GC analysis expect the ones containing methanol, which is not compatible with the GC column used, and therefore CCA production was confirmed by TLC analysis. In some combinations conversion was not detected (ND).

Catalyst	Solvent	Catalyst solubility	Conversion (%)
Zinc Chloride ($ZnCl_2$)	Acetonitrile	Soluble	4.8
	Methanol	Soluble	ND
	Ethanol	Soluble	0.6
	Isopropanol	Insoluble	1.6
Chiral Catalyst	Methanol	Soluble	ND
	Isopropanol	Soluble	1.5
Aluminium Chloride ($AlCl_3$)	Acetonitrile	Insoluble	37.5
	Methanol	Soluble	ND
	Ethanol	Soluble	0.1
	Isopropanol	Insoluble	0.2
	Acetonitrile + 5% (v/v) MeOH	Insoluble	ND
	Acetonitrile + 10% (v/v) MeOH	Soluble	ND
	Acetonitrile + 5%(v/v) EtOH	Insoluble	10.6
	Acetonitrile + 10%(v/v) EtOH	Insoluble	3.9
	Acetonitrile + 20% (v/v)EtOH	Soluble	0.8
	Acetonitrile + 5% (v/v) iPrOH	Insoluble	12.8
	Acetonitrile + 10% (v/v)H_2O	Soluble	ND
	Acetonitrile + 30% (v/v)H_2O	Soluble	ND

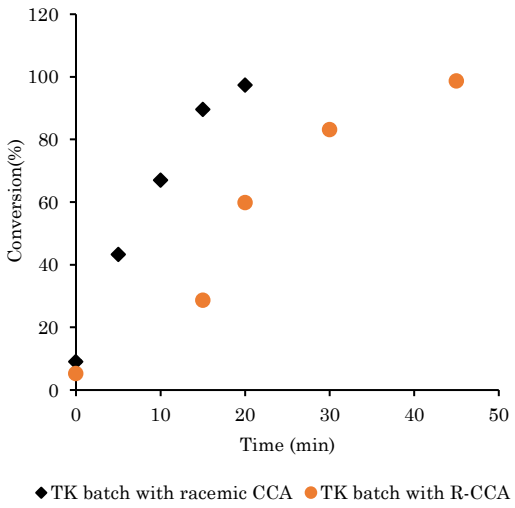

Figure 6.18: Comparison of TK activity towards racemic CCA and R-CCA.
Conversions were calculated based on HPA depletion measured by HPLC. The data suggests that TK can convert R-CCA and HPA to form DCDHP.

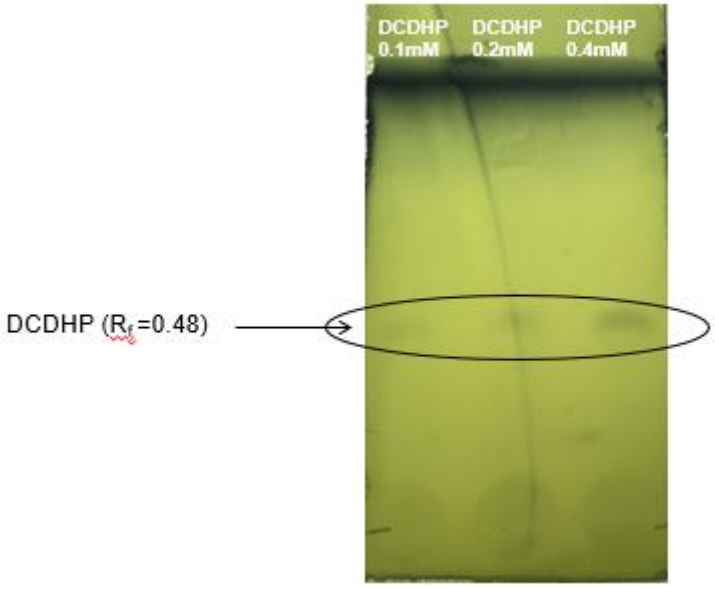

Figure 6.19: DCDHP visibility test on the TLC assay.
DCDHP is visible at low concentration on the TLC assay.

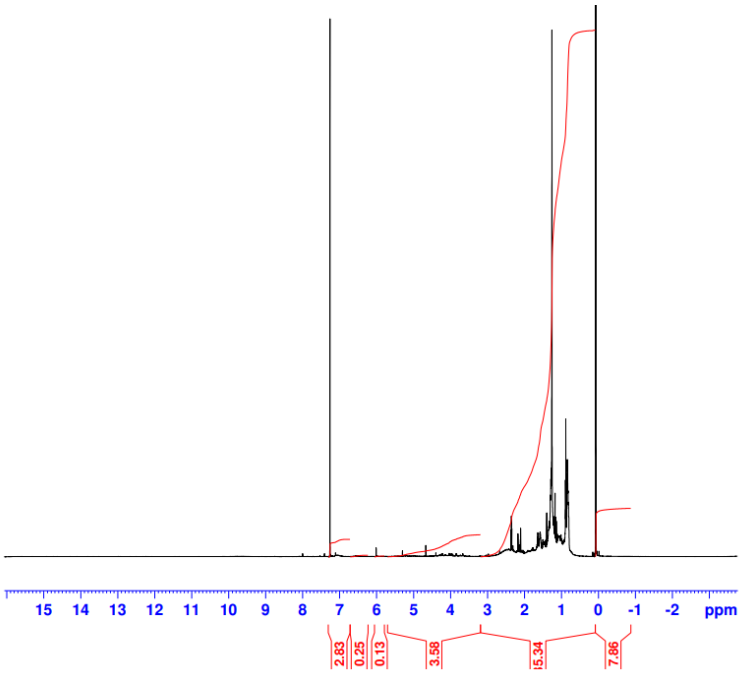

Figure 6.20: ^{1}H NMR of DCDHP.

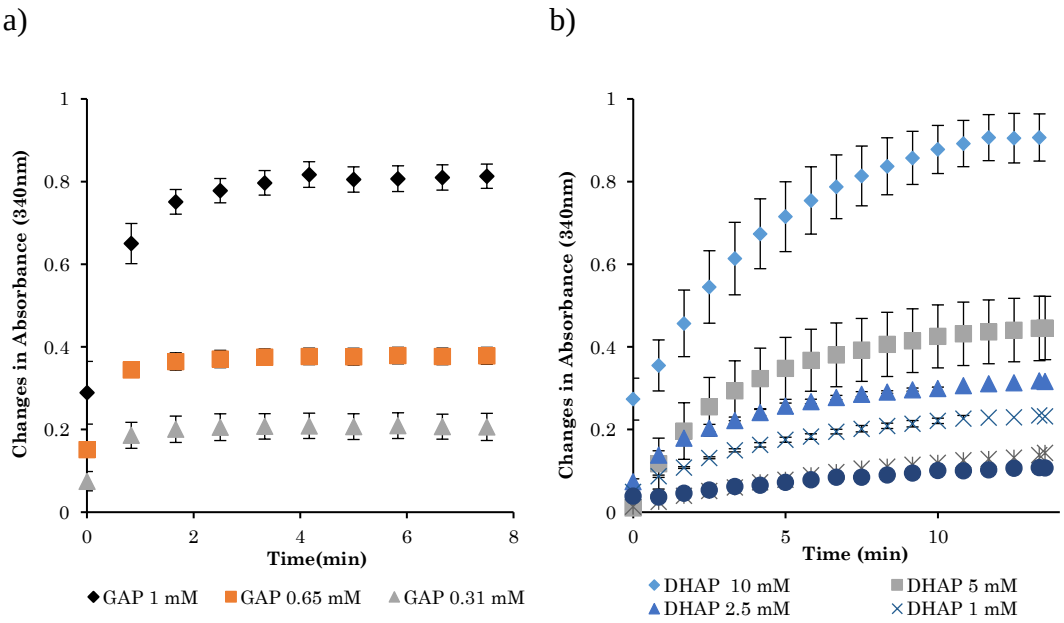

Figure 6.21: GAPDH and TPI-GAPDH activity assays.
a) GAPDH batch reaction using different concentrations of GAP (1 – 0.31 mM). b) TPI-GAPDH forward batch reaction using with different concentrations of DHAP (10 – 0.25 mM); reactions were done 50 mM glycine-phosphate buffer pH 8.5 with enzyme concentrations of 1 U.ml^{-1}. Error bars represent mean ±SD (n=3).

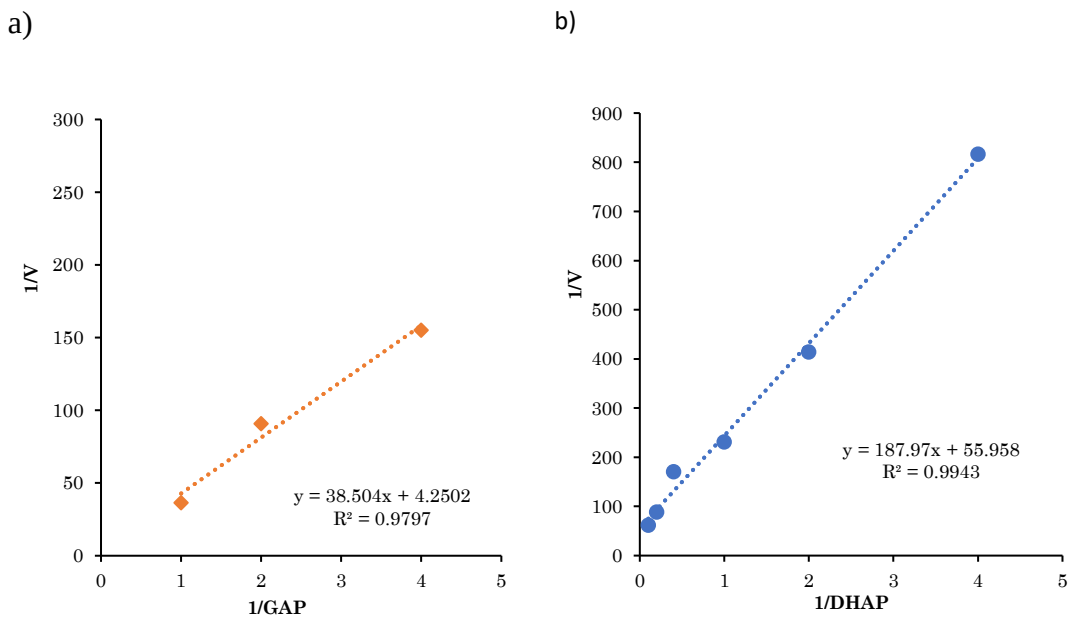

Figure 6.22: Lineweaver Burk plots from GAPDH and TPI-GAPDH catalysed reactions.

a) Lineweaver Burk plot from GAPDH batch reaction using different concentrations of GAP (1 – 0.31 mM); b) Lineweaver Burk plot from TPI-GAPDH forward batch reaction using with different concentrations of DHAP (10 – 0.25 mM); Michaelis constant (Km) and maximum reaction velocity (Vmax) of GAPDH and TPI were determined according to double-reciprocal Lineweaver–Burk plots. GAPDH had a Vmax equal to 0.235 $mM.min^{-1}$ and a Km equal to 9.06 mM. TPI demonstrated activity with a Vmax equal to 0.018 $mM.min^{-1}$ and a Km equal to 3.36 mM. The obtained kinetic values are in-line with the ones reported in other studies under similar conditions (Moellering and Cravatt, 2013a; Mukai *et al.*, 2013b, 2017)

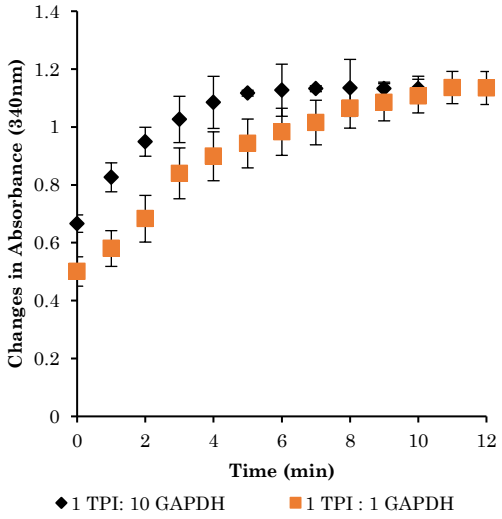

Figure 6.23: Effect of GAPDH concentration on TPI-GAPDH batch reactions.
Reactions were carried without with 1 U.ml^{-1} TPI: 1 U.ml^{-1} GAPDH and with 1 U.ml^{-1} TPI: 10 U.ml^{-1} GAPDH, with 10 mM of DHAP and 0.4 mM NAD+ in 50 mM glycine-phosphate buffer pH 8.5; no significant different was found between the two sets of data; Error bars represent mean ±SD (n=3).

a)

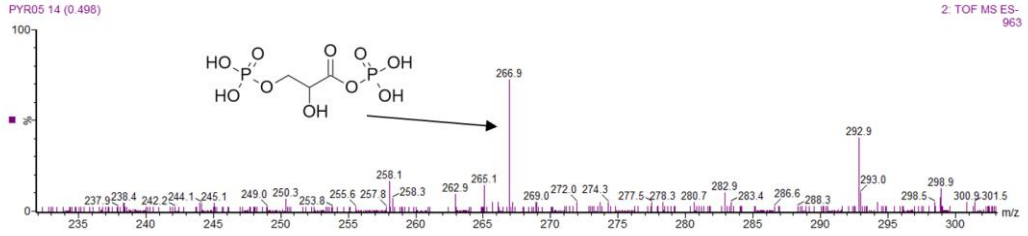

b)

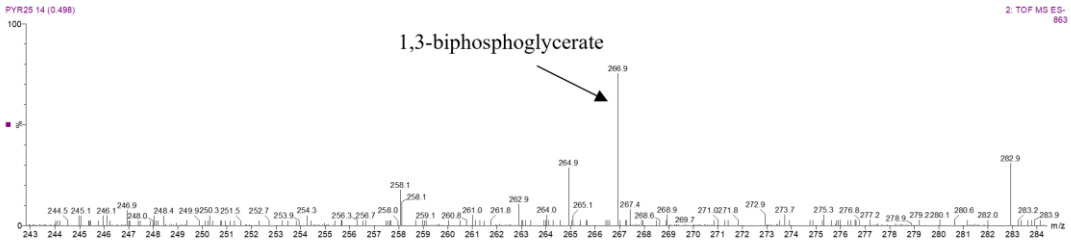

Figure 6.24: LC-MS chromatogram from TPI-GAPDH and TPI-GAPDH-LDH batch reaction.
a) Chromatogram from TPI-GAPDH batch reaction with a signal of m/z 266.9 in negative ion mode is visible, suggesting the presence of 1,3-biphosphoglycerate in the reaction mixture; b) chromatogram from TPI-GAPDH-LDH batch reaction with a signal of m/z 266.9 in negative ion mode is visible, suggesting the presence of 1,3-biphosphoglycerate in the reaction mixture.

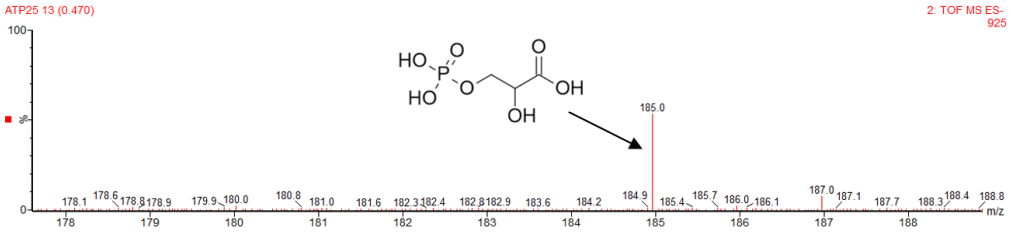

Figure 6.25: LC-MS chromatogram from PGK assay.
A signal of m/z 185 in negative ion mode is visible, suggesting the presence of 3-PGA in the reaction mixture.